
Theses and Dissertations

Spring 2012

On the role of intracranial aneurysm morphology in stable versus unstable lesions

Manasi Ramachandran
University of Iowa

Follow this and additional works at: <https://ir.uiowa.edu/etd>



Part of the [Biomedical Engineering and Bioengineering Commons](#)

Copyright © 2012 Manasi Ramachandran

This dissertation is available at Iowa Research Online: <https://ir.uiowa.edu/etd/2965>

Recommended Citation

Ramachandran, Manasi. "On the role of intracranial aneurysm morphology in stable versus unstable lesions." PhD (Doctor of Philosophy) thesis, University of Iowa, 2012.

<https://doi.org/10.17077/etd.uxcjttg>

Follow this and additional works at: <https://ir.uiowa.edu/etd>



Part of the [Biomedical Engineering and Bioengineering Commons](#)

ON THE ROLE OF INTRACRANIAL ANEURYSM MORPHOLOGY IN STABLE VERSUS
UNSTABLE LESIONS

by

Manasi Ramachandran

An Abstract

Of a thesis submitted in partial fulfillment
of the requirements for the Doctor of
Philosophy degree in Biomedical Engineering
in the Graduate College of
The University of Iowa

May 2012

Thesis Supervisor: Associate Professor Madhavan L. Raghavan

ABSTRACT

Most intracranial aneurysms (IA) that are unruptured during clinical screening remain stable over time with no measurable change or symptoms if left untreated. However, a few do grow larger and may rupture. The ability to preemptively identify aneurysms that will become unstable over time (i.e., those that will grow and/or rupture) can result in timely intervention for these few patients while avoiding unnecessary treatment for countless others. So far, reports have primarily assessed potential rupture factors in IAs between ruptured lesions and unruptured lesions. These factors (that discriminate rupture status) do not necessarily distinguish unruptured aneurysms that tend towards growth and/or rupture over a period of time from those that remain stable. The hypothesis motivating this study is that aneurysm shape morphology provides critical information that will indicate instability in unruptured aneurysms. We tested this hypothesis in a large population multi-center prospective longitudinal cohort study of unruptured IAs.

A total of 198 study subjects were recruited at four clinical centers – Penn State Hershey Medical Center, Massachusetts General Hospital, Thomas Jefferson University Hospital and University of Iowa Hospitals and Clinics. All had at least one unruptured IA and were placed on follow-up without immediate intervention. Three-dimensional volumetric scans were obtained from the clinics. Three dimensional models were created from the source data using levelset segmentation techniques implemented in the Vascular Modeling ToolKit (VMTK). Five size and six shape indices were calculated on the isolated aneurysm geometry: Size indices - Height (H), max. diameter (Dmax), neck diameter (Dn), volume (V), and surface area (SA) and Shape Indices - Undulation index (UI), Aspect ratio (AR), Ellipticity index (EI), Non-sphericity index (NSI), Bulge Location (BL), and Bottleneck factor (BF). Pressure-induced wall tension was calculated using Finite element analysis. An isotropic, polynomial model was used after a comparative study of different modeling choices was performed and the 95th percentile max. principal stress (Peak Wall Stress - PWS) was chosen to be the index of maximum wall tension. Independent studies were performed to document validity of methods used, to quantify

sensitivity of these indices (in turn, of the segmented geometries) to imaging modality and to quantify variability in segmented geometries between investigators. Researchers were blinded from the follow-up status of IAs to avoid any user bias in the analysis. During follow-up, aneurysms were labeled as “grown” or “stable” by radiologists. Study subjects were assigned to one of two groups based on clinical outcome: Unstable group (grown or ruptured) or Stable group (remained same or lesser size). Statistical analysis was then performed on the computed indices. One hundred ninety eight aneurysms were followed for an average of 607 days. Over the follow-up period, 26 were lost to follow up, 150 were found to be stable, 20 had grown, 1 deceased, 1 could not be located on the angiogram and none had ruptured. Also, of the total 198, 53 were electively treated during follow-up. Non-parametric Mann-Whitney U-tests were performed for index to test for statistically significant difference between the stable ($n_1 = 150$) and the unstable group ($n_2 = 21$). None of the indices differentiated the two groups in a statistically significant manner. Receiver Operating Characteristics (ROC) curve analysis was consistent with these findings.

Is aneurysm morphology (size and shape) a risk factor for IA growth/rupture? We sought to test this hypothesis in a study design that is unique in many ways – it is the first large population study of longitudinal cohorts; the study population was prospectively recruited at multiple clinical sites; the study population was predominated by small aneurysms (88% of IAs in the study population were less than 7 mm). The results of this large population cohort study suggest that previously reported metrics of aneurysm cannot serve as prognostic indicators of longitudinal outcome.

Abstract Approved:

Thesis Supervisor

Title and Department

Date

ON THE ROLE OF INTRACRANIAL ANEURYSM MORPHOLOGY IN STABLE
VERSUS UNSTABLE LESIONS

by
Manasi Ramachandran

A thesis submitted in partial fulfillment
of the requirements for the Doctor of
Philosophy degree in Biomedical Engineering
in the Graduate College of
The University of Iowa

May 2012

Thesis Supervisor: Associate Professor Madhavan L. Raghavan

Graduate College
The University of Iowa
Iowa City, Iowa

CERTIFICATE OF APPROVAL

PH.D. THESIS

This is to certify that the Ph.D. thesis of

Manasi Ramachandran

has been approved by the Examining Committee
for the thesis requirement for the Doctor of Philosophy
degree in Biomedical Engineering at the May 2012 graduation.

Thesis Committee: _____
Madhavan L. Raghavan, Thesis Supervisor

Krishnan B.Chandran

Joseph M.Reinhardt

Jia Lu

David Hasan

To Amma and Appa

ACKNOWLEDGMENTS

I would like to thank my advisor, Dr. M.L. Raghavan for the great teacher and mentor that he has been throughout my PhD. He has tirelessly provided guidance making me a better writer, orator and thinker. In the words of Henry Adams, “A teacher affects eternity; he can never tell where his influence stops”.

Thanks to my committee members for serving in my committee. Special thanks to Dr. Hasan and Dr. Lu for helping with the multimodality and modeling choices study. Thanks to Dr. Harbaugh, Dr. Ogilvy, Dr. Rossenwasser and Dr. Policeni for their overall guidance and support in this project.

My gratitude to: Steve Lin and Tatiana Correa for helping me manage the clinical data and segmenting 3D models; Ben Dickerhoff for his help with organizing the segmentation protocol and performing the user sensitivity study; Shouhua Hu for performing the inverse analysis as part of the modeling choices study; Rohini Retarekar for setting up the flow loop used for the multimodality study; Deborah Hoffman, Michael Philips, Melissa Witt and Ben Berkowitz for data collection and clinical coordination.

Thanks to my uncle, H.Madhavan for introducing me to Biomedical engineering. Thanks to Anupama.L.Reddy for her support through the years. Thanks to Kathleen, Christine, Vasudha, Renu and a few others who have made this journey worthwhile. Most importantly, thanks to Chris Reardon for supporting me through the latter PhD years and for proving to me that the cliché – “home is where the heart is” – is in fact true.

Finally, thanks to my parents for all their hard work in reaching above and beyond their means and giving me the best of everything. This PhD has been possible only because of the encouragement and inspiration they have provided.

ABSTRACT

Most intracranial aneurysms (IA) that are unruptured during clinical screening remain stable over time with no measurable change or symptoms if left untreated. However, a few do grow larger and may rupture. The ability to preemptively identify aneurysms that will become unstable over time (i.e., those that will grow and/or rupture) can result in timely intervention for these few patients while avoiding unnecessary treatment for countless others. So far, reports have primarily assessed potential rupture factors in IAs between ruptured lesions and unruptured lesions. These factors (that discriminate rupture status) do not necessarily distinguish unruptured aneurysms that tend towards growth and/or rupture over a period of time from those that remain stable. The hypothesis motivating this study is that aneurysm shape morphology provides critical information that will indicate instability in unruptured aneurysms. We tested this hypothesis in a large population multi-center prospective longitudinal cohort study of unruptured IAs.

A total of 198 study subjects were recruited at four clinical centers – Penn State Hershey Medical Center, Massachusetts General Hospital, Thomas Jefferson University Hospital and University of Iowa Hospitals and Clinics. All had at least one unruptured IA and were placed on follow-up without immediate intervention. Three-dimensional volumetric scans were obtained from the clinics. Three dimensional models were created from the source data using levelset segmentation techniques implemented in the Vascular Modeling ToolKit (VMTK). Five size and six shape indices were calculated on the isolated aneurysm geometry: Size indices - Height (H), max. diameter (Dmax), neck diameter (Dn), volume (V), and surface area (SA) and Shape Indices - Undulation index (UI), Aspect ratio (AR), Ellipticity index (EI), Non-sphericity index (NSI), Bulge Location (BL), and Bottleneck factor (BF). Pressure-induced wall tension was calculated using Finite element analysis. An isotropic, polynomial model was used after a

comparative study of different modeling choices was performed and the 95th percentile max. principal stress (Peak Wall Stress - PWS) was chosen to be the index of maximum wall tension. Independent studies were performed to document validity of methods used, to quantify sensitivity of these indices (in turn, of the segmented geometries) to imaging modality and to quantify variability in segmented geometries between investigators. Researchers were blinded from the follow-up status of IAs to avoid any user bias in the analysis. During follow-up, aneurysms were labeled as “grown” or “stable” by radiologists. Study subjects were assigned to one of two groups based on clinical outcome: Unstable group (grown or ruptured) or Stable group (remained same or lesser size). Statistical analysis was then performed on the computed indices. One hundred ninety eight aneurysms were followed for an average of 607 days. Over the follow-up period, 26 were lost to follow up, 150 were found to be stable, 20 had grown, 1 deceased, 1 could not be located on the angiogram and none had ruptured. Also, of the total 198, 53 were electively treated during follow-up. Non-parametric Mann-Whitney U-tests were performed for index to test for statistically significant difference between the stable ($n_1 = 150$) and the unstable group ($n_2 = 21$). None of the indices differentiated the two groups in a statistically significant manner. Receiver Operating Characteristics (ROC) curve analysis was consistent with these findings.

Is aneurysm morphology (size and shape) a risk factor for IA growth/rupture? We sought to test this hypothesis in a study design that is unique in many ways – it is the first large population study of longitudinal cohorts; the study population was prospectively recruited at multiple clinical sites; the study population was predominated by small aneurysms (88% of IAs in the study population were less than 7 mm). The results of this large population cohort study suggest that previously reported metrics of aneurysm cannot serve as prognostic indicators of longitudinal outcome.

TABLE OF CONTENTS

LIST OF TABLES	iv
LIST OF FIGURES	v
CHAPTER	
1 BACKGROUND AND SIGNIFICANCE.....	1
1.1 Intracranial Aneurysms and its Prevalence.....	1
1.2 Disease Consequence and Management.....	2
1.3 Current Knowledge on Intracranial Aneurysm Morphology.....	3
1.4 Current Knowledge of Pressure-Induced Wall Tension in Intracranial Aneurysms.....	6
1.5 Current Knowledge of Hemodynamics Within Cerebral Aneurysms.....	7
1.6 Dissertation Overview	8
2 3D SEGMENTATION AND ITS CHALLENGES	10
2.1 Basic Methods	10
2.2 Presence of Skull in CTA – ICA Aneurysms	11
2.3 Merging of Vascular Structures - ACOM and Pericallosal Aneurysms	13
2.4 Presence of Thrombus	15
3 ANEURYSM ISOLATION.....	17
4 SENSITIVITY OF QUANTIFIED INTRACRANIAL ANEURYSM GEOMETRY TO IMAGING MODALITY.....	21
4.1 Introduction.....	21
4.2 Methods	23
4.2.1 Imaging of aneurysm flow phantom using multiple scan modalities	23
4.2.2 Collection of multiple modality scans from aneurysm patients.....	27
4.2.3 3D Segmentation	28
4.2.4 Morphometrics	30
4.3 Results.....	31
4.4 Discussion.....	37
4.5 Conclusion	40
5 ON THE ROLE OF MODELING CHOICES IN ESTIMATION OF CEREBRAL ANEURYSM WALL TENSION	41
5.1 Introduction.....	41
5.2 Methods	42
5.2.1 Numerical Simulations	44
5.2.2 Tension Indices Based on Curvature.....	48
5.2.3 Tension Indices Based on Clinical Measurements.....	49

5.3 Results.....	49
5.3.1 Numerical Simulations	49
5.3.2 Tension Indices Based on Curvature	51
5.3.3 Tension Indices Based on Clinical Measurements	52
5.4 Discussion.....	53
5.5 Conclusion	56
6 CHARACTERIZATION OF IN-VIVO MECHANICAL PROPERTIES OF CEREBRAL ARTERIES USING CRANIOTOMY VIDEO.....	58
6.1 Background.....	58
6.1.1 Craniotomy Video	58
6.1.2 Estimation of Arterial Mechanical Properties	58
6.2 Materials and Methods	59
6.2.1 Video Source	59
6.2.2 Measurements.....	59
6.2.3 Estimation of Mechanical Properties.....	60
6.3 Results and Conclusion.....	61
7 MORPHOLOGY OF INTRACRANIAL ANEURYSMS AND THEIR CORRELATION TO INTRACELLULAR SIGNALING PATHWAYS.....	62
7.1 Summary.....	62
8 PROTOCOL FOR VASCULAR SEGMENTATION AND ITS USER SENSITIVITY	64
8.1 Introduction.....	64
8.2 Methods	65
8.2.1 Study Population	65
8.2.2 3D Segmentation and Isolation	65
8.3 Results and Discussion	75
8.4 Conclusion.....	81
9 LONGITUDINAL COHORT STUDY.....	82
9.1 Data Collection	82
9.2 Segmentation and Isolation.....	84
9.3 Morphometric Analysis of Initial Scans and Clinical Follow-up.....	92
9.4. Morphometric Analysis of Follow-up scans of Unstable Aneurysms	99
9.5 Discussion.....	107
9.5.1 Sensitivity to imaging modalities.....	109
9.5.2 User Variability in the segmentation process	110
9.5.3 Role of Modeling Choices	110
9.5.4 Limitations	111
9.5.5 Future Studies	112
9.6 Conclusion.....	112
REFERENCES	114
APPENDIX.....	118
Segmentation Protocol.....	118

LIST OF TABLES

Table 1: Parameters for scanning flow phantom in four modalities.....	26
Table 2: Parameters used for patient scans of four modalities.	27
Table 3: Average and standard deviation of morphometric indices calculated for modalities across eight levels of smoothing.....	32
Table 4: Percent error between height and diameter provide by vendor to height and diameter measured on models from the four modalities.....	33
Table 5: Shape indices calculated for each of the three patients.	33
Table 6: Patients and their aneurysm demographics as obtained from medical records.....	42
Table 7: Modeling choices made during finite element analysis of cerebral aneurysm geometries.	45
Table 8: Stress indices calculated using different. Values presented as mean \pm standard deviation.	54
Table 9: Average and standard deviation of size and shape indices calculated across 10 aneurysm models.	73
Table 10: Coefficient of Repeatability (CR) calculated for models segmented by User1 and User 2.....	76
Table 11: Range of measurement for each index measured on 199 aneurysm dome models.....	87
Table 12: Area under the ROC curve (AUC) calculated for the each index. AUC of "Null" is 0.50.	91
Table 13: Increase in morphometric indices measured in 17 "unstable" aneurysms listed as min-median-max.....	98

LIST OF FIGURES

Figure 1: Circle of Willis	2
Figure 2: Example of a saccular aneurysm occurring at the Basilar Artery.	4
Figure 3: Definitions of shape indices used by Raghavan et al (45).	5
Figure 4: 3D segmentation of CTA images of flow phantom.	11
Figure 5: Sample slice of CTA showing ICA aneurysm with skull impinging on it.	12
Figure 6: 3D segmentation of sample ICA aneurysm after the removal of skull.	13
Figure 7: Segmentation of Left Pericallosal Aneurysm a) 3D model. b) CTA slice showing showing proximity of left and right Pericallosal arteries c) CTA slice showing aneurysm and artery presenting poor intensity gradients.	14
Figure 8: 3D segmentation of Pericallosal arteries merged due to lack of discernable intensity gradients.....	15
Figure 9: (left to right) Front and back view of 3D aneurysm model, CTA image slice demonstrating thrombus in aneurysm.	16
Figure 10: Examples of aneurysms isolated (shown in red) from their parent vasculature.	17
Figure 11: SCA branching off Basilar aneurysm, 10b: Ophthalmic branching off ICA aneurysm.	18
Figure 12: Segmentation repeated for aneurysms in Figure 12 to remove small branch arising from aneurysms.....	19
Figure 13: Example of PCA branching off from Basilar aneurysm.	20
Figure 14: Phantom of circle of Willis with an ACOM aneurysm.	24
Figure 15: Frontal view of the mold used for making in-vitro phantom, along with dimensions of arteries and the aneurysm (provided by vendor).....	24
Figure 16: Schematic diagram of flow loop consisting of phantom, pump, Inlet/Outlet tank, valve.	25
Figure 17: 3D segmentation of the vasculature from all four modalities. The views and scales are roughly similar between models shown.	28
Figure 18: 3D segmentations of the aneurysm and parent vessel. Also shown is the aneurysm dome isolated from its parent vasculature (highlighted as a darker shade).....	29
Figure 19: Two corresponding views of 3D models from Patient1, Patient2 and Patient3. Aneurysm sac is shown as a darker shade.	31

Figure 20: Graphical representation of size indices measured on patient-aneurysms with 3DRA on the x-axis and CE-MRA/TOF-MRA/CTA on the y-axis.....	34
Figure 21: Graphical representation of shape indices measured on patient-aneurysms with 3DRA on the x-axis and CE-MRA/TOF-MRA/CTA on the y-axis.....	35
Figure 22: Representative aneurysm models – at a basilar tip and at an MCA (isolated-aneurysm sac highlighted in red).....	43
Figure 23: Sample course and fine meshes for an aneurysm dome model.....	46
Figure 24: Sample of absolute peak value of maximum principal stress occurring due to irregular element in the mesh.	47
Figure 25: Stress calculated using numerical simulations with variations in modeling choices. Plots compare each modeling choice.....	49
Figure 26: Stress calculated using numerical simulations with variations in interpretation choices. Plots compare each interpretation choice.....	50
Figure 27: 95th percentile maximum principal stress calculated for aneurysm domes modeled as polynomial, isotropic model Vs. 95th percentile Km based stress.	51
Figure 28: 95th percentile maximum principal stress calculated for aneurysm domes modeled as polynomial, isotropic model Vs. stress calculated using clinical information – Dmax and H a) assuming ellipsoidal geometries b) assuming spherical geometries.	51
Figure 29: Maximum Principal Stress distribution on aneurysm geometries, including and excluding contiguous vasculature.	52
Figure 30: Histogram showing distribution of stresses calculated using finite element analysis and using curvature calculations.	53
Figure 31: Diameter measurements on an ACA at diastolic (a) and systolic (b) states using ImageJ	58
Figure 32: Basilar aneurysm located in the volumetric CTA scan.	64
Figure 33: VOI of the aneurysm and its contiguous vasculature chosen.....	65
Figure 34: Segmentation stages of Basilar Artery (left to right, top to bottom).....	67
Figure 35: Segmentation of aneurysm (left). Segmented model of aneurysm merged with the contiguous vasculature.....	68
Figure 36: Aneurysm Isolation. a) Isolated aneurysm dome and its contiguous vasculature, b) Mesh quality of isolated aneurysm dome.....	69

Figure 37: 3D segmentation of aneurysm (highlighted in color) and its contiguous vasculature. Segmentation by user 1 shown in red and by user 2 shown in blue.....	70
Figure 38: Three cross sections of all 10 aneurysm models. Highlighted in Red Models by User 1, in blue – Models by User 2	71
Figure 39: Bland- Altman plots for size indices calculated for each aneurysm model, isolated using different and same cutting planes.	74
Figure 40: Bland- Altman plots for shape indices calculated for each aneurysm model, isolated using different and same cutting planes.	75
Figure 41: Bar chart showing number of patient scans in each of the three imaging modalities.....	78
Figure 42: Bar chart showing the number of aneurysms at each location.	80
Figure 43:3D models of isolated ICA aneurysms.....	81
Figure 44:3D models of isolated MCA aneurysms.....	82
Figure 45:3D models of isolated Ophthalmic aneurysms.....	83
Figure 46:3D models of isolated ACA aneurysms.	84
Figure 47:3D models of isolated AComm aneurysms.....	84
Figure 48:3D models of isolated Bslar aneurysms.	85
Figure 49:3D models of isolated PComm aneurysms.....	85
Figure 50:3D models of isolated aneurysms located at PCA, PICA, SCA and Vertebral arteries.....	85
Figure 51: Histogram showing distribution of Dmax ranging from 1.4 to 16.4 mm.....	88
Figure 52: Histogram showing distribution of NSI ranging from 0.27 – 4.94.	88
Figure 53: Histogram showing distribution of PWS ranging from 0.073 – 1.012 MPa.....	89
Figure 54: Receiver Operating Characteristics (ROC) curves for each index. “Null” represents zero predictive capability. Most indices are close to “Null” indicating the absence of their predictive capability.....	90
Figure 55: Comparison between maximum diameter measurements provided by clinics and maximum diameter data measured on isolated aneurysm models obtained after segmentation.	92
Figure 56: ACA aneurysms – initial (blue) and follow-up (red) segmentation. Follow-up segmentations show increase in aneurysms size.....	93

Figure 57: AComm aneurysms – initial (blue) and follow-up (red) segmentations. Follow-up segmentations show increased in aneurysm size.....	94
Figure 58: ICA aneurysms – initial (blue) and follow-up (red) segmentation. Follow-up segmentations show increase in aneurysms size.....	95
Figure 59: Basilar and SCA aneurysms – initial (blue) and follow-up (red) segmentation. Follow-up segmentations show increase in aneurysms size.....	96
Figure 60: PComm and MCA aneurysms – initial (blue) and follow-up (red) segmentation. Follow-up segmentations show increase in aneurysms size.....	97

CHAPTER 1

BACKGROUND AND SIGNIFICANCE

1.1 Intracranial Aneurysms and its Prevalence

Intracranial aneurysms (IA) are local dilations that occur in cerebral vasculature. While some of these aneurysms grow and rupture causing subarachnoid hemorrhage, resulting in morbidity and mortality, most IAs remain stable causing no harm. Since unruptured cerebral aneurysms rarely present symptoms, they are usually discovered either after hemorrhage or by serendipity [1]. Due to its asymptomatic nature, the measurement of prevalence and incidence of the disease vary considerably [2]. Reported prevalence of IAs vary from 0.4 to 6% of the population depending upon the nature of study: prospective or retrospective, angiographic or autopsy based, study population and aneurysm characteristics [2]. Average prevalence in adults with no specific risk factors was 2.3% and it was found to increase with autosomal dominant polycystic kidney disease (ADPKD), familial disposition, age, smoking, hypertension and atherosclerosis [2]. Most commonly, IAs occur at the circle of Willis which is a unique vascular region because several arteries join together to form a circle. This circular formation of vessels ensures that if some of these arteries are blocked, the other arteries belonging to the circle ensures blood circulation to the brain. Middle cerebral artery (MCA), Anterior Communicating Artery (ACOM), Anterior Cerebral Artery (ACA) and Internal Carotid Artery (ICA) shown in Figure 1 are some of the arteries in the circle of Willis and are also common arteries where aneurysms occur [1, 3].

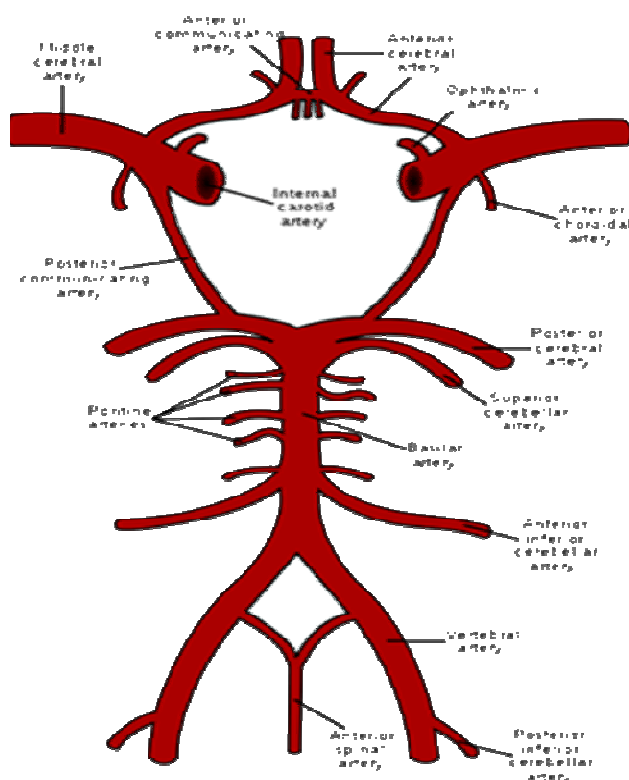


Figure 1: Circle of Willis

1.2 Disease Consequence and Management

Reported IA rupture rates vary from 0.1% to 5% [1, 4] and 10 to 20% of patients with a ruptured aneurysm die immediately [1]. Risk of rupture was found to be higher in women, for symptomatic aneurysms and in the posterior circulation of the cerebral circulation[2]. Management of these lesions remains largely controversial [3].

Management decisions include whether or not to treat them and which one of two methods of treatment to employ. The two methods of treatments used are 1. Surgical clipping 2. Endovascular coiling – the former being more invasive than the latter. The International Subarachnoid Aneurysm Trial (ISAT) compared the safety and effectiveness of endovascular coiling to surgical clipping by enrolling 2143 patients with

ruptured IAs and assigning them randomly to surgical clipping (n = 1070) or endovascular coiling (n = 1073) [5-6]. They found that endovascular coiling reduced the absolute risk of patient dependency or death by 7.4% at a 1-year follow-up. However, late re-bleeding of treated IAs was found to be more common after endovascular coiling than after surgical clipping [5]. Both treatment methods present a set of serious complications and the overall mortality caused by IAs, combining both treated and untreated lesions, adds up to 40 to 50% [4]. The risk of aneurysm treatment is found to be equal to or sometimes, exceeding risk of rupture [3, 7]. Hence, the decision whether to treat an IA rather than to leave it alone is crucial to the management of this disease. Today, treatment criteria for cerebral aneurysms is influenced by several clinical factors such as patient's age, family history, location of the lesion, being symptomatic and presence of thrombus [1, 3]. Size of the aneurysm plays a huge part in this treatment decision [1, 3, 7] and therefore has been studied widely.

1.3 Current Knowledge on Intracranial Aneurysm

Morphology

Intracranial aneurysm range in size from as small as 1.5 mm to 26 mm or more [1] and studies suggest that aneurysm size correlates with rupture and in turn, with subarachnoid hemorrhage. However, many cases of subarachnoid hemorrhage have been reportedly due to the rupture of small aneurysms [8] i.e. of aneurysms less than 7 mm in size. In order to prevent rupture, unruptured IAs, as small as, 4mm are chosen for treatment [9-12]. It has been recognized that size alone is not a reliable indicator of rupture [1, 3] and other aspects of aneurysm morphology such as shape, perhaps, play a role.

90% of cerebral aneurysms are saccular in shape [1]. Saccular aneurysms present themselves as an outpouching of the parent vessel with a visible neck and a sac region. An example of a saccular aneurysm geometry is shown here in Figure 2.

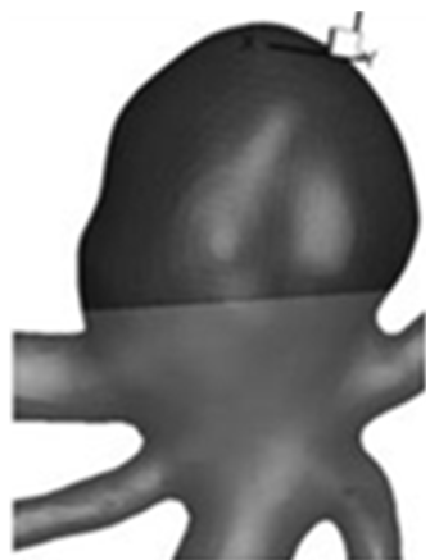


Figure 2: Example of a saccular aneurysm occurring at the Basilar Artery.

Advanced imaging and image processing techniques provide the capability to thoroughly characterize these aneurysms. So, three dimensional (3D) cerebral aneurysm geometries can be reliably quantified in terms of both size and shape. However, as opposed to size, it is difficult to quantify shape due to its subjective nature. Shape features in aneurysms are often discussed in subjective terms such as daughter sacs , multiple lobes [13-15] and surface irregularities [16]- perceptions of which could vary between users. In order to eliminate the subjectivity involved in aneurysm shape, it is necessary to quantify these shape features using objective, continuous indices.

Research groups, so far, have focused mainly on two dimensional (2D) shape features of these saccular aneurysms. Aspect ratio is one such index that has often been used to quantify aneurysm morphology [17-18] using 2D angiograms. Aspect ratio - the ratio of height to neck width, was suggested by Ujiie et al. [17-18] to be indicative of rupture. However, other research groups found that rupture correlation with aspect ratio did not reach statistical significance [19-20]. Another such 2D shape index – size ratio

was defined as the maximum stretch of the aneurysm dome from the neck center divided by the parent vessel diameter [19, 21]. Size ratio correlated with aneurysm rupture both in retrospective [19, 22] and prospective assessments [23] of rupture risk . Although size ratio takes into account the aneurysm location by incorporating vessel size, it does not account for the asymmetrical, three dimensional nature of aneurysm geometries.

Our research group, for the first time, developed three dimensional indices using computational and differential geometry techniques to quantify aneurysm shape [24]. These indices are calculated on segmented 3D models of IAs where each index accounts for one or more shape features. Several of these shape indices correlated to rupture status when they were tested on a retrospective population of 27 aneurysms [24]. These 3D shape indices shown in Figure 3 along with size indices such as maximum diameter, height, volume, surface area and neck diameter quantifies aneurysm geometries with considerable rigor. In the current study, these indices are tested using a prospective analysis on a large cohort of patients.








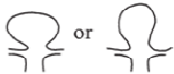
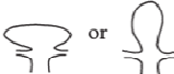

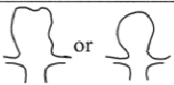
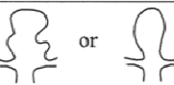






Shape Index	Low	Medium	High
Undulation index (UI)			
Aspect ratio (AR)			
Ellipticity index (EI)			
Non-sphericity index (NSI)			
Conicity parameter (CP)			
Bottleneck factor (BF)			

Figure 3: Definitions of shape indices used by Raghavan et al (45).

1.4 Current Knowledge of Pressure-Induced Wall Tension in Intracranial Aneurysms

Estimations of pressure-induced tension in the cerebral aneurysm sac wall may serve as metrics that help stratify patients according to rupture risk. Wall tension on patient –specific cerebral aneurysm geometries can be estimated at varying levels of computational sophistication – 1) By performing numerical simulations such as Finite element analysis (FEA) 2) Using geometrical information like curvature distributions 3) Using clinical measurements such as height (H) and maximum diameter (Dmax). The challenge is to pick one or more wall tension indices based on its predictive value while keeping computational methods as simple as possible, thus saving computational time and cost.

Research groups have performed Finite Element Analysis (FEA) defining aneurysm wall properties with simple material models such as linear elastic models [25-26] or more sophisticated models like hyperelastic Fung-type model [27-28]. As of now, anisotropic, hyperelastic Fung-type model is considered to be the gold standard in modeling IAs and therefore its material parameters have been defined and used in previous studies of cerebral aneurysm wall tension [29-30]. More recently, Isaken et al performed fluid-structure analysis to calculate wall tension distribution on one patient-specific aneurysm, modeling a flexible aneurysm wall and suggested that such a simulation could be used for rupture prediction [31]. In addition to wall tension studied in cerebral aneurysms, wall tension estimation methods are widely discussed in abdominal aortic aneurysms (AAA) as well. For instance, Reeps et al performed a comparative study of different modeling choices made in numerical simulations performed on four patient-specific AAAs and concluded that sophistications in modeling choices influence quantitative results [32].

Apart from numerical simulations, wall tension estimation can be simplified to using only the available geometrical information. If the segmented patient-specific

geometry is assumed to be the deformed configuration and its wall is considered to be membrane, wall tension distribution can be estimated using geometrical information only. The Laplace equation which is $\kappa_1 T_1 + \kappa_2 T_2 = P$ where κ_1 and κ_2 are the two principal curvatures and T_1 and T_2 are the principal stress resultants [33] allows us to estimate aneurysm wall tension from curvature information.

As the third and final step of simplification, aneurysm wall tension can be estimated using clinically measured values – height and maximum diameter. Aneurysm geometries can be assumed as spherical or ellipsoidal and the Laplace equation to calculate wall tension can be simplified [33]. Research groups have used the Laplace equation derived for a sphere – Wall Tension = (pressure x radius)/2 to calculate wall tension in saccular cerebral aneurysms [26, 34-36].

Often, the focus is on what the best of these methods for wall tension estimation are. Ideal method would be to perform FEA with appropriate modeling choices - anisotropic finite elastic model [30, 37], shell-like behavior [38], a large enough vasculature in the analysis domain to minimize edge-effects at the aneurysm sac, and an inverse solution scheme [38] to address the pre-deformed nature of the sac under in vivo imaging. In the current study, whether (and to what extent) these rigorous modeling choices affect the predictive value of aneurysm wall tension in stratifying patients based on rupture risk is assessed.

1.5 Current Knowledge of Hemodynamics Within Cerebral Aneurysms

With respect to rupture prediction in cerebral aneurysms, estimations of wall tension and IA morphology have been discussed above. Apart from these, hemodynamics within the cerebral aneurysm sac and its surrounding vasculature is often studied for IA rupture prediction. It is believed that hemodynamics plays a strong role in IA rupture and in its pathogenesis [39-41]. Research groups have often analyzed complex flow patterns,

multiple vortices, impingement regions and particle residence time both in experimental [42-44] and computational studies[39-40, 45]. In computational studies, different hemodynamic environments were simulated in 2D and 3D models in order to generate hemodynamic indices. Some of these hemodynamic indices are: wall shear stress (WSS), wall shear stress area (WSSA), wall shear stress gradient (WSSG), oscillatory shear index (OSI), number of vortices (NV), size of inflow jet, area of impingement and relative residence time (RRT) [39-40, 45]. These are important indices and some of them have been shown to significantly distinguish ruptured from unruptured aneurysms. Hemodynamics of IAs is an independent study in itself and is beyond the scope of this thesis project. However, it is worth emphasizing that the role of hemodynamics played in the pathogenesis and rupture risk of IAs is an important piece of the puzzle.

1.6 Dissertation Overview

The hypothesis of this project is that IA morphology, quantified as size, shape and wall tension can be used as a prognostic indicator of rupture. This hypothesis will be assessed using a longitudinal cohort study of 200 patients who present initially with unruptured IAs and followed over a period of 1-4 years.

As a first step, methods to segment the aneurysm and its contiguous vasculature as well as methods to isolate the aneurysm dome from its contiguous vasculature were established. In order to perform such a longitudinal cohort study assessing IA morphology, it is necessary to ascertain that combining source data from multiple modalities and multiple users performing segmentations does not introduce variability in results or in findings. Therefore, two independent studies - to assess the sensitivity of quantified intracranial aneurysm geometry to imaging modality and user variability- were performed. In order to assess sensitivity to imaging modality, two independent approaches to assess sensitivity to scan modality were used: 1) using a flow phantom of the cerebral vasculature with an ACOM aneurysm that is scanned by all three modalities;

and 2) patients who have all been scanned by one common modality and at least one another modality. 3D segmentation was performed on all datasets and their morphometric indices were compared to assess sensitivity to image modality. In order to assess sensitivity to user variability, segmentations were performed by two users on 10 selected patient IAs and their indices were calculated. Both quantitative assessments (comparison of indices) and qualitative assessments (comparison of 3D surface models) were performed on all of the segmented models.

Also, appropriate modeling choices should be made for the calculation of wall tension distribution when a large population of patient-specific geometries are being analyzed, keeping in mind the computational cost and time as well as physiologic accuracy. Hence a comparative study of wall tension estimation methods of varying levels of sophistication was performed. The objective of this study is to test the importance of: 1) Numerical simulations - modeling choices and interpretation choices, 2) Tension indices based on curvature calculations and 3) Tension indices based on clinical measurements– in stratifying aneurysms based on wall tension in a study population.

Results from both these preliminary studies were incorporated in the longitudinal study of about 200 aneurysms. These patient-specific IAs were quantified, in a blinded prospective study, by calculating size, shape and wall-tension indices. After IA quantification on initial scans was completed, clinical rupture and growth status were collected at the end of the follow-up period. The clinical status was correlated with measured indices to identify correlations, if any.

CHAPTER 2

3D SEGMENTATION AND ITS CHALLENGES

2.1 Basic Methods

Three dimensional models were created from the source data using levelset segmentation techniques [46] implemented in the Vascular Modeling ToolKit (VMTK). VMTK comprises of algorithms implemented as C++ libraries in Visualization ToolKit (VTK) and Image Processing ToolKit (ITK). It combines these C++ classes using Python scripts enabling 3D segmentation, mesh generation and other image processing functions of vascular structures from medical images. The levelset initialization methods, referred to as colliding fronts and fast marching [47] were used to reconstruct the parent vasculature and the aneurysm respectively. Colliding fronts method involves selecting two seed points at either ends of a vascular segment. A 3D surface is generated between these points, based on intensity gradients, automatically ignoring side branches. This procedure is repeated for every segment of the required vasculature and they are merged together as one single model. The fast marching method used to reconstruct aneurysms involves selecting one seed point at the center of the aneurysm with target points selected randomly along its outer boundary. A 3D aneurysm surface is generated and this surface is then merged with the rest of the segmented vasculature. The deformable models were evolved by applying evolution parameters within a set range – number of iterations (200-300), propagation scaling (0-1), curvature scaling (0-1) and advection scaling (0-1). Detailed reviews of these methods have been published by its authors earlier [46-48]. Segmentation of vascular structures was performed on control geometries to ensure that 3D segmentations were as accurate as their source images. One such segmentation of control geometry is shown in Figure 5.

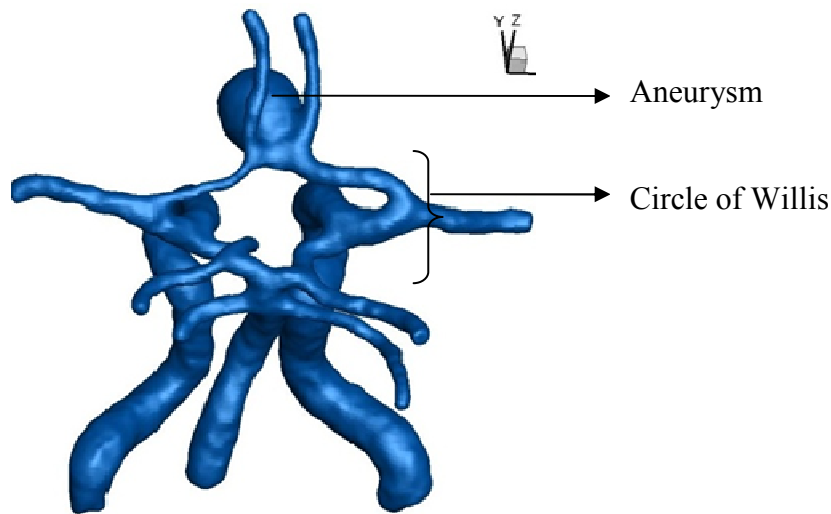


Figure 4: 3D segmentation of CTA images of flow phantom.

Segmentation of patient specific geometries presented certain challenges, which were not faced while segmenting the above flow phantom vasculature. Some of those challenges and special cases are discussed below:

2.2 Presence of Skull in CTA – ICA Aneurysms

Segments of Internal Carotid Arteries (ICA) and Ophthalmic Arteries exist in close proximity to the skull. Sometimes, when these arteries are required to be segmented and the scanning modality is CTA, the presence of the skull interferes with the geometric reconstruction of the aneurysm.

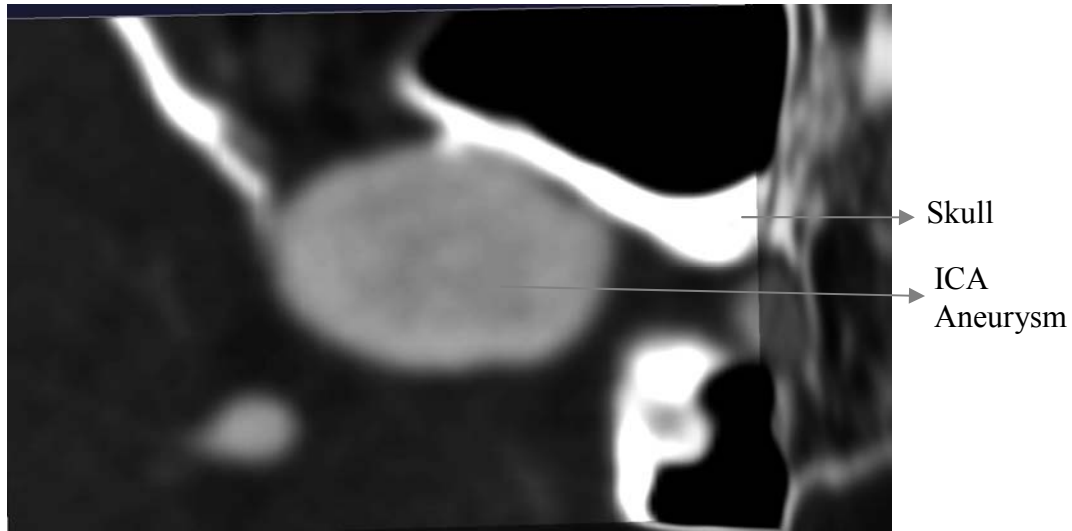


Figure 5: Sample slice of CTA showing ICA aneurysm with skull impinging on it.

In order to obtain accurate segmentations of ICA and Ophthalmic aneurysms, the skull was subtracted out from the image before vascular structures were segmented. The skull was defined as an isosurface using its threshold value in the levelset segmentation algorithm. It was then excluded from the vascular segmentation using the feature correction and image composing algorithms in VMTK. For detailed explanations of these methods, please refer to tutorials in vmtk.org and the PhD thesis of Luca Antiga [49]. Using these algorithms, the 3D segmentation of ICA aneurysms can be obtained without the interference of nearby skull as shown in Figure 7.

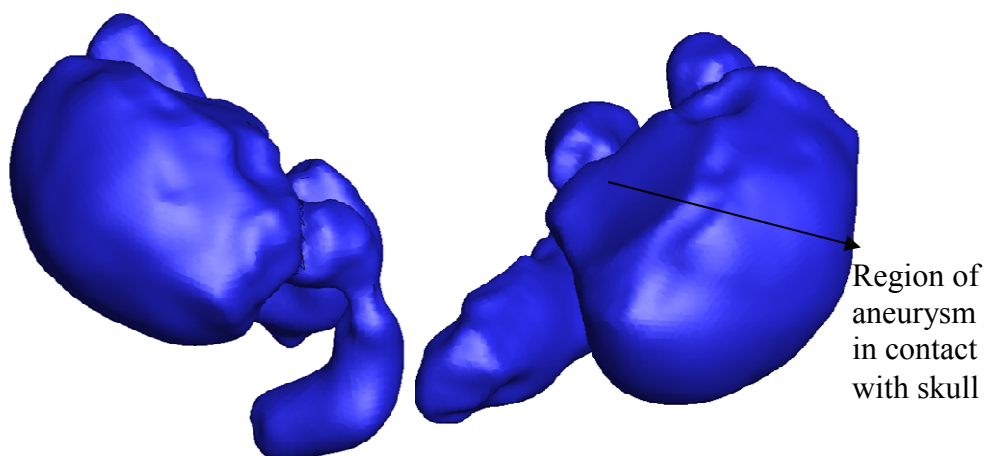


Figure 6:3D segmentation of sample ICA aneurysm after the removal of skull.

2.3 Merging of Vascular Structures - ACOM and

Pericallosal Aneurysms

Pericallosal arteries, also known as, the distal anterior cerebral arteries are small arteries of 1.6 mm diameter. They present themselves in angiographic studies 50-67% of the time [50-51]. The left and right Pericallosal arteries run parallel to each other and often overlap. Pericallosal arteries bear about 5% of saccular aneurysms, most of which are small aneurysms [52]. Usually, the presentation of these structures in the angiographic source images is of poor intensity gradients and this makes it difficult to capture their 3D geometry using the VMTK segmentation algorithms. In most cases, successful segmentation is possible by defining stringent upper and lower intensity values and choosing appropriate seed points to define small vascular segments at each time. In addition to this, surface shrinking algorithms implemented in VMTK can be used to ensure that any two vascular structures do not unrealistically merge due to their geographical proximity.

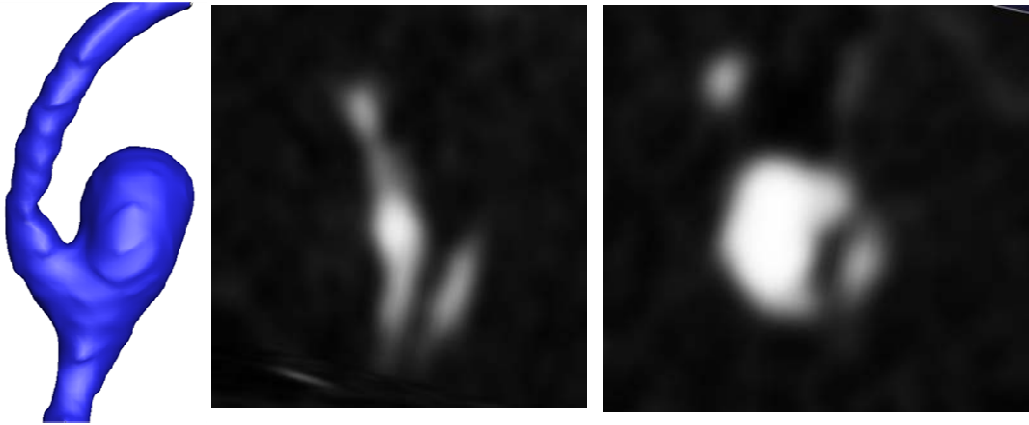


Figure 7: Segmentation of Left Pericallosal Aneurysm a) 3D model. b) CTA slice showing showing proximity of left and right Pericallosal arteries c) CTA slice showing aneurysm and artery presenting poor intensity gradients.

A left Pericallosal aneurysm of height 4.5 mm and max.diameter 4.2 mm is shown in Figure 8a. Although both the right and the left Pericallosal arteries lie close to the aneurysm and to each other, this 3D segmentation of the aneurysm geometry is not perturbed by their proximity. However, in certain cases where two structures whose separation cannot be discerned in their source images, their 3D segmentation merge them together as shown in Figure 9. So far, merging of vascular structures as in Figure 9 has not occurred at the aneurysm sac itself. However, if it does, so as to completely perturb the geometry of the aneurysm under study, those aneurysms will be left out from the morphometric analysis.

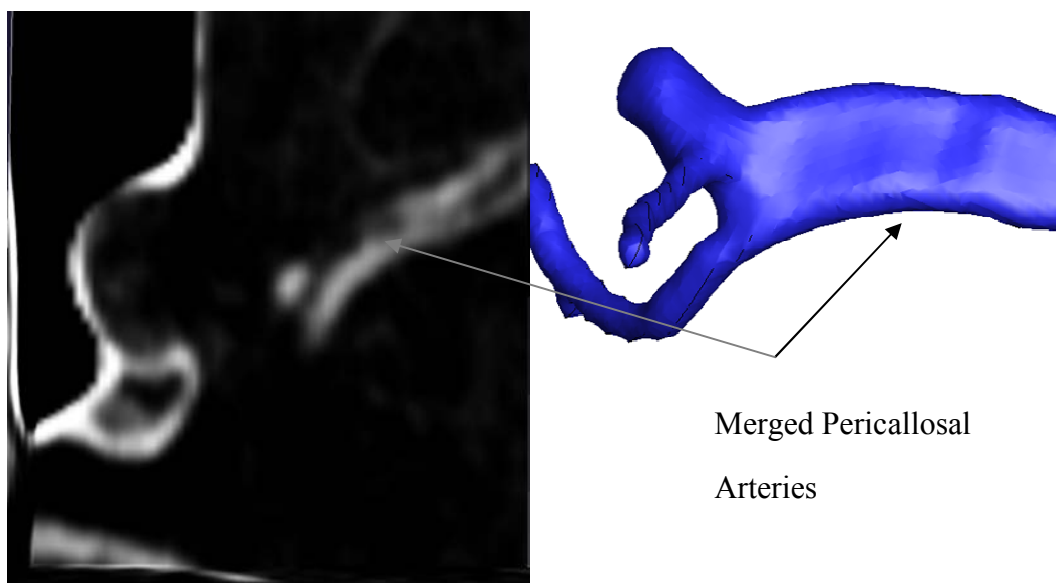


Figure 8:3D segmentation of Pericallosal arteries merged due to lack of discernable intensity gradients

2.4 Presence of Thrombus

Presence of thrombus in aneurysms obstructs the 3D reconstruction process because the Hounsfield unit of thrombus in an angiographic image is similar to air. This leads to the 3D model appearing incomplete with the presence a “hole” in the geometry. Please refer to Figure 10 below. These aneurysms were excluded from the morphometric analysis of this project. However, occurrence of thrombus in our study was quite rare. In our experience of segmenting around eighty aneurysms, we have found three aneurysms that contained thrombus in them.

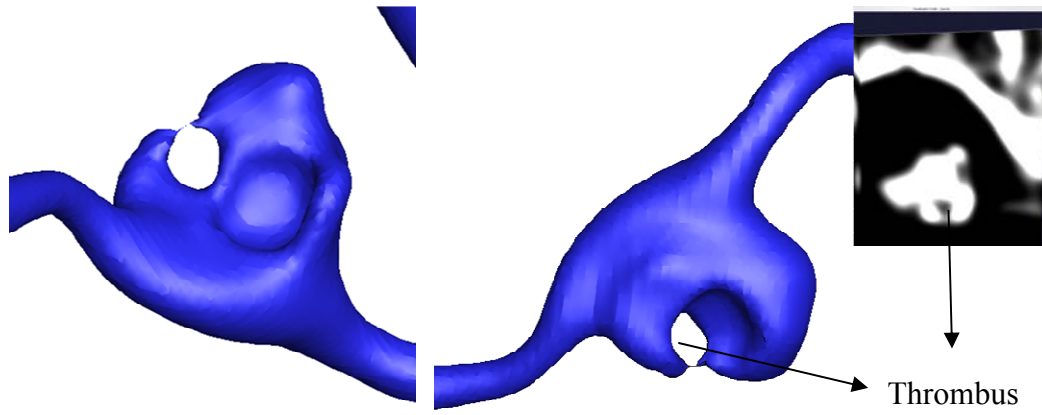


Figure 9: (left to right) Front and back view of 3D aneurysm model, CTA image slice demonstrating thrombus in aneurysm.

CHAPTER 3

ANEURYSM ISOLATION

In order to quantify the aneurysm morphology, aneurysms needed to be isolated from their contiguous vasculature. One way to isolate aneurysms would be to define a single plane in 3D space that would separate the aneurysm from its parent vessels. This method of isolating aneurysms from their parent vasculature was previously reported by Ma et al [53]. In this process, a plane is chosen with manual discretion using the 3D visualization software called TECPLOT 360 (2009 Release, Tecplot Inc., Bellevue, WA). The aneurysm is isolated at this plane using the isolation algorithm implemented in computing software program MATLAB (version 7.8, The Mathworks Inc., Natick, MA). For further details regarding the implementation of this method, please refer [54]. Size and shape indices are calculated for these isolated aneurysm geometries. This isolation method makes the quantification of aneurysm geometry simpler by providing an unambiguous neck plane, height, etc.

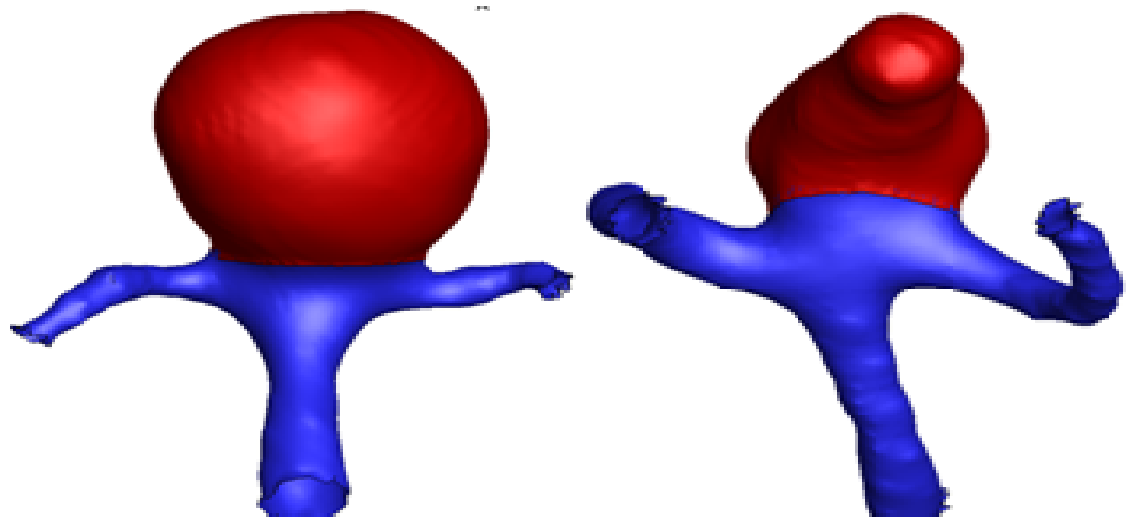


Figure 10: Examples of aneurysms isolated (shown in red) from their parent vasculature.

Inter-user and intra-user consistency in choosing a plane for isolating the aneurysm was to be ensured so that this task was fairly repeatable. The cutting plane is chosen in such a manner that it would reflect the plane where a surgeon would perhaps place a surgical clip while treating the aneurysm during a craniotomy procedure. Despite thus codifying this process, the cutting plane remains dependent upon the user's discretion to some extent. Due to the choice of the cutting plane, residues of aneurysm geometries are sometimes left behind without the entire aneurysm being included in the morphometric analysis.

Such special cases were discussed with clinical collaborators to ensure that consistent cutting plane decisions were made for all aneurysms that posed any ambiguity in being isolated. A clear criterion for aneurysm isolation is jeopardized when a small artery arises from the aneurysm dome. Examples of such a scenario is when a Superior Cerebellar Artery (SCA) shoots off from a basilar aneurysm and when an ophthalmic artery arises from an ICA aneurysm. In those cases, a considerable part of the aneurysm sac geometry would be left behind from the analysis as shown in Figure 12.

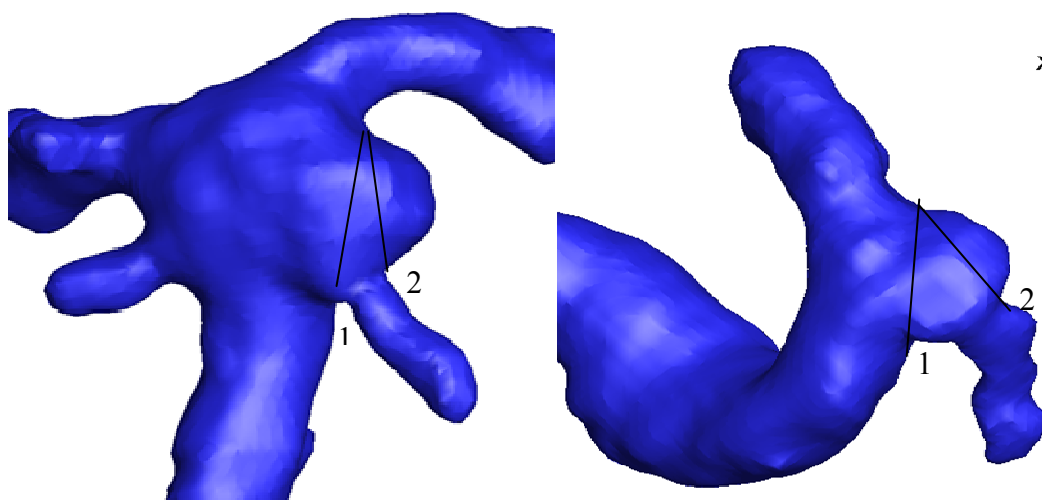


Figure 11: SCA branching off Basilar aneurysm, 10b: Ophthalmic branching off ICA aneurysm.

Figure 12 shows two cutting planes labeled “1” and “2” for each aneurysm. Clinical measurements of size such as maximum diameter and height of the aneurysm would be made using plane “1”. However, if aneurysm isolation is performed based on the general criteria, they would be cut using plane “2”. All the morphometric indices calculated henceforth would be a misrepresentation for these aneurysms. Therefore, in order to maintain consistency with clinical measurements and to eliminate ambiguity in aneurysm isolation another criterion was defined for these special cases. Branches such as SCA (off Basilar) and ophthalmic artery (off ICA) are small branches arising from fairly large vessels. In the angiographic source images, these branches are of much less intensity compared to the parent vessel and sometimes do not present themselves due to low flow in them. After discussing these cases, it was decided that, these branches would be left out from the segmentation process, in order keep cutting planes consistent. Segmentation of aneurysms shown in Figure 12 was repeated and the side branches arising from these aneurysms were left out (Figure 13).

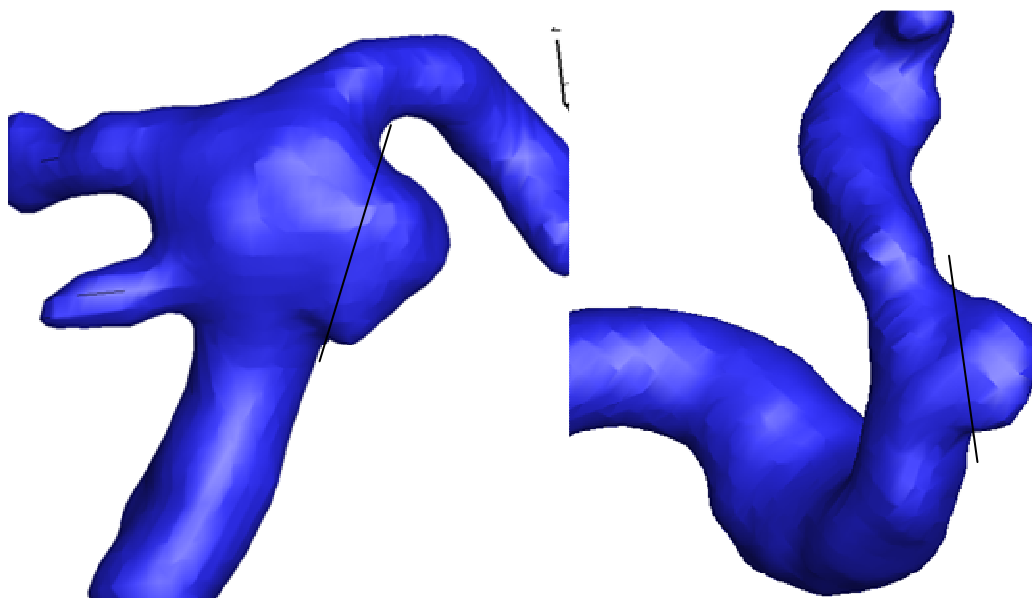


Figure 12: Segmentation repeated for aneurysms in Figure 12 to remove small branch arising from aneurysms.

For those cases where the side branches arising from aneurysms were as large as or larger than the parent vessel, they were left intact and the default cutting plane criterion was employed. Figure 14 shows an example for the second case where Posterior Cerebral Artery (PCA) branches off from Basilar aneurysm. For this aneurysm, PCA was kept intact and cutting plane “2” was chosen for isolating the aneurysm.

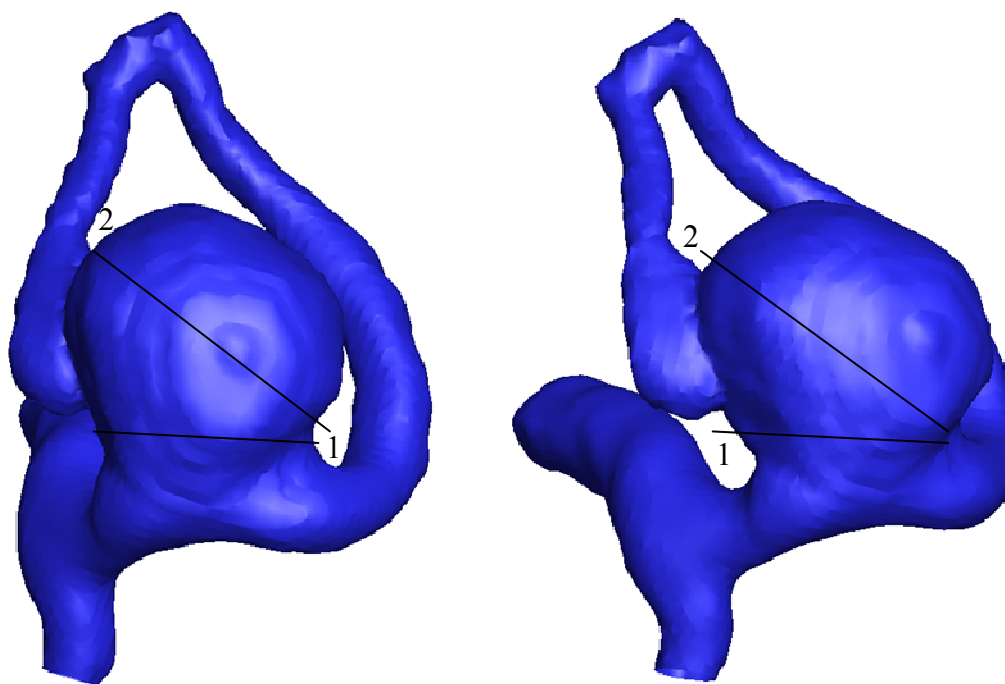


Figure 13: Example of PCA branching off from Basilar aneurysm.

CHAPTER 4

SENSITIVITY OF QUANTIFIED INTRACRANIAL ANEURYSM GEOMETRY TO IMAGING MODALITY

4.1 Introduction

In the diagnosis and clinical management of cerebral aneurysms, patients are routinely subjected to volumetric scans, but these can be one of four three-dimensional (3D) modalities – 3D Rotational Angiography (3DRA), Computed Tomography Angiography (CTA), Contrast Enhanced Magnetic Resonance Angiography (CE-MRA) and Time-Of-Flight MRA (TOF-MRA). The choice of the imaging modality for a particular situation is dictated by various considerations such as invasiveness, spatial and temporal resolution, radiation exposure, contrast medium, need for depicting surrounding tissue or blood flow, and capability for retrospective manipulation [55]. These differing merits and demerits of modalities are often leveraged for a given clinical case. However, it is worthwhile to wonder if the morphology of the aneurysm – its size and shape – is specifically sensitive to the modality. Addressing this issue can have important implications at the clinic and in the research lab. It is not uncommon for patients who are followed with unruptured intracranial aneurysms to be imaged by one modality in one year and a different modality in a subsequent year. If changes are noted in aneurysm morphology (say, a new lobulation), can image modality be confidently eliminated as a factor? Sensitivity to modality may also have important implications for many ongoing longitudinal research studies on whether computational modeling may be effective in predicting rupture or growth risk. For these studies to have a large enough patient population, data from multiple modalities may need to be lumped together. Here too, the issue of whether aneurysm morphology measurements are sensitive to imaging modality becomes critical.

Rigorous studies on whether or to what extent the aneurysm's shape and size will be different between the four imaging modalities is lacking in the literature. To our knowledge, there is no study, in existing literature that compares even aneurysm size in human subjects scanned using all the four imaging modalities. The studies that do exist on this topic are confined to the sensitivity of basic manual measurements of aneurysm sizes – often in comparison to 2D- DSA (Digital subtraction angiography)[55-64]. In a study of elastase-induced aneurysm models in rabbits, Doerfler et al. [59] reported that CTA, TOF-MRA and CE-MRA were well correlated with DSA for measuring aneurysm size- height, width and neck. Fahrig et al.[65] constructed rigid-walled phantom models of the circle of Willis with a spherical basilar aneurysm in a simulated flow loop and imaged the phantom using TOF-MRA, DSA and CTA . They measured vessel diameter on CTA and TOF-MRA images and found that the measurements were within 4% error compared to prescribed vessel diameters. They did not report measurements on the aneurysm. Pötter et al.[66], compared volume measurements of a rigid-walled phantom of an anterior communicating (ACOM) artery aneurysm in a pulsatile flow loop, imaged using CTA, TOF- MRA and 3DRA. They found that both CTA and 3DRA were more accurate than TOF-MRA (with statistical significance) and 3DRA was more accurate than CTA (without statistical significance). Data from human subjects were however not assessed. Kouskouras et al. [61] compared aneurysm size (maximum diameter and neck diameter) measure from TOF-MRA, CTA and DSA to those measurements made surgically with the focus on evaluating CTA in the pre-surgical planning of cerebral aneurysm. They also noted shape characteristics (irregularities and lobulations) but these shape characteristics were not clearly defined in the study. In summary, these studies are confined to basic aneurysm size measurements made on a phantom [66] , an animal model [59] and only one study on human subjects [61]. Moreover, these studies do not address all the four imaging modalities. All of these three studies make measurements on planar slices rather than accommodating the three-dimensional nature of imaging.

With recent advances in the use of computational tools for assessing three-dimensional aneurysm size and shape, it is imperative that the sensitivity of the three-dimensional morphology of the aneurysm to image modality be assessed with rigor. The objective of our study is to assess whether and by how much size and shape measurements of 3D models of intracranial aneurysms differ among image modalities. We use two independent approaches: 1) using a flow phantom of the cerebral vasculature with an ACOM aneurysm that is scanned by all three modalities; and 2) patients who have all been scanned by one common modality and at least one another as well. 3D segmentation was performed on all datasets and their morphometric indices were compared to assess sensitivity to image modality.

4.2 Methods

4.2.1 Imaging of aneurysm flow phantom using multiple scan modalities

A silicone flow phantom consisting of the complete circle of Willis with a saccular aneurysm at the ACOM was used (Shelley Medical Imaging Technologies, Canada). The model is anatomically realistic and was built by the lost wax technique, using cadaver molds (Figure 14). The phantom has four inlets- two common carotids and two vertebral arteries. The two common carotids then split into external and internal carotids. The six outlets of the phantom are two branches from the Middle Cerebral Arteries (MCAs), both on the left side and right side - M1, M2 and two Anterior Cerebral Arteries (ACAs). The phantom contains a saccular aneurysm at the anterior communicating artery with about 3.5 mm neck diameter and height of 13 mm (as specified by manufacturer). Dimensions for all other arteries are shown in Figure 15.

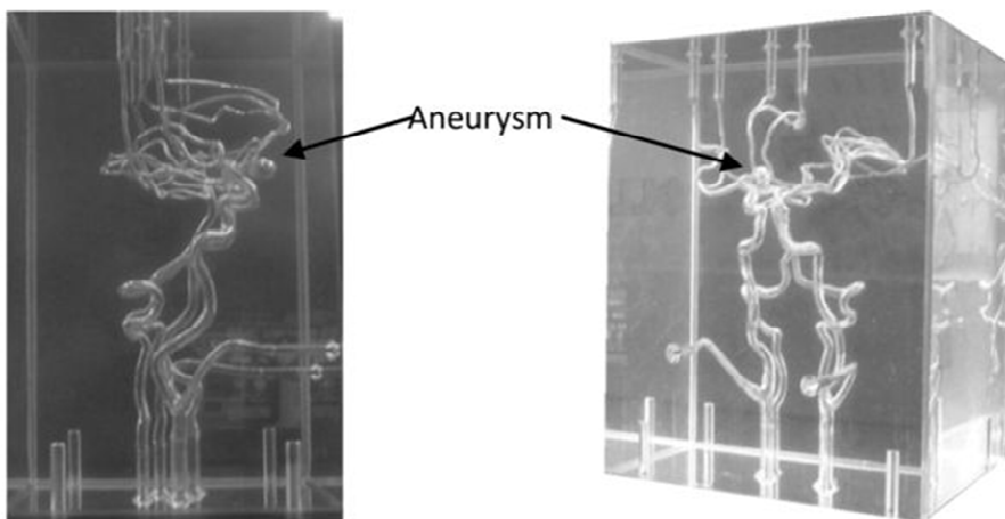


Figure 14: Phantom of circle of Willis with an ACOM aneurysm.

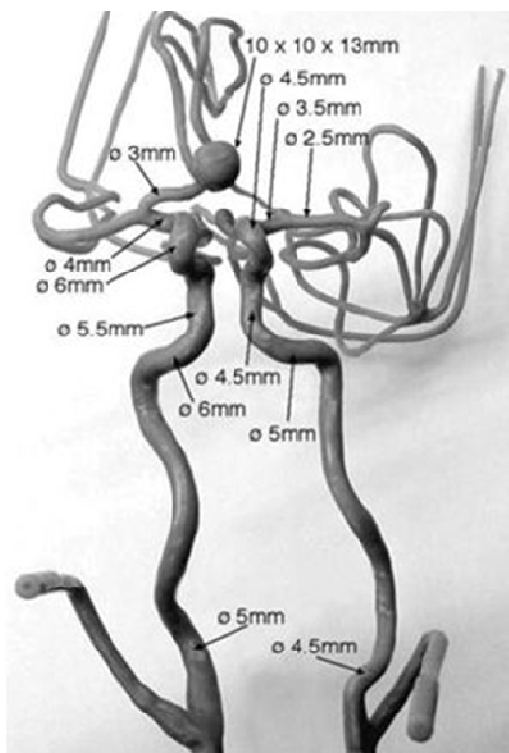


Figure 15: Frontal view of the mold used for making in-vitro phantom, along with dimensions of arteries and the aneurysm (provided by vendor).

In order to simulate blood flow through the phantom, a flow loop was set up (Figure 16). In the flow loop, the inlet/outlet tank was filled with 6 liters of 0.9% saline. Saline from the tank was passed through the pump to the four inlets of the phantom. In the flow loop, the external carotids were occluded to confine the flow domain to the relevant vessels and therefore the flow rate at the common carotid inlets was made equal to that of the internal carotids. A peristaltic pump maintained steady flow at the inlet of 800 cc/min. The flow rates at the inlets were controlled using pinch valve flow resistors to ensure that they are roughly physiological: 275 cc/min at the left and right ICAs, 100 and 80 cc/min at the left and right vertebral arteries.[65, 67]

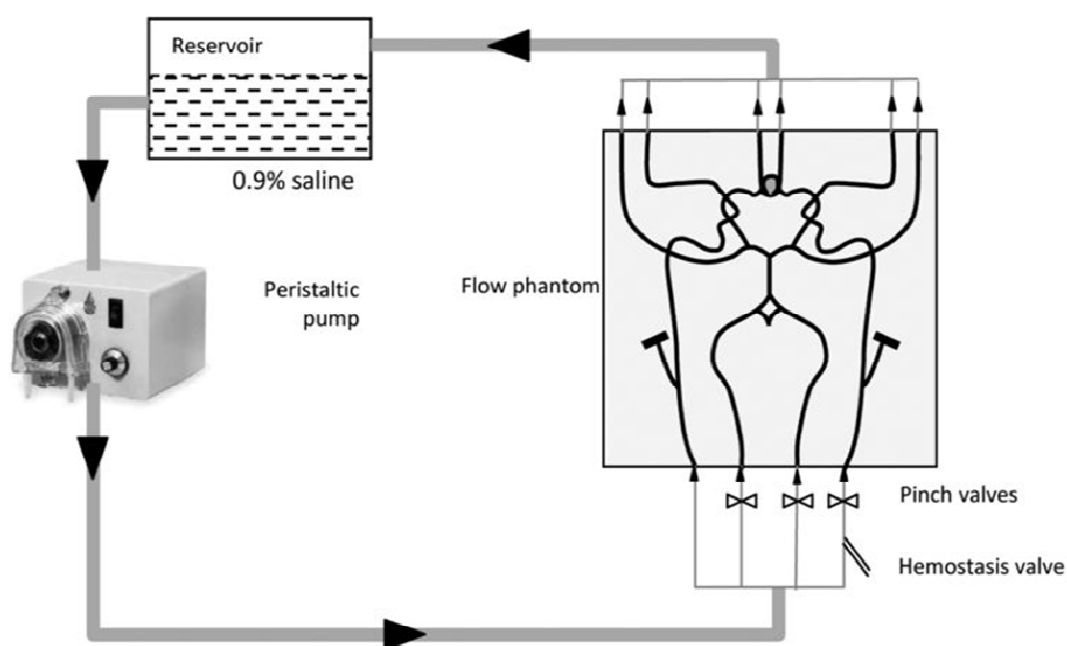


Figure 16: Schematic diagram of flow loop consisting of phantom, pump, Inlet/Outlet tank, valve.

Scans were performed on the phantom by four imaging modalities at the University of Iowa Hospital and Clinics following to the extent possible, scanning

protocols used for aneurysm patients. Time delays for scanning were based on the discretion of radiology personnel, as would be the case during patient scans. Table 1 shows the parameters used for the four modalities.

Modality	Scanner Type	Voxel Size	Contrast Medium Added to Inlet/Outlet Tank	Miscellaneous Parameters
CE-MRA	Siemens 1.5T Avanto MRI	0.625 x 0.625 x 1	20 ml Gadolinium	Repetition time 3.17 s, flip angle 30°, echo time 1.12s
TOF-MRA	Siemens 1.5T Avanto MRI	0.429 x 0.429 x 0.8	N/A	Repetition time 39 s, flip angle 25°, echo time 7.2s
CTA	Siemens Sensation 64	0.309 x 0.309 x 1	150 ml Iohexol	N/A
3DRA	Siemens Axiom Artis	0.468 x 0.468 x 0.499	34.5 ml Iopamidol	N/A

Table 1: Parameters for scanning flow phantom in four modalities.

4.2.2 Collection of multiple modality scans from aneurysm patients

Scans from three patients with aneurysms at the AComm, MCA and Basilar arteries at the University of Iowa Hospitals were retrieved. Institutional IRB approval was obtained for this study (IRB# 200912759). Each of these patients was scanned using 3DRA and one of the following modalities: CTA, CE-MRA and TOF-MRA. Therefore, 3DRA – the common modality among all three subjects – was compared to: CE-MRA in Patient1 (interval between scans: 1 day), TOF-MRA in Patient2 (0 days) and CTA in Patient3 (0 days). Specifications of the scans are listed in Table 2.

Modality	Voxel Size	Miscellaneous Parameters
CE-MRA	0.625 x 0.625 x 0.8	repetition time 3.17 s, flip angle 30°, echo time 1.12s
TOF-MRA	0.429 x 0.429 x 1	repetition time 39 s, flip angle 25°, echo time 7.2s
CTA	0.390 x 0.390 x 1	N/A
3DRA	0.218 x 0.218 x 0.218	N/A

Table 2: Parameters used for patient scans of four modalities.

4.2.3 3D Segmentation

Three dimensional models were created from the source data using levelset segmentation techniques as implemented in the Vascular Modeling ToolKit (VMTK) [46]. The levelset initialization methods, referred to as colliding fronts and fast marching

were used to segment the parent vasculature and the aneurysm respectively.[68] The deformable models were evolved by applying segmentation parameters within a set range – number of iterations (200-300), propagation scaling (0-1), curvature scaling (0-1) and advection scaling (1). Detailed reviews of these methods have been published by its authors earlier[46, 48, 68]. Considering the fact that the phantom-aneurysm was a relatively large (height of 13 mm) ACOM aneurysm, special attention needed to be paid to the segmentation of the Pericallosal arteries, since there was a tendency for the aneurysm to overlap with those arteries, due to geometric proximity.

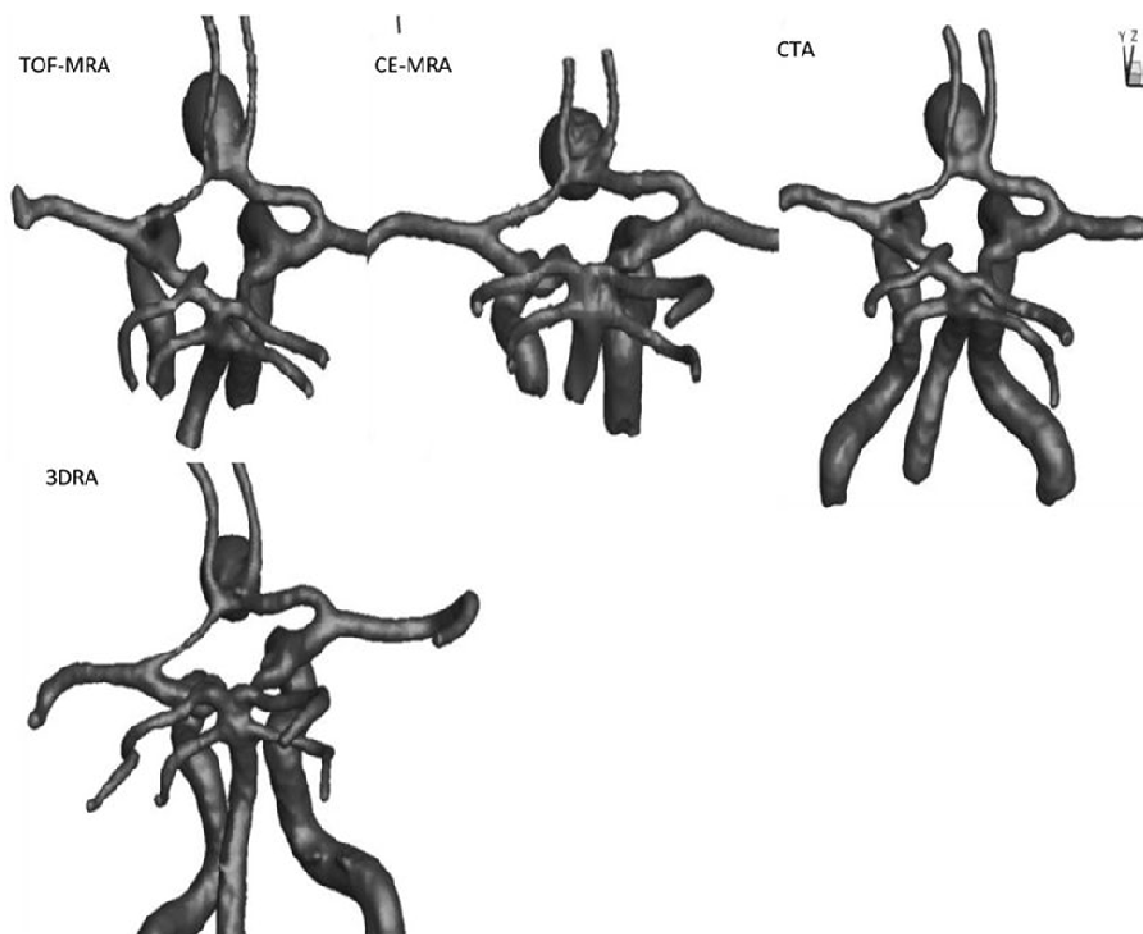


Figure 17: 3D segmentation of the vasculature from all four modalities. The views and scales are roughly similar between models shown.

The 3D segmentations of the phantom model obtained from each of the four scanning modalities are shown in Figure 17. The segmented images were then smoothed using Taubin's non shrinking algorithm implemented in VMTK [69]. In order to better document the sensitivity of the segmentation to the smoothing parameters, the two smoothing parameters - number of iterations and passband were perturbed with values of 40, 60, 80, 100 and 0.1, 0.01 respectively and resulting segmentations recorded for each smoothing parameter value [48]. Thus, for each modality, eight models with eight different iteration-passband combinations were created for each of five scans for a total of 40 segmentations of the phantom ACOM aneurysm model.

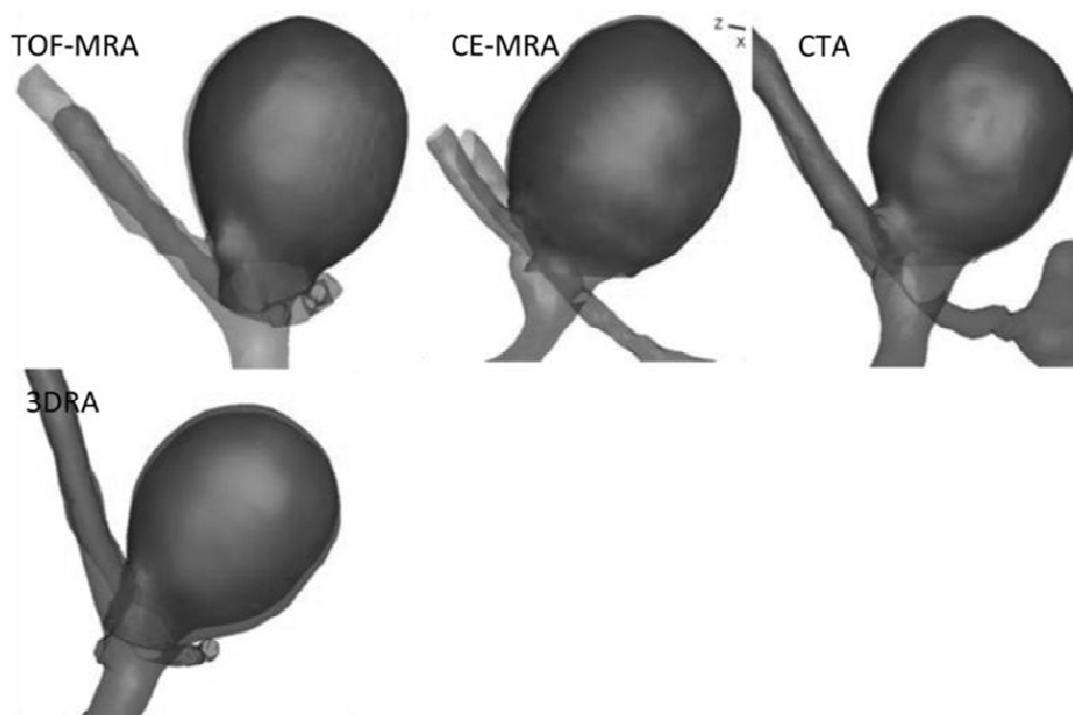


Figure 18: 3D segmentations of the aneurysm and parent vessel. Also shown is the aneurysm dome isolated from its parent vasculature (highlighted as a darker shade).

5.2.4 Morphometrics

The aneurysm sac was isolated from the contiguous vasculature using a visually determined cutting plane as previously reported.[59] The cutting plane was chosen, so that, it would reflect the plane where a surgeon would, perhaps, place a surgical clip while treating the aneurysm by a craniotomy procedure. In spite of the above criteria, the cutting plane remains dependent upon the user's discretion to some extent. Once the aneurysm dome was isolated from the parent vessels, five size and six shape indices were calculated for each 3D model using methods reported earlier [24, 59]:

1. Size indices: Height (H), maximum diameter (Dmax), neck diameter (Dn), volume (V), and surface area (SA).
2. Shape indices:
 - a. Aspect ratio (AR): ratio of neck diameter to height.
 - b. Bottleneck factor (BF): Ratio of neck diameter to max diameter.
 - c. Bulge location (BL): Distance from neck plane to largest cross-section as a fraction of total height.
 - d. Undulation index (UI): Measure of lobulations in the aneurysm surface.
 - e. Ellipticity index (EI): Measure of ellipticity of aneurysm.
 - f. Non-sphericity index (NSI): Aggregate measure of deviation from spherical shape due to ellipticity and undulation.

4.3 Results

Three-dimensional segmentations of aneurysms and their contiguous vasculature for the phantom-aneurysm are shown in Figure 18 and those for the patient-aneurysms are shown in Figure 19.

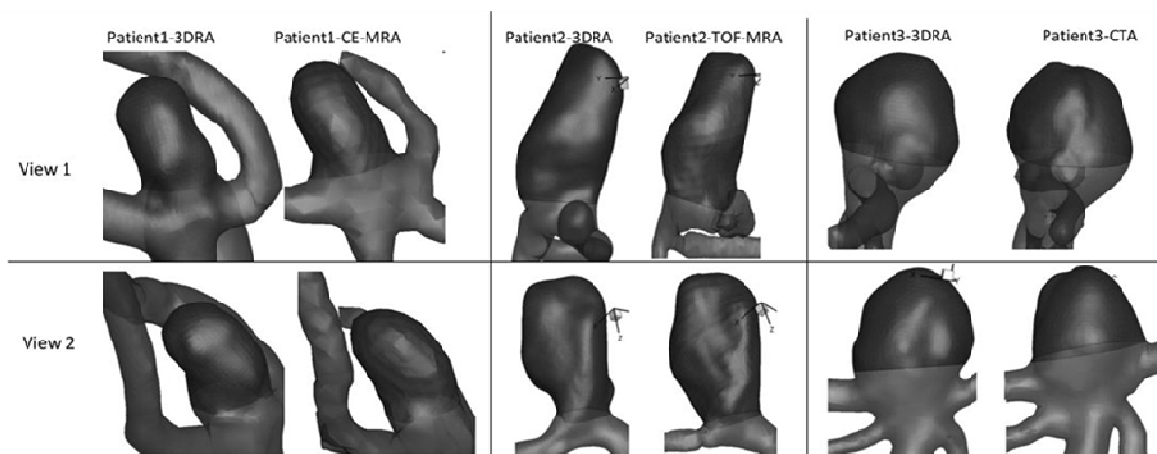


Figure 19: Two corresponding views of 3D models from Patient1, Patient2 and Patient3. Aneurysm sac is shown as a darker shade.

Upon performing geometric analysis, all indices were calculated and tabulated. Table 3 lists the geometric indices of the phantom-aneurysm with their mean and standard deviation due to different levels of smoothing for each scan modality. The standard deviation for the indices were less than 3% of the mean indicating that the indices are not sensitive to smoothing levels, within the range tested.

Indices	CE-MRA	TOF-MRA	CTA	3DRA
Height (mm)	12.4 ± 0.2	12.9 ± 0.1	12.5 ± 0.2	12.5 ± 0.6
Max. Diameter (mm)	10.5 ± 0.01	10.3 ± 0.1	10.4 ± 0.01	10.4 ± 0.01
Neck Diameter (mm)	4.3 ± 0.2	5.0 ± 0.1	5.0 ± 0.1	5.5 ± 0.6
Aspect Ratio	2.9 ± 0.2	2.6 ± 0.1	2.5 ± 0.1	2.3 ± 0.3
Volume (mm ³)	731.9 ± 4.3	733.8 ± 4.0	728.2 ± 2.6	753.6 ± 15.7
Surface area (mm ²)	390.6 ± 4.8	390.8 ± 3.5	386.4 ± 2.7	388.3 ± 12.3
Bottleneck Factor	2.42 ± 0.13	2.06 ± 0.07	2.10 ± 0.08	1.92 ± 0.21
Bulge Location	0.50 ± 0.01	0.55 ± 0.009	0.54 ± 0.008	0.54 ± 0.01
Undulation Index	0.023 ± 0.01	0.021 ± 0.01	0.019 ± 0.00	0.015 ± 0.01
Non Sphericity Index	0.202 ± 0.01	0.200 ± 0.00	0.195 ± 0.00	0.181 ± 0.02
Ellipticity Index	0.197 ± 0.005	0.195 ± 0.001	0.190 ± 0.003	0.177 ± 0.010

Table 3: Average and standard deviation of morphometric indices calculated for modalities across eight levels of smoothing.

Owing to the (subjective) choice of neck plane, neck diameter and indices associated with it such as aspect ratio and bottleneck factor, showed greater sensitivity, but still low. The seemingly elevated sensitivity of undulation index is of little consequence because the values were near zero due to the lack of any undulations on the phantom-aneurysm. In general, the values of indices are consistent across 3DRA, CTA, CE-MRA and TOF-MRA models. Dimensions of the phantom-aneurysm as given by the vendor (Shelley Medical Imaging Technologies, Ontario, Canada) are a height of 13 mm and a diameter of 10 mm. Assuming the numbers are accurate, comparison between ‘actual’ values and estimated values of both height and diameter is shown in Table 4. Morphometric indices calculated for patient aneurysm models are displayed in Table 5.

Index	CE-MRA	TOF -MRA	CTA	3DRA
Height	4.6%	0.8%	3.8 %	3.8 %
Max. Diameter	5.0%	3.0%	4.0%	4.0%

Table 4: Percent error between height and diameter provide by vendor to height and diameter measured on models from the four modalities.

Patient #	Patient 1		Patient 2		Patient 3	
	3DRA	CE-MRA	3DRA	TOF-MRA	3DRA	CTA
Height (mm)	5.5	5.8	13.6	14.6	5.9	5.8
Max. Diameter (mm)	4.1	4.2	9.0	8.4	7.1	7.5
Neck Diameter (mm)	4.1	4.1	5.8	6.1	6.6	7.3
Aspect Ratio	1.3	1.4	2.3	2.4	0.9	0.8
Volume (mm ³)	62.9	69.9	628.0	635.2	179.7	184.0
Surface area (mm ²)	72.6	79.2	368.7	378.4	131.9	131.5
Bottleneck Factor	1.00	1.03	1.54	1.37	1.08	1.02
Bulge Location	0	0.26	0.41	0.43	0.26	0.13
Undulation Index	.0660	0.088	0.054	0.074	0.009	0.018
Non Sphericity Index	0.164	0.177	0.237	0.250	0.073	0.056
Ellipticity Index	0.145	0.153	0.219	0.225	0.070	0.052

Table 5: Shape indices calculated for each of the three patients.

Comparison of shape and size indices between 3DRA and CE-MRA/TOF-MRA/CTA for patient-aneurysms is shown in Figure 20 and 21.

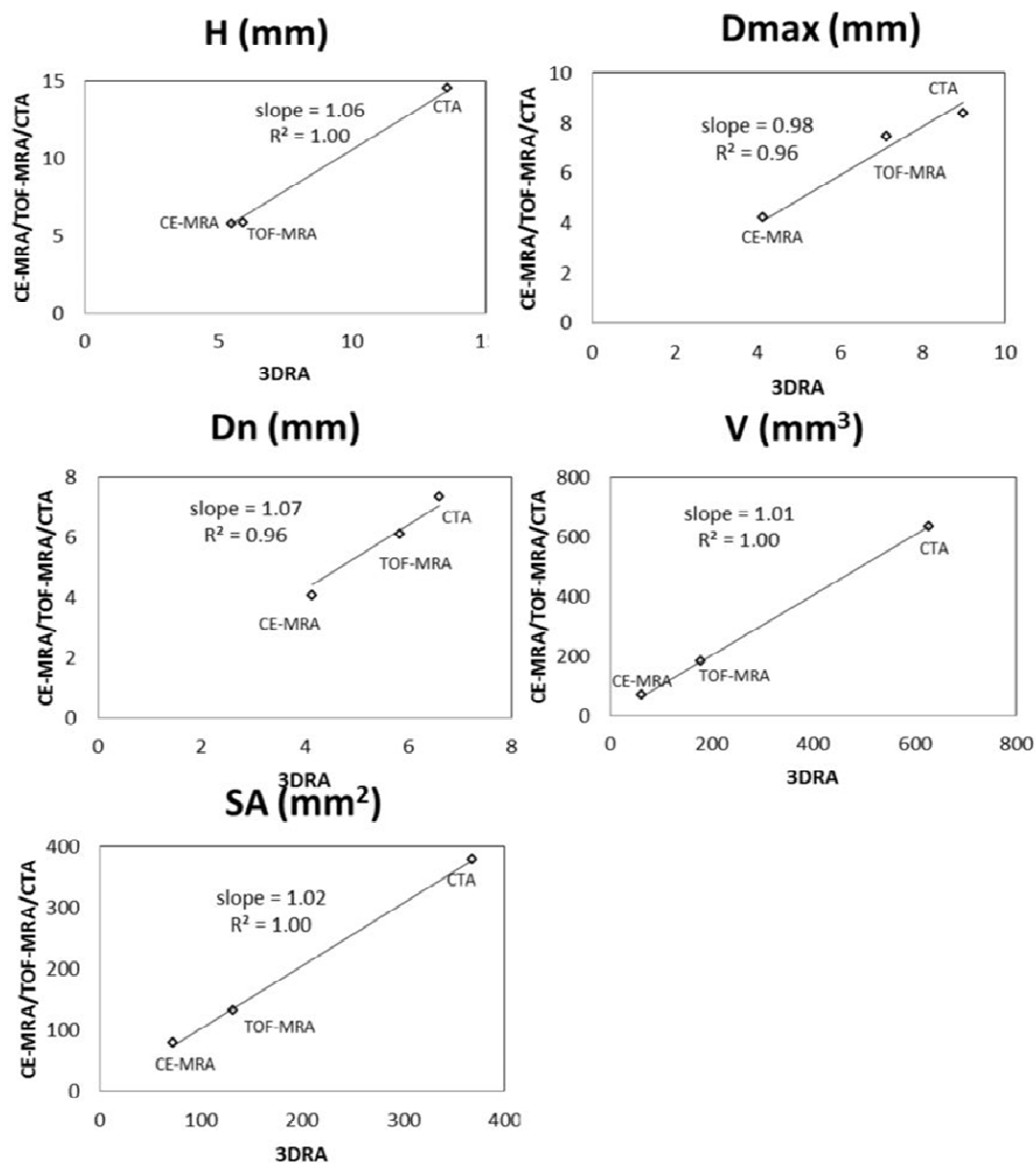


Figure 20: Graphical representation of size indices measured on patient-aneurysms with 3DRA on the x-axis and CE-MRA/TOF-MRA/CTA on the y-axis

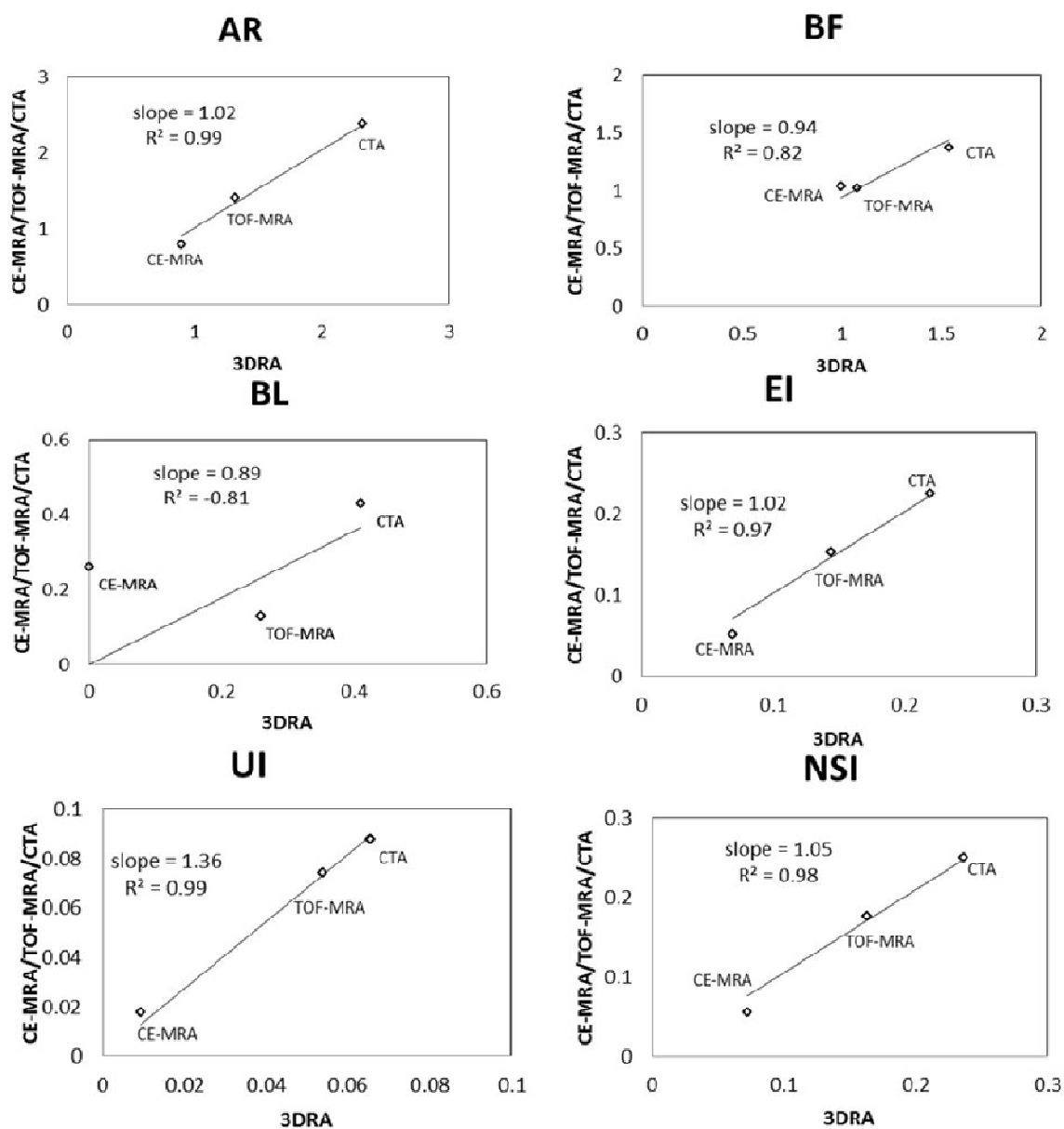


Figure 21: Graphical representation of shape indices measured on patient-aneurysms with 3DRA on the x-axis and CE-MRA/TOF-MRA/CTA on the y-axis.

4.4 Discussion

The choice of imaging modality in the clinical management of unruptured intracranial aneurysms is often driven by many clinical factors. It is inevitable then that multi-site studies on aneurysms that are essential for recruiting large study populations will accumulate data from different imaging modalities. Assessing the appropriateness of lumping quantified geometric measures computed from such multi-modality data for statistical analysis is important. Simply put, would an aneurysm's quantified geometric characteristics differ simply because the modality is different? The current study assessed rigorously whether and to what extent 3D measures of aneurysm size and shape is sensitive to scan modality. All scan modalities were obtained for a single ACOM aneurysm flow phantom and compared. Although the flow phantom used was morphologically realistic and provides some definitiveness in comparisons, one could argue that it does not present with the true complexity and variations of image data from human subjects. The quality of phantom images may be a best case scenario with the absence of skull and other tissue structures. Our studies with the phantom are still valuable because it permitted our evaluation of all four modalities in a single aneurysm and the geometry being imaged is known a priori. The phantom-aneurysm comparisons were augmented by the study with human subjects. Ideally, such a study would involve a population of patients, each of whom have been scanned by all four modalities within a short period of time (days or weeks, not months or years) so that paired comparisons of geometric indices maybe conducted. But in practice, such data is scarce. Therefore, scans from three human subjects who all had 3DRA scans and one each of the other modalities were assessed.

Visual inspection of the phantom-3D models in Figure 20 and the patient-3D models in Figure 21, suggest agreement between 3DRA, CE-MRA, TOF-MRA and CTA. To quantitatively assess similarity between modalities for each index of the phantom-aneurysm, a similarity metric was defined as the ratio of standard deviation of the means

to the mean of the means for each modality. An index was judged to be similar between modalities when its similarity metric is less than 5%. Seven of the indices were similar: H (2%), Dmax (1%), V (2%), SA (1%), BL (4%), NSI (5%) and EI (5%). However, the Dn (10%), AR (10%), and BF (10%) are not similar between modalities. The common feature among these latter indices is that they are all related to the choice of neck plane. Neck diameter is affected by choice of neck plane with small differences in the location and orientation of the neck plane likely causing large variations in measured indices. Aspect ratio and bottleneck factor are calculated from the neck diameter and hence affected by it. The undulation index had a similarity ratio of 18%, but that is inconsequential since the seeming dissimilarity may be attributed to the fact that it is extremely small (0.01 to 0.02; the phantom aneurysm had little to no perceptible undulation) and so tiny fluctuations result in large percent errors. In patient-aneurysms, the similarity metric defined above cannot be used since only any two modalities were available in each subject. Fortunately however, the three subjects had aneurysms of varying sizes, permitting a combined assessment of each index for all three subjects as done in Figure 22 and 23. A straight line relationship for an index on these graphs would suggest that the three aneurysms would be stratified in exactly the same manner by both indices and a slope of close to 1 indicates that the absolute values of the index is the same for both modalities. In human subjects too, the indices associated with the neck plane, namely, neck diameter (Dn), bottleneck factor (BF) and bulge location (BL) performed the worse than the other indices. The worst among these, BL is the normalized height at which the maximum diameter of the aneurysm occurs (i.e., BL=0 if the largest cross-section is at the neck, and BL=1 if at the dome). This index too is highly sensitive to how the neck plane is chosen in aneurysms that do not have a clear plane of maximum dimension (cylindrical shapes). If the neck plane has a flare due to the inclusion of the vessel geometry, it may become the largest cross section for such aneurysm shapes

resulting in $BL=0$. But with slight differences in angle of the neck plane, the height-axis of the aneurysm varies significantly and this causes BL to vary significantly as well.

The subjectivity and lack of consistency in isolating the aneurysm from its parent vasculature is a clear limitation of the segmentation approach, but not related to or resulting in sensitivity to imaging modality. A single investigator performed all the analyses to minimize subjectivity. In this context, a nifty technique for automated aneurysm isolation proposed by Ford et al. is noteworthy.(15) A second limitation of this study is with regard to how 3DRA was assessed in the phantom. The contrast was directly mixed to the fluid in the reservoir for all phantom-aneurysm scans. This reasonably reflects the situation for CTA and MRA scans, but may not for 3DRA scans where it would have been better to inject the contrast at the ICA. The reason for mixing the contrast was to accommodate contrast flow-related issues with the scanning. On the one hand, ACOM aneurysms are particularly vulnerable to poor contrast flow from unilateral injection.(7, 19) On the other hand, the experiments involved steady flow of fluid in the flow phantom as opposed to the more realistic pulsatile flow because the latter is technically challenging to accomplish within the constraints of the clinical setting. But steady flow may further aggravate poor mixing of the contrast with the flow medium resulting in a scan that is not reflective of clinical 3DRA scanning. Indeed, another set of 3DRA scan was performed on the phantom with 34.5 ml of Iopamidol injected in the right ICA through a homeostasis valve in the flow loop as would be done in patients, except under steady flow conditions. The 3DRA scans were performed on a Siemens Axiom Artis and the subtraction angiographic images were obtained with a voxel size of $0.187 \times 0.187 \times 0.187$ mm with matrix 512×512 . It was noted that this 3DRA model presented with more surface undulations and the source images had poor and unrealistic intensity gradients. These were absent when 3DRA was performed with contrast mixed in the reservoir. Bash et al.(3) observed that DSA performed poorly under low flow conditions, perhaps, the same phenomenon is observed here with low flow

regions caused by an 11mm AComm aneurysm and the poor mixing of contrast to flow medium under steady flow conditions. 3DRA scans of large patient-aneurysms need to be investigated independently.

4.5 Conclusion

The volumetric imaging modalities commonly used for intracranial aneurysm scanning – CTA, CE-MRA, TOF-MRA, and 3DRA – provide a consistent measure of its actual morphology. Subjectivity in the choice of the neck (aneurysm-isolation) plane does contribute to variations in some of the size and shape indices, but this is not attributable to sensitivity to modality per se. The study results suggest that the sensitivity of quantified intracranial aneurysm morphology to 3D scan modality is unlikely to have a significant impact on large-scale studies that lump data from multiple modalities.

CHAPTER 5

ON THE ROLE OF MODELING CHOICES IN ESTIMATION OF CEREBRAL ANEURYSM WALL TENSION

5.1 Introduction

Estimations of pressure-induced tension or stress resultant in the intracranial aneurysm (IA) sac wall have been proposed as metrics that help stratify patients according to rupture risk – the underlying claim being that aneurysms with high wall tension are more likely to fail [31, 37]. Wall tension on patient-specific IAs can be estimated using varying levels of measured information and after making different modeling choices. At its simplest, the ‘size’ of the IA – a standard clinical measure used for diagnosis of severity and treatment planning – may be used to calculate aneurysm wall tension under the assumption that it has a spherical or ellipsoidal shape (depending on whether its ‘size’ is known from one or more orientations, respectively). However, if volumetric image data is available, the aneurysm geometry in its true three-dimensional complexity may be segmented. This rich measured information may be leveraged for estimating a more region-specific distribution of wall tension [26, 33-34]. Region-specific aneurysm wall tension may be estimated in two essential ways: 1) By using the generalized Laplace law for arbitrary convex membranes based on surface principal curvatures [33], 2) By using the finite element (FE) method for stress analysis of the pressurized structure [31, 37]. Irrespective of the approach used, one could conceivably claim that the use of rich three-dimensional (3D) aneurysm morphology – as opposed to using just clinical size measurements – will have to yield more reliable estimations of wall tension and better able to distinguish aneurysms vulnerable to high wall tension. But how much more valuable and critical is the 3D morphological information to wall tension estimations? This remains unclear. Answering this question has important practical implications. Consider that wall tension computed from basic size measurements turns

out to stratify aneurysms approximately as effectively as 3D FE analyses. The ease of such simple calculations may then permit studies that test the hypothesis that high wall tension correlates to high rupture risk with very large populations. When data collection and analysis is simple, investigators can afford to accommodate study populations that are orders of magnitude greater than if they have to collect volumetric images, and perform segmentation in order to leverage 3D morphological information. Larger study populations can certainly contribute to greater reliability in findings. Further, the ease of calculations would also translate into ease of using wall tension indices in a clinical setting for quick biomechanical assessments.

Now, within studies that leverage patient-specific 3D morphological information, FE analysis itself may be performed by employing differing modeling choices (material or geometric nonlinearity, anisotropy, etc.) [25-32]. In most studies of IA wall tension, these modeling choices are assumed to be consistent across the study population since patient-specific information (e.g. patient-specific material parameters, contact constraints with skull, etc) are not, often, available to be incorporated. When modeling parameters are consistently applied to a study population, are the findings – specifically how we interpret them – affected significantly by which models are used? The objective of this study is to assess and document how the wall tension estimates and the ability to stratify aneurysms based on wall tension is affected by these different approaches using a population of aneurysms.

5.2 Methods

Computed Tomography Angiographic (CTA) images of 26 saccular (9 ruptured and 17 unruptured), patient-specific cerebral aneurysms were obtained as listed in Table 6.

		Unruptured aneurysms (n=17)	Ruptured aneurysms (n=9)
Variables	Median age, years	59.0 (43-71)	58.0 (39-82)
	Women‡	12	3
Location	Middle cerebral	8	4
	Internal carotid	4	-
	Anterior	1	2
	Basilar artery	1	1
	Posterior	1	1
	Pericallosal artery	2	1

Table 6: Patients and their aneurysm demographics as obtained from medical records.

Three dimensional (3D) models of these aneurysms and their contiguous vasculature were created from the source data using levelset segmentation techniques [46] as implemented in the Vascular Modeling ToolKit (VMTK- open source software, <http://vmtk.org/>). VMTK comprises of algorithms implemented as C++ libraries in Visualization ToolKit (VTK) and Image Processing ToolKit (ITK). It combines C++ classes using Python scripts enabling 3D reconstruction, mesh generation and other image processing functions of vascular structures from medical images. The parent vasculature and the aneurysm were reconstructed using levelset initialization methods - colliding fronts and fast marching [47] respectively . Detailed reviews of these methods have been published by its authors earlier [46-48]. Aneurysm domes were then isolated from their contiguous vasculature using the method previously reported by Ma et al [53]. In this method, a plane is chosen with manual discretion using the 3D visualization software TECPLOT 360 (2009 Release, Tecplot Inc., Bellevue, WA) and the aneurysm is isolated at this plane using an isolation algorithm implemented in the computing software

MATLAB (version 7.8, The Mathworks Inc., Natick, MA). Further details regarding the implementation of this method is discussed in previously reported work [53].

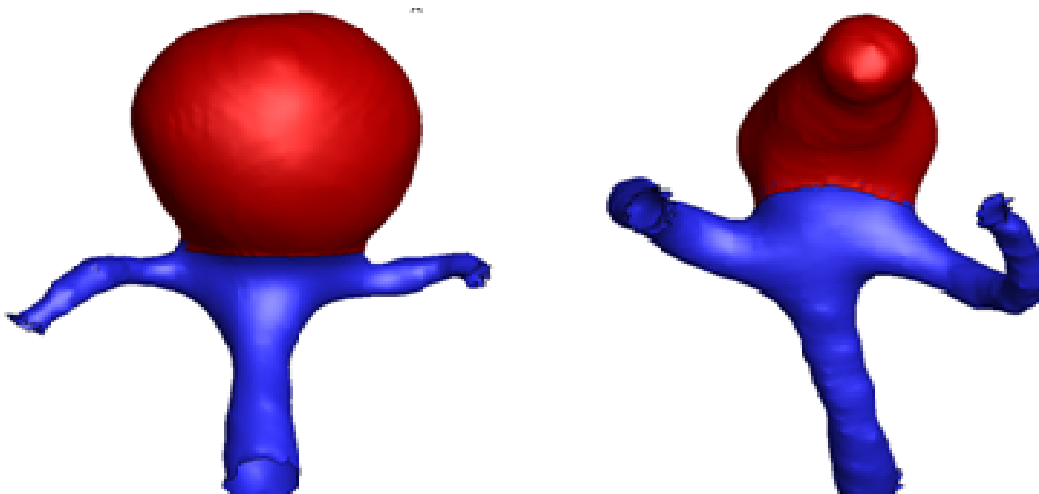


Figure 22: Representative aneurysm models – at a basilar tip and at an MCA (isolated-aneurysm sac highlighted in red)

The cutting plane is chosen in such a manner that it would reflect the plane where a surgeon would perhaps place a surgical clip while treating the aneurysm during a craniotomy procedure. By this criterion, inter-user and intra-user consistency, in choosing a plane for isolating the aneurysm, was ensured so that this task was fairly repeatable.

5.2.1 Numerical Simulations

Finite element stress analysis was repeatedly performed on isolated aneurysm sacs from all study subjects using different modeling choices listed in Table 7. For each analysis, shell elements of uniform thickness $86\ \mu\text{m}$ and a transverse shear of stiffness of $2.4\ \text{N/mm}$ were used [37]. The neck was fixed, a uniform blood pressure of $100\ \text{mmHg}$ was applied and solved using Abaqus (ver. 6.9-1, Dassault Systèmes Simulia Corp., Providence, RI).

Role of Material Models: Forward finite element analysis was performed using the four different material models listed in Table 10. Material parameters for the Fung and the linear elastic model were obtained from literature [30, 37]. Material parameters for the 3rd order polynomial model were estimated such that under biaxial extension, a tissue would have an identical stress-strain response to the isotropic Fung model as reported earlier [70]. The analyses were solved as non-linear geometries.

Role of Geometric Modeling: Forward finite element analysis was performed using the linear elastic model with same parameters as above and the analyses was run using both linear and nonlinear geometries.

Role of Geometric Truncation: In order to assess what role, if any, that exclusion of the contiguous vasculature would play on computed peak wall stress index, analyses were repeated for aneurysms from all study subjects but with their contiguous vasculature (see Figure 22). Here, the vessel ends, not the sac neck was fixed. Other choices used were: forward, nonlinear geometric analysis with isotropic polynomial model.

Role of Solution Schemes: So far, most studies have assumed that the aneurysm geometry obtained from in vivo images to be the stress-free configuration. In reality, images from in vivo arterial structures are in a pre-deformed state, being subjected to arterial pressure. In order to address this issue, our collaborators introduced an inverse elastostatic approach using which aneurysm mechanics can be more accurately studied [38, 71]. Hence, forward and inverse finite element shell stress analysis was repeatedly performed on 26 aneurysm dome models using finite element analysis program FEAP. Fung-type material model and parameters above was used for analyses. In inverse analyses, model parameter values were chosen to ensure convergence. But we have shown earlier [38] that in the inverse scheme, this has no effect on stress estimations owing to the fact that the deformed geometry is known a priori.

Modeling Choices	Material Models	<ol style="list-style-type: none"> 1. Orthotropic Fung-type model where, $W = c e^{[c_1 E_{11}^2 + c_2 E_{22}^2 + c_3 E_{11} E_{22} + c_4 E_{12}^2]}$ with $c=28 \text{ N/mm}^2$, $c_1=17.58$, $c_2=12.19$, $c_3=7.57$, $c_4=4.96$ [30, 37]. 2. Isotropic Fung-type model with $c = 28 \text{ N/mm}^2$, $c_1=14.89$, $c_2=14.89$, $c_3=7.57$, $c_4=4.96$ [37]. 3. Isotropic 3rd order polynomial model where, $W = a(I_c - 3) + b(I_c - 3)^2 + c(I_c - 3)^3$ with $a=3.00 \text{ N/mm}^2$, $b=-14.35 \text{ N/mm}^2$ and $c=63.57 \text{ N/mm}^2$. 4. Linear elastic model (small deformation) with $E=100 \text{ N/mm}^2$ and $n=0.49$ [37].
	Geometric Modeling	<ol style="list-style-type: none"> 1. Linear geometry 2. Nonlinear geometry
	Geometric Truncation	<ol style="list-style-type: none"> 1. Aneurysm dome only 2. Aneurysm dome with contiguous vasculature
	Solution Schemes	<ol style="list-style-type: none"> 1. Forward solution scheme 2. Inverse solution scheme
	Mesh Quality	<ol style="list-style-type: none"> 1. Fine mesh 2. Coarse mesh
Interpretation Choices	Failure Stress	<ol style="list-style-type: none"> 1. Maximum principal stress 2. Von Mises stress
	Maximum Principal Stress	<ol style="list-style-type: none"> 1. Absolute peak value 2. 95th percentile value 3. 50th percentile value

Table 7: Modeling choices made during finite element analysis of cerebral aneurysm geometries.

Role of Mesh Quality: Forward finite element analysis was performed using meshes of two qualities (see Figure 23). The fine mesh was obtained by re-meshing the course mesh at a maximum element area to be 0.2 while aspect ratio, normal angle tolerance and collapse angle were maintained at 1.2, 0.2 and 0.2 respectively. Other choices used were: forward, nonlinear geometric analysis with isotropic polynomial model.

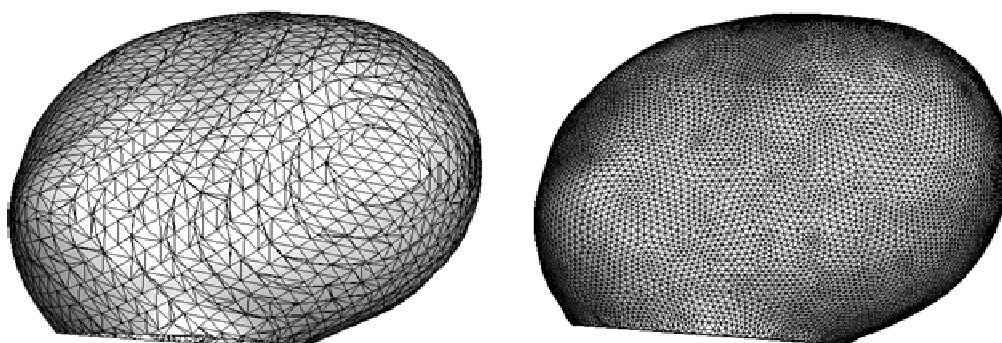


Figure 23: Sample course and fine meshes for an aneurysm dome model.

Role of Interpretation Choices: Apart from the modeling choices made during FEA, choices are also made on quantities of interest for the interpretation of results. Since it is believed that rupture occurs when wall tension exceeds wall strength, maximum wall tension is often the quantity of interest [27, 31]. To gain an understanding of failure, Maximum principal stress or Von Mises stress distributions are often observed. As an index of maximum wall tension, the absolute peak value of maximum principal stress can be observed. However, the absolute peak value of wall stress distributions tend to strongly depend on small geometrical irregularities thus resulting in an anomalous stress index [72]. Refer to Figure 26. Considering 95th percentile wall stress as an index ensures a more robust measurement of peak wall stress. Therefore the interpretation choices compared were: 1) Absolute peak value versus 95th percentile maximum

principal stress 2) 95th percentile versus 50th percentile maximum principal stress 3)
Maximum principal stress versus Von Mises stress.

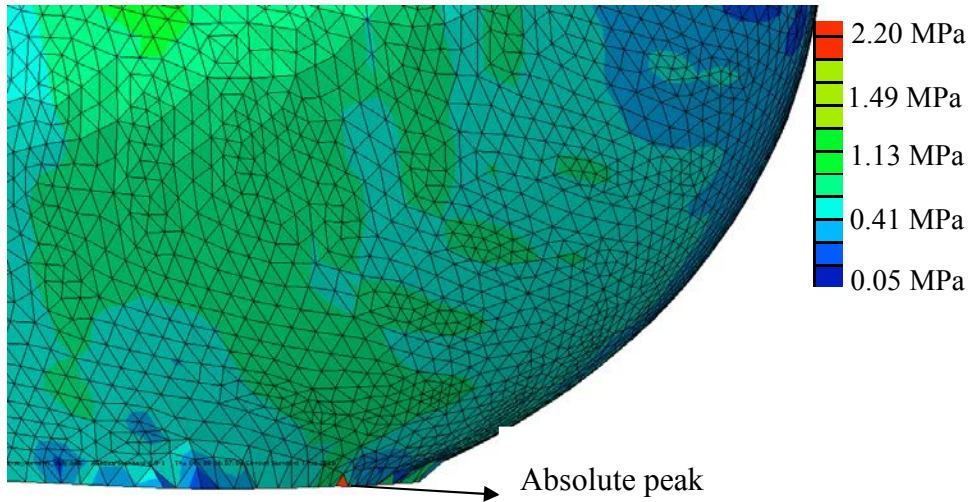


Figure 24: Sample of absolute peak value of maximum principal stress occurring due to irregular element in the mesh.

5.2.2 Tension Indices Based on Curvature

Two principal curvatures (κ_1, κ_2) of the aneurysm surface were calculated for the 26 patient aneurysm dome models [37, 53]. Assuming the aneurysm wall to be a membrane and its deformation to be axisymmetric [33], stress distribution was obtained using: $\sigma_1 = \frac{P}{2\kappa_m t}$ where σ_1 is the maximum stress, κ_m is mean curvature ($\frac{\kappa_1 + \kappa_2}{2}$), P is a pressure of 100 mmHg and t is an assumed thickness of 0.089 mm. 95th and 50th percentile value of σ_1 was considered as the index.

5.2.3 Tension Indices Based on Clinical Measurements

Height (H) and maximum diameter (Dmax) was measured on all 26 aneurysm dome models.

1) Assuming patient-aneurysm geometries to be spherical, maximum stress was calculated with the measured maximum diameter as $\sigma_1 = \frac{PR}{2t}$ where $R = D_{max}/2$.

2) Assuming patient-aneurysm geometries to be ellipsoidal, maximum stress was calculated as $\sigma_1 = \frac{Pa^2}{2t(a^2 \sin^2 \varphi + b^2 \cos^2 \varphi)^{1/2}}$ where a, b are deformed major and minor axis of the ellipsoid and φ is angle made by the normal, at any point, to the major axis of the ellipsoid. Height (H/2) and maximum diameter (Dmax/2) measurements of the patient geometries were used to calculate dimensions of ellipsoid, a being the maximum of the two.

5.3 Results

5.3.1 Numerical Simulations

For material model assessment, the relationship of 95th percentile maximum principal stress between the gold standard – Fung anisotropic model – and all other material models are shown in figure 4. The plots show the slope and R^2 values of each linear fit. The comparison of 95th percentile maximum principal stress for aneurysms with and without contiguous vasculature and that for forward versus inverse solution schemes are shown in Figure 25 – both were linearly related. Similarly 95th percentile stress values calculated on both fine and coarse meshes of the aneurysm models share a linear relationship as shown in Figure 25.

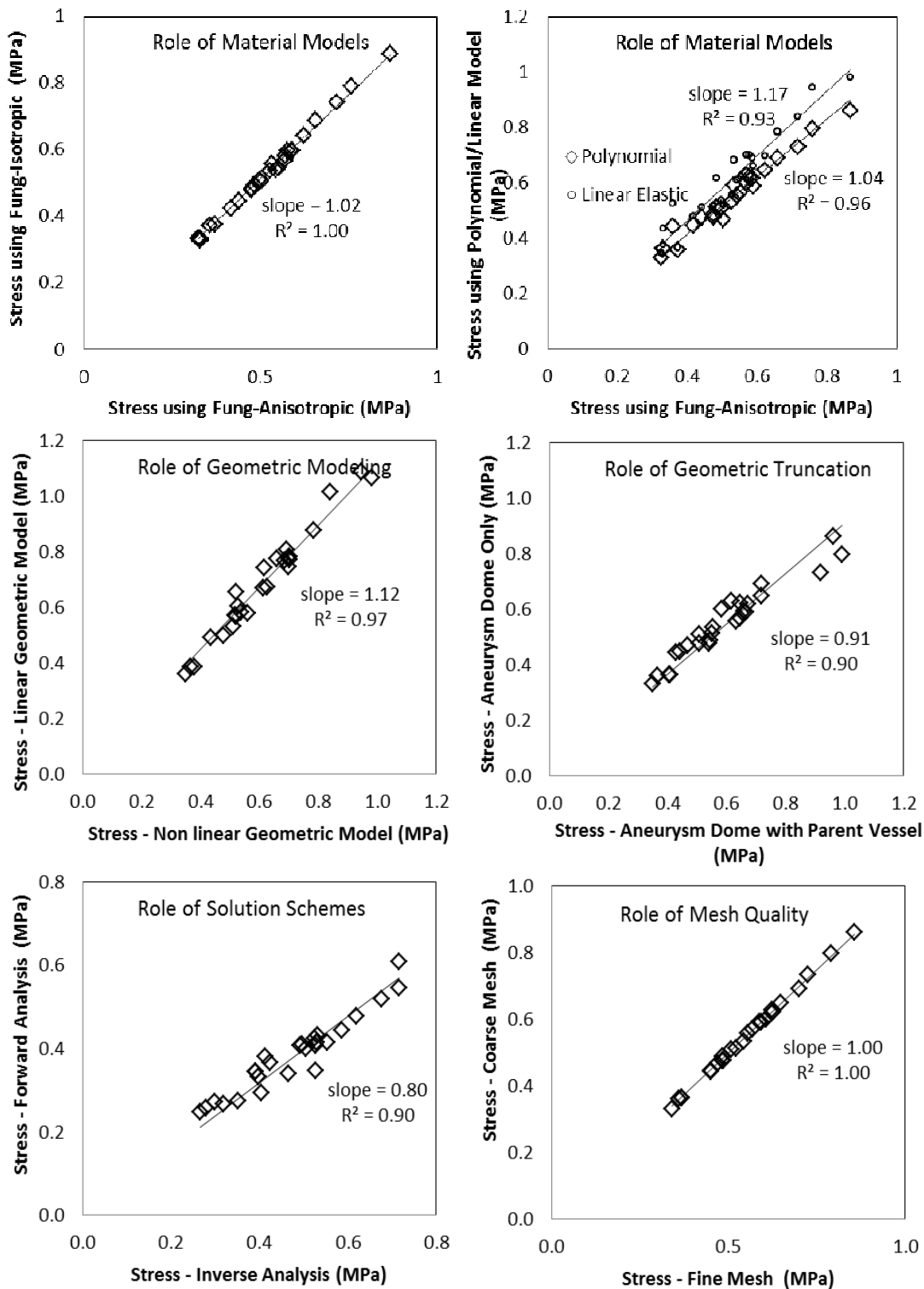


Figure 25: Stress calculated using numerical simulations with variations in modeling choices. Plots compare each modeling choice.

For the assessment of interpretation choices, the comparison of 95th percentile maximum principal stress to absolute peak value and the 50th percentile maximum principal stress is shown in Figure 28. The former comparison has a near-linear relationship with a few outliers while the latter comparison is also linear but with a low slope. The relationship between 95th percentile maximum principal stress and Von Mises stress was linear as shown in Figure 26.

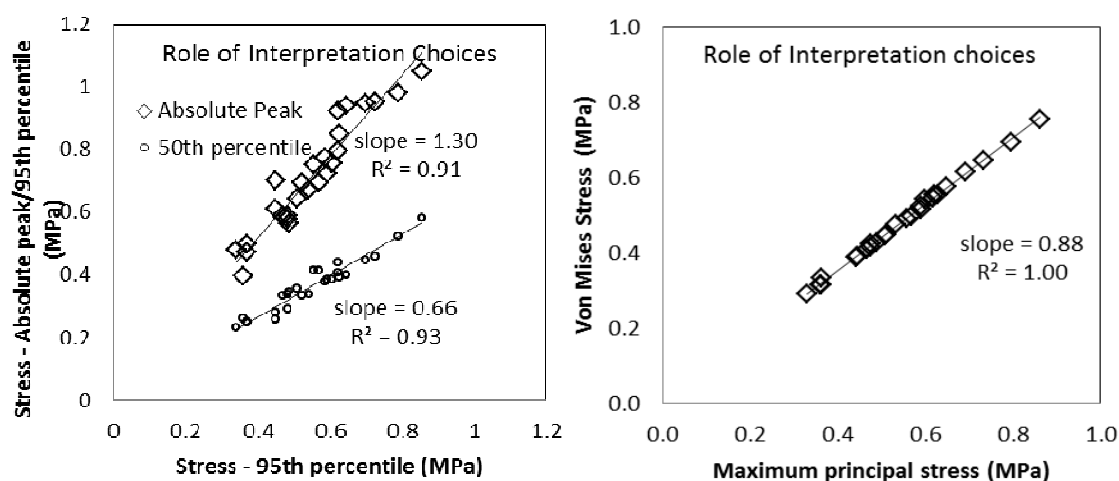


Figure 26: Stress calculated using numerical simulations with variations in interpretation choices. Plots compare each interpretation choice.

5.3.2 Tension Indices Based on Curvature

The comparison between 95th percentile maximum principal stresses and 95th percentile κ_m based stresses did not prove to have any sort of perceivable relationship as illustrated in Figure 27.

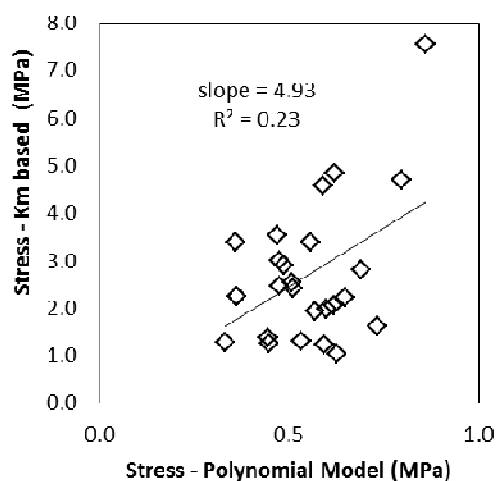


Figure 27: 95th percentile maximum principal stress calculated for aneurysm domes modeled as polynomial, isotropic model Vs. 95th percentile Km based stress.

5.3.3 Tension Indices Based on Clinical Measurements

The relationship between stresses calculated assuming ellipsoidal geometries to 95th percentile maximum principal stress obtained from numerical simulations follows a fairly linear trend but with 3 significant outliers (Figure 28a). On the other hand, an improved linear relationship is observed between stresses in models assumed to be spherical and the 95th percentile maximum principal stress suggesting that numerically calculated 95th percentile stress is perhaps strongly correlated with Dmax (Figure 28b).

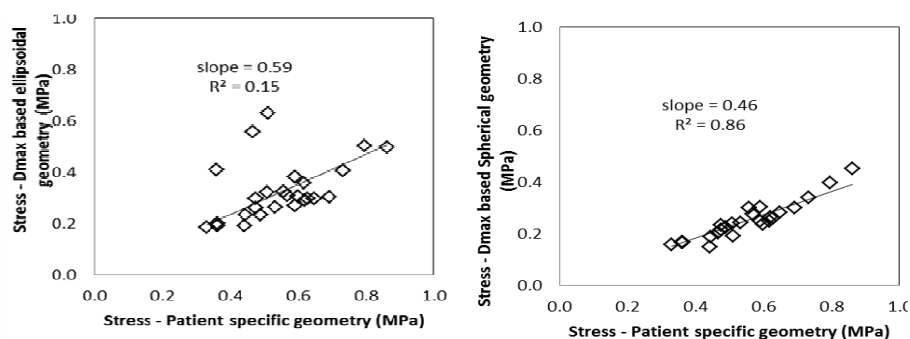


Figure 28: 95th percentile maximum principal stress calculated for aneurysm domes modeled as polynomial, isotropic model Vs. stress calculated using clinical information – Dmax and H a) assuming ellipsoidal geometries b) assuming spherical geometries.

5.4 Discussion

Would the inferences from a stress analysis of a given cerebral aneurysm population be any different when different modeling choices are made? We sought to address this question using the 95th percentile maximum principal stress as an index on a population of 26 patient specific aneurysms. On material models, both the Fung-isotropic and polynomial-isotropic models show a clear linear relationship to anisotropic Fung model, despite the latter's apparent sophistication and realism. Also, both forward and inverse solution schemes show a linear relationship as well. This suggests that if one were to rank aneurysms according to wall stress, the ranking would be no different whether an isotropic or an anisotropic model and whether a forward or an inverse solution is employed, not to mention any model functional form. Indeed, even the linear elastic model results in a near-linear relationship with the anisotropic Fung model. Similarly, a linear relationship was found for the 95th percentile stress between aneurysm models with and without the contiguous vasculature. The locations of these 95th percentiles in the aneurysm dome and the patterns of stress distributions were also similar between truncated models and their non-truncated counterparts as shown in Figure 29.

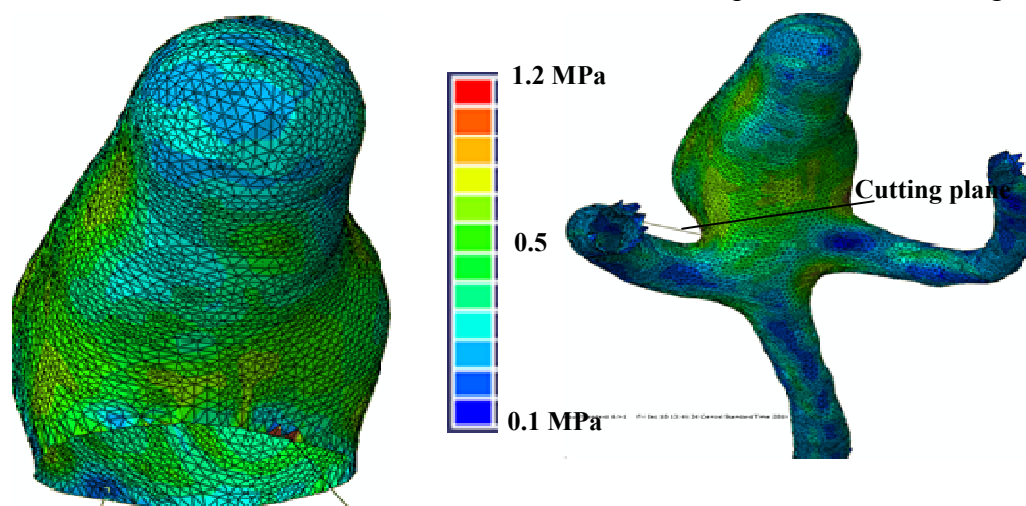


Figure 29: Maximum Principal Stress distribution on aneurysm geometries, including and excluding contiguous vasculature.

This suggests that truncated models are likely sufficient for stress analysis. Here however, caution is warranted. In the non-truncated models, only the stress in the aneurysm sac region was used to determine the 95th percentile stress. But peak stresses did occur in some cases at the neck regions which were excluded by this criterion. Since cerebral aneurysms rupture predominantly at the fundus of the aneurysm, in a region away from the neck [14, 73], truncation at the neck might not affect inferences from the stress analysis.

The lack of a relationship between stresses calculated from mean curvature and stresses from numerical simulations is because the relationship defined between stress and curvature does not hold true at flat and concave regions of aneurysm geometries. At flat regions where curvature tends to zero, stress tends to infinity. This is further illustrated by the vast spread in curvature-based stress distribution compared to stresses calculated using other methods. Refer to Figure 30.

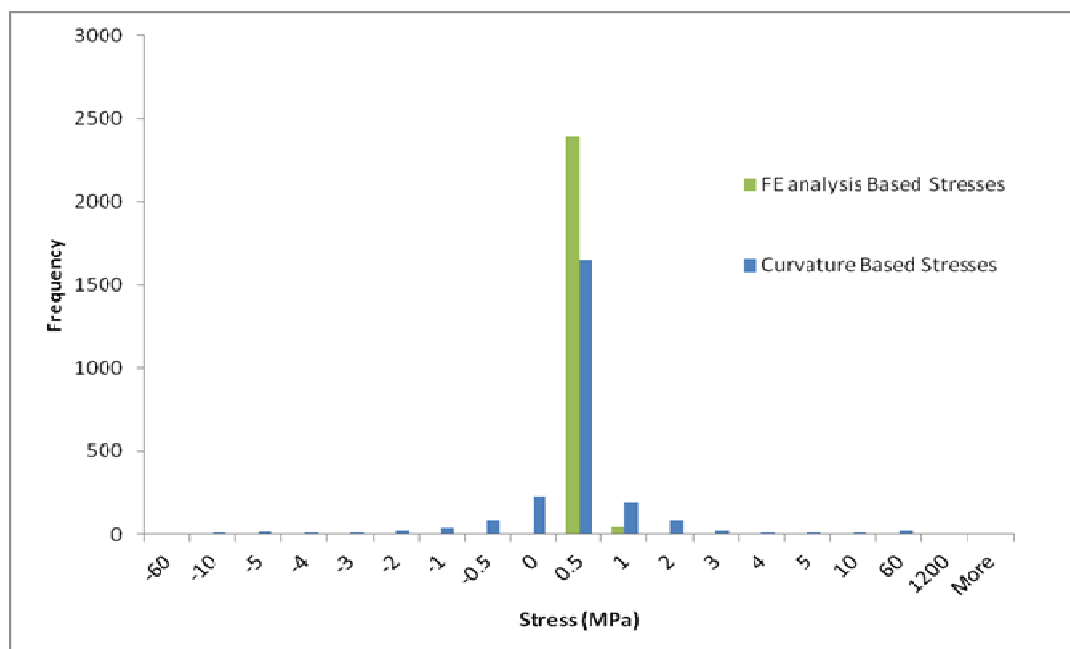


Figure 30: Histogram showing distribution of stresses calculated using finite element analysis and using curvature calculations.

The near -linear relationship observed between stresses calculated using maximum diameter measurements and stresses calculated from numerical simulations of patient- aneurysms suggests that numerically calculated 95th percentile stresses are strongly correlated to size information. It also warrants another question. Can both methods differentiate ruptured from unruptured aneurysms with the same accuracy? Two-tailed independent student-t tests performed to observe standard error, mean and standard deviation values while differentiating the two groups using: 1) 95th percentile maximum principal stress numerically calculated on isolated aneurysm dome modeled as anisotropic, Fung model, 2) 95th percentile maximum principal stress numerically calculated on isolated aneurysm dome model modeled as isotropic, polynomial model, 3) Stress calculated using maximum diameter measurement ($\frac{PR}{2t}$). Results are listed in Table 8. None of the values reached statistical significance. Perhaps, because the data chosen for this study, both ruptured and unruptured are large aneurysms, without much variation in size.

Stress	Ruptured (n = 9)	Unruptured (n = 17)
95 th percentile stress (Anisotropic, Fung model)	0.543 ± 0.160 Error = 0.053	0.517 ± 0.121 Error = 0.029
95 th percentile stress (Isotropic, Polynomial model)	0.569 ± 0.151 Error = 0.050	0.538 ± 0.126 Error = 0.031
Stress using ($\frac{PR}{2t}$)	0.258 ± 0.098 Error = 0.033	0.255 ± 0.063 Error = 0.031

Table 8: Stress indices calculated using different. Values presented as mean ± standard deviation.

It is, however, worth emphasizing that the insensitivity to modeling choices is only true because the focus is on stratifying subjects with geometry being the only patient-specific information used. In this study, aneurysms with thrombus were left out and contact constraints (For example: skull touching ICA aneurysms) were not modeled. It is of prime importance to note that if additional patient-specific information such as contact constraints is involved, then modeling choices will indeed start to matter in a substantive manner.

5.5 Conclusion

From the results, it can be concluded that sophistication in computational models will not affect the stratification of aneurysms, as long as boundary conditions and forces are consistent across the patient population. It is crucial to understand that these modeling choices play a significant role once patient-information is not uniform across the population.

CHAPTER 6

CHARACTERIZATION OF IN-VIVO MECHANICAL PROPERTIES OF CEREBRAL ARTERIES USING CRANIOTOMY VIDEO

6.1 Background

Characterization of the mechanical properties of intracranial arteries and aneurysms has been hampered by scarcity of specimens and/or inadequate resolution of diagnostic imaging. In vivo assessments using dynamic imaging data is rare due to lack of data and limited scan resolution relative to arterial wall motion and image registration. This project utilized tissue characteristics that are currently available in literature. In this context, one source of valuable information that has seldom been leveraged is the microsurgical videos routinely generated during open craniotomy surgeries such as intracranial aneurysm clipping. In this proof-of-concept study, the ability to utilize microscope-video recorded in the operating room during craniotomy for extracting distensibility information on intracranial arteries was evaluated for use in future studies.

6.1.1 Craniotomy Video

Craniotomy videos are recorded during brain microsurgery to aid in this operation. They are routinely recorded during intracranial aneurysm clipping. The video clips used for this pilot study was captured from a fixed position using a Zeuss microscope at 640 x 480 pixels, at a rate of 30 fps. The scale was extracted from surgical implants of known dimensions. Spatial resolutions of these craniotomy videos were better than cerebral angiograms.

6.1.2 Estimation of Arterial Mechanical Properties

Diameter variation of candidate artery under physiological pressure wave may be measured by digitization of video frames. Thus, arterial compliance maybe estimated directly. For the estimation of arterial mechanical properties, arterial wall was assumed to

be a membrane. This membrane assumption allows ignoring residual stress and for determination of variation of stress resultant (tension – N/m) in the arterial wall during cardiac cycle using $t = \frac{1}{2} PD$ where t-tension; P-pressure; D-diameter. For a given material model (membrane formulation), pressure (known) maybe derived as a function of current diameter (known), zero-pressure diameter (unknown) and material parameters (unknown). The equation for Hooke's law - $P = \frac{2E_t}{D_0} \left(1 - \frac{1}{D}\right)$ where D_0 – zero pressure diameter and E_t – Membrane modulus.

Pressure-diameter data can be fit to model to estimate D_0 and material parameters simultaneously.

6.2 Materials and Methods

6.2.1 Video Source

The craniotomy video for a patient with an exposed anterior cerebral artery (ACA) was used for this analysis. It is a three-second video clip prior to beginning of surgical procedure. The specifications of which are 640 x 480 pixels; 30 frames per second with 1 pixel being 0.16 mm. Pulsation of the ACA was visually perceptible in these videos.

6.2.2 Measurements

Distinct material reference points were identified along the ACA wall by exploiting texture information using public domain, java-based image processing software - ImageJ. Image sequences randomized in order to blind the investigator during digitization. Arterial points were tracked for every frame during that time period for four cardiac cycles in the chosen video clip. For demonstration purposes in this study, a pressure wave was assumed to vary from 80 to 120 mmHg. Pressure recorded in the OR will need to be used for assessment of mechanical properties.

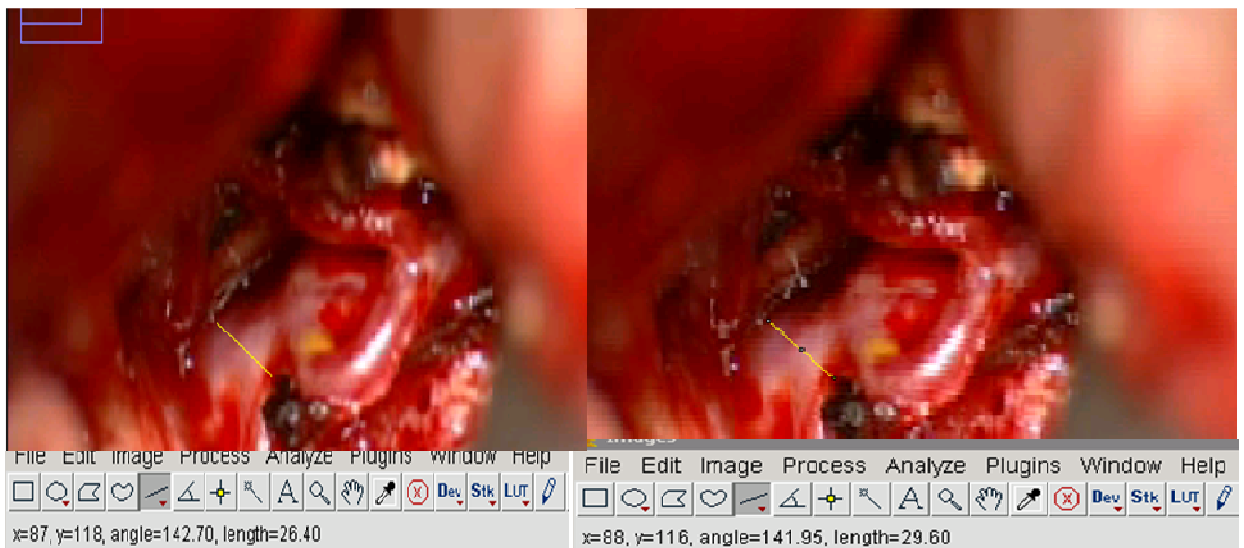


Figure 31: Diameter measurements on an ACA at diastolic (a) and systolic (b) states using ImageJ

6.2.3 Estimation of Mechanical Properties

Compliance was estimated for the ACA displayed in Figure 14. Material parameters for three models were evaluated: Linear elastic (Hooke's), hyperelastic 1 (NeoHookean), and hyperelastic 2 (2nd order polynomial of the first invariant of C). Pressure-diameter relationship was derived for each model as function of D_0 and parameters :

$$\text{Hooke's law: } P = f(D, D_0, E_t)$$

E_t – Tension modulus

$$\text{Hyperelastic 1: } P = f(D, D_0, m)$$

Strain Energy per unit surface area:

$$W = m(I_c - 3)$$

$$\text{Hyperelastic 2: } P = f(D, D_0, a, b)$$

Strain Energy per unit surface area:

$$W = a(I_c - 3) + b(I_c - 3)^2$$

$P=f(D)$ was fit to pressure-diameter data for the patient's ACA to estimate D_0 and material parameters using Newton Raphson nonlinear regression technique. Mechanical property measures were compared to report by Toth et al. [74] on an in vitro pressure-inflation study of anterior cerebral artery.

6.3 Results and Conclusion

Variation of diameter across four cardiac cycles is in correspondence with the systolic and diastolic movement of the vessel was noted. The dilation of the artery can be seen in Figure 15. Figure 16 displays the pressure – diameter data measured is fit with the three material models in order to calculate zero pressure material parameters of the arterial wall. This is a pilot study of extracting mechanical properties from OR videos and the usage of OR videos for extraction for tissue properties requires further study. Therefore, the material parameters and tissue property used for wall tension calculation (discussed above) was obtained from literature, rather than from being calculated using OR videos. The results of this study was not utilized in other parts of the project.

CHAPTER 7

MORPHOLOGY OF INTRACRANIAL ANEURYSMS AND THEIR CORRELATION TO INTRACELLULAR SIGNALING PATHWAYS

Disclosure: This work was a collaborative effort with our collaborators in the Department of Neurosurgery, Helsinki Central Hospital, Helsinki, Finland. Data and specimen collection and protein-signaling measurements and statistical analysis performed by the Helsinki group. My contributions included image segmentation, morphometric analysis and results interpretation. This work has been accepted for publication: Laaksamo E, Ramachandran M, Juhana F Riikka, T.Marc, B.Friedlander Robert, M.Harbaugh Robert, E.Juha, H.Mika, N.Raghavan Madhavan, L.Aki, L., *“Intracellular Signaling Pathways and Size, Shape, and Rupture History of Human Intracranial Aneurysms”*, Neurosurgery, 2012.

7.1 Summary

The pathogenesis of cerebral aneurysms and their reasons for rupture remain largely unclear. Two different scientific approaches to understand their behavior are 1) Assessing aneurysm morphology 2) Assessing proteins in aneurysm wall. While our group assesses aneurysm morphology, the neurosurgery research group at the Helsinki University Central Hospital studies the role of Mitogen Activated Protein Kinases in the pathogenesis and rupture of cerebral aneurysms.

Mitogen Activated Protein (MAP) Kinases are a class of signaling proteins that get activated within the MAP kinase cascade in order to stimulate a cellular response. This family of intracellular signaling proteins consists of c-Jun N-terminal kinase (JNK), p38 and Extracellular signal-regulated kinase (ERK) [75]. MAPKs are activated or deactivated by their phosphorylation triggered by upstream kinases i.e. MAP3K activates MAP2K which in turn activates MAPK. This set of activation is stimulated by

extracellular stimuli such as mechanical stretch, inflammatory cytokines, growth factors and cellular stress. They are responsible for cellular activities – growth, proliferation, differentiation and apoptosis [75]. They are up-regulated or down-regulated for the treatment of various diseased states. It is well accepted that MAPKs are involved in vascular remodeling. For instance, in abdominal aortic aneurysms, it was shown that JNK activates transcription factor c-Jun and regulates the expression of matrix metalloproteinases (MMPs) involved in wall degradation [76]. However, the role of MAPKs in the pathogenesis of cerebral aneurysms is still fairly unknown [75]. Laaksamo et al [75] at the University of Helsinki, Finland studied the expression and phosphorylation of MAPKs and other proteins in ruptured and unruptured human intracranial aneurysms.

Their results suggested that certain proteins and their phosphorylation states (P54 JNK, phospho-p54 JNK, P38, phospho-p38) might be involved in IA growth [75]. Similarly, previous morphometric studies [24, 53-54] performed by our group showed that certain shape indices were associated with aneurysm growth/rupture (non sphericity index, undulation index). The pathogenesis of IAs is presumed to be due to vascular remodeling where their increase in size, development of irregular shape characteristics and consequently, their rupture are, perhaps, reflective of the re-modeling process. It is also known that these signaling proteins are responsible for or play a role in the re-modeling process. Hence it is reasonable to wonder if there is certain morphometric wall features triggered as a response to certain proteins. Hence the objective of this study was to find correlations, if any, between these protein indices and the morphometric indices on a set of intracranial aneurysms. These correlations would, perhaps, provide us with better understanding of IA development and wall degeneration.

Reference to the publication listed above provides further details on the methods, results and discussions of this study.

CHAPTER 8

PROTOCOL FOR VASCULAR SEGMENTATION AND ITS USER SENSITIVITY

Disclosure: This work was collaboratively performed with Benjamin Dickerhoff, then Research Engineer in the BioMechanics of Soft Tissues Lab, Biomedical Engineering. My contributions include development of image analysis protocol and acting as one of two users for image segmentation. The role of second user, review of the image analysis protocol, comparisons between users and statistical analyses were performed by B.Dickerhoff.

8.1 Introduction

A protocol was developed to ensure consistency in the process of segmenting patient specific aneurysms. Since data handling and segmentation will be performed by multiple users with different levels of experience, a protocol with a standardized step by step approach makes the process more streamlined. The protocol organizes classes from VMTK's segmentation procedure discussed in Chapter 2 and 3 in a set of sequential steps. This reduces variability introduced in the segmented 3D models due to vascular segmentation being performed by multiple users. It also shortens the time taken to segment each 3D model. In addition to this, the protocol ensures uniform naming schemes for the segmented and archived files. However, it is difficult to completely eliminate subjectivity in choices made by a user during segmentation. Choices made during the selection of seed points, threshold values and evolution parameters involve user discretion. Since with angiographic images, vessel boundaries are not always clearly defined, subjective judgments are necessarily made in this account. Hence a study was performed to assess variations between users in segmented geometries and their measured morphometric indices.

8.2 Methods

8.2.1 Study Population

Ten of the patient- aneurysms were chosen for the study. The study population includes 3 internal carotid artery (ICA) aneurysms, 2 middle cerebral artery (MCA) aneurysms, 1 anterior cerebral artery (ACA) aneurysm, 1 superior cerebellar artery (SCA) aneurysm, 1 anterior communicating artery (ACOM) aneurysm, 1 posterior communicating artery (PCOM) aneurysm, and 1 basilar artery aneurysm. Out of the 10 scans for the chosen patient- aneurysms, there were 6 CTAs and 4 TOF-MRA scans. The average resolution of the scans were 0.38 x 0.38 x 0.63 mm.

8.2.2 3D Segmentation and Isolation

The segmentation protocol was developed based on topics discussed in Chapter 2 and 3. This protocol was used to segment IA geometries chosen for this study. The protocol uses VMTK and involves the following steps:

1. Locating the aneurysm: The volumetric scan is opened using VMTK dicom viewer and its slices are browsed through to locate the aneurysm based on the clinically provided location. Once the aneurysm is located, the x,y,z coordinate of the scan at this location is noted.
2. Selecting a VOI: A Volume of Interest (VOI) comprising of the located aneurysm and its contiguous vasculature is then selected. Care is taken to ensure that all of the contiguous vasculature is included in the VOI, so that all inlets and outlets can be accurately defined while performing hemodynamic simulations using these segmented 3D models.

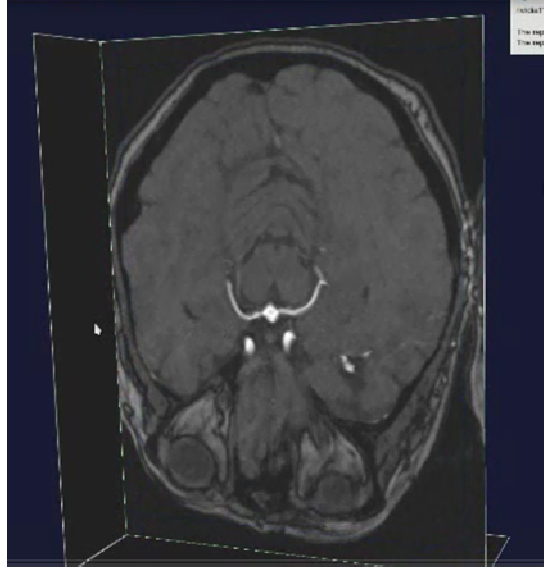


Figure 32: Basilar aneurysm located in the volumetric CTA scan.

3. Removal of Bone: Next, features of the scan that might interfere with the segmentation of the aneurysm and its contiguous vasculature are defined in order to be subtracted from the rest of the segmentation. This step is commonly employed while segmenting ICA or Ophthalmic aneurysms due to their close proximity to the skull. Using VMTK's level set segmentation algorithm, the skull is segmented by choosing "Threshold" as the initialization method. An appropriate threshold value is entered and an initial model of the skull is generated. The generated model is then evolved with evolution parameters - number of iterations (300), propagation scaling (0), curvature scaling (0) and advection scaling (1) - set to their default values. The bone segmentation is then saved as a feature and will be subtracted from the rest of the segmentation.

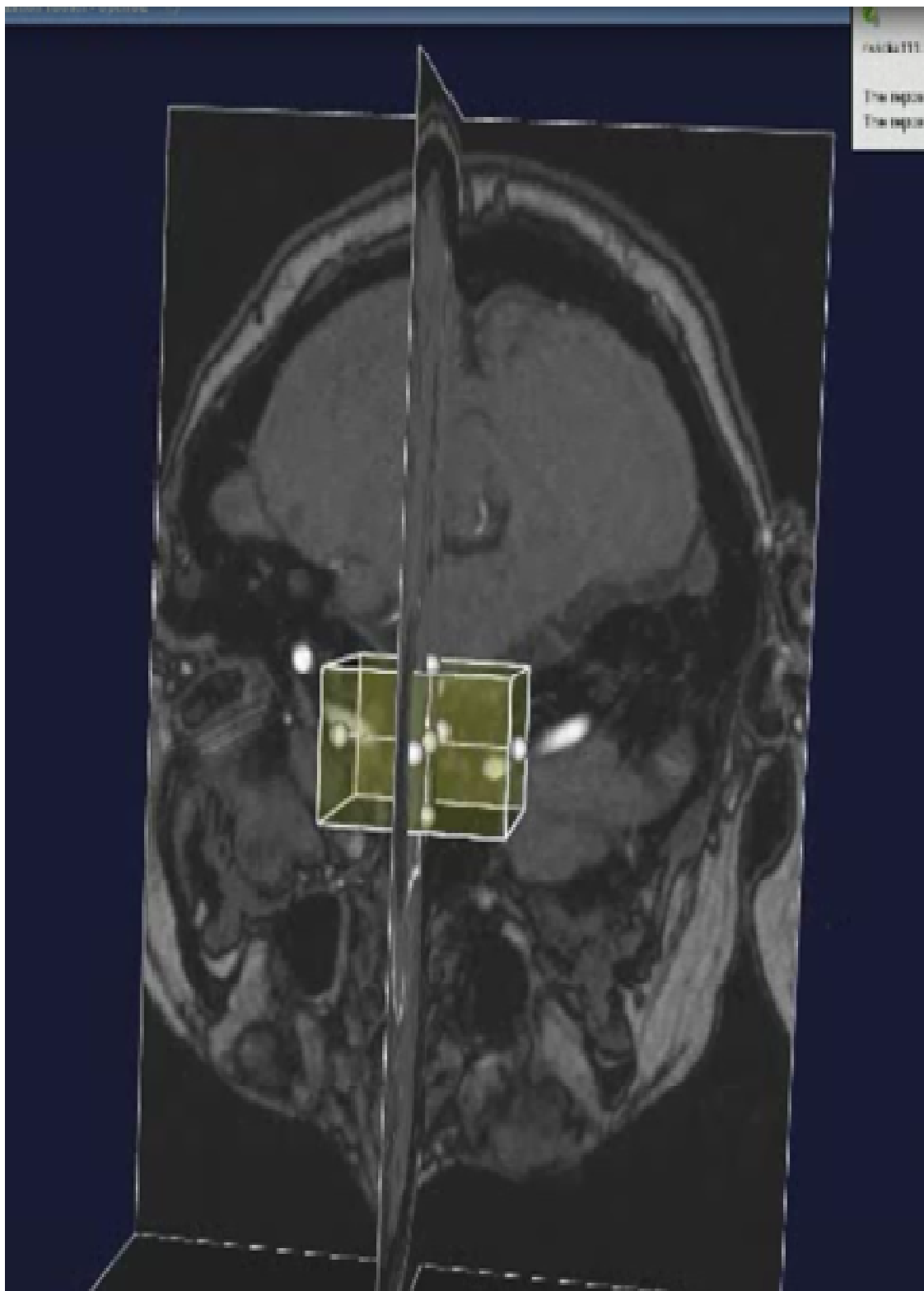


Figure 33: VOI of the aneurysm and its contiguous vasculature chosen.

4. Segmentation of Contiguous Vasculature: Using VMTK's level set segmentation algorithm, the contiguous vasculature is segmented by choosing "colliding fronts" is chosen as the initialization method. "Colliding Fronts" is the initialization method suitable for vessel segmentation since it is designed for cylindrical geometries. Appropriate upper and lower threshold values are chosen by scanning through the dicom images and these values are entered. Source and target seed points for a vessel are picked and an initial model of the vessel is generated. The generated, deformable model is then evolved to form a smooth, continuous surface. The deformable models were evolved by applying segmentation parameters within a set range – number of iterations (200-300), propagation scaling (0-1), curvature scaling (0-1) and advection scaling (1) until the evolved model is satisfactory. The slices are run through the 3D surface to ensure that it complies with the threshold gradients of the angiographic images. This process is repeated for each of the contiguous vessels and they are merged together.
5. Segmentation of aneurysm: As the next step, the aneurysm geometry is segmented using VMTK's level set segmentation algorithm. "Fast marching" is chosen as the initialization method, upper and lower threshold values are chosen as described in the previous step and is entered. One source seed point is picked in the center of the aneurysm geometry and several target seed points along the boundary of the aneurysm geometry. An initial model is generated based on the input parameters. This generated model is then evolved to form a smooth, continuous surface by applying segmentation

parameters within a set range – number of iterations (200-300), propagation scaling (0-1), curvature scaling (0-1) and advection scaling (1). The segmented aneurysm geometry is then merged with the contiguous vasculature.

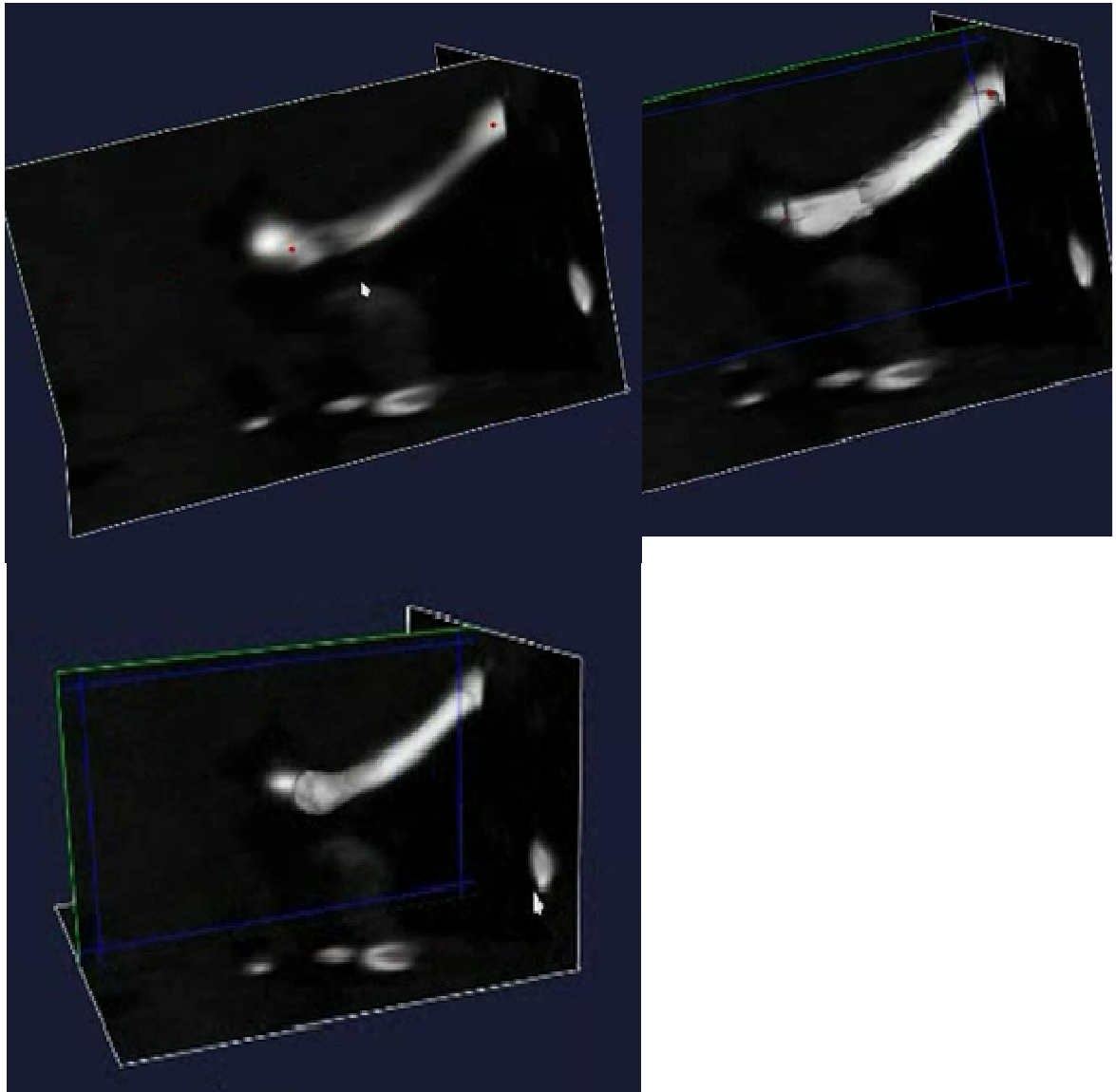


Figure 34: Segmentation stages of Basilar Artery (left to right, top to bottom).

6.

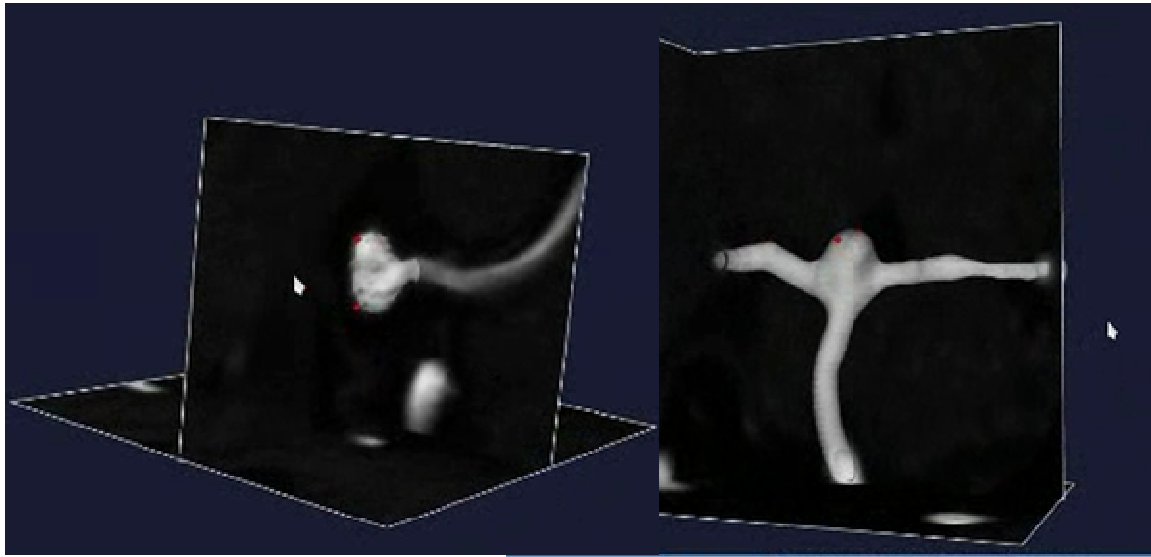


Figure 35: Segmentation of aneurysm (left). Segmented model of aneurysm merged with the contiguous vasculature.

7. Isolation of Aneurysm Dome: The aneurysm dome is then isolated from its contiguous vasculature using a plane where a surgeon would place a surgical clip during craniotomy. The aneurysm dome is then remeshed with maximum element area set to be 0.2 along with aspect ratio, normal angle tolerance and collapse angle set to 1.2, 0.2 and 0.2 respectively. This ensures that there are no convergence issues while performing finite element analysis to calculate wall tension.

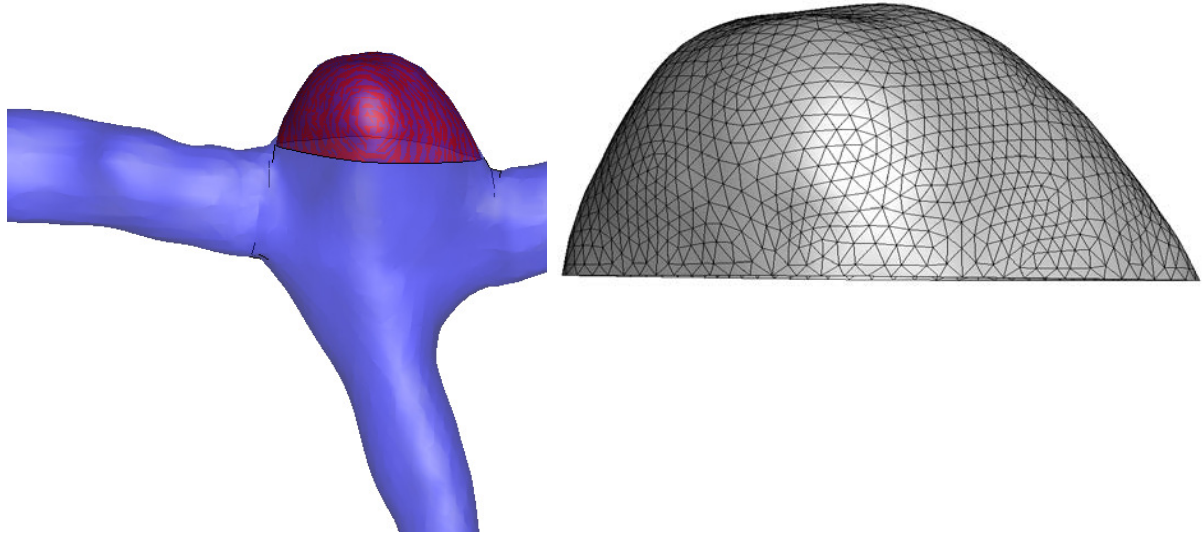


Figure 36: Aneurysm Isolation. a) Isolated aneurysm dome and its contiguous vasculature, b) Mesh quality of isolated aneurysm dome.

For the user sensitivity study, the 10 selected aneurysms were independently segmented and their domes isolated by 2 users, using the segmentation protocol described above. The 3D surface models of the aneurysm along with its contiguous vasculature as segmented by both users is shown in Figure 38.

Once the aneurysms were segmented and isolated using the protocol, five size and six shape indices, discussed earlier, were calculated for all of these 20 models. For visual examination of the independently segmented and isolated surfaces and their boundaries, refer Figure 39. Observation of Figure 39 shows that extracted boundaries, in general, matched closely. However the neck plane boundary showed varying levels of disparity between user models with Subject 7 showing the greatest shape difference.

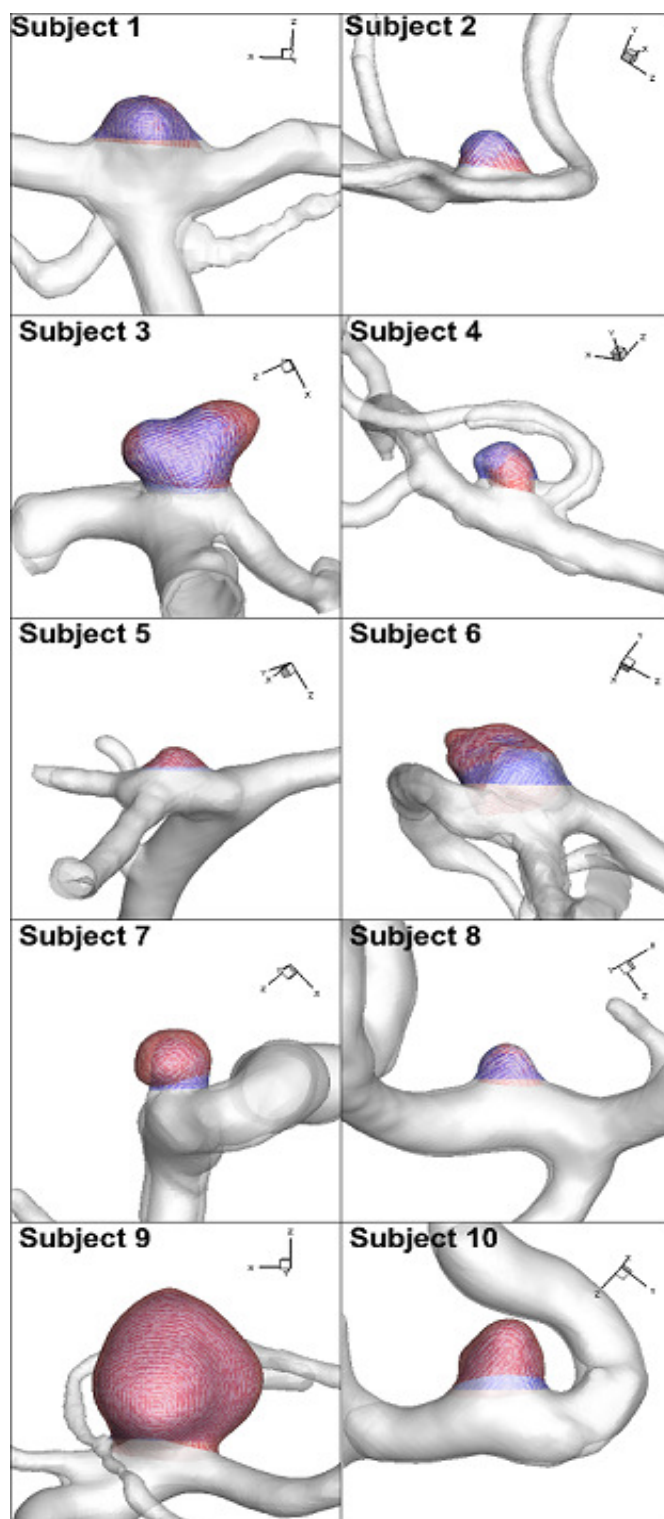


Figure 37: 3D segmentation of aneurysm (highlighted in color) and its contiguous vasculature. Segmentation by user 1 shown in red and by user 2 shown in blue.

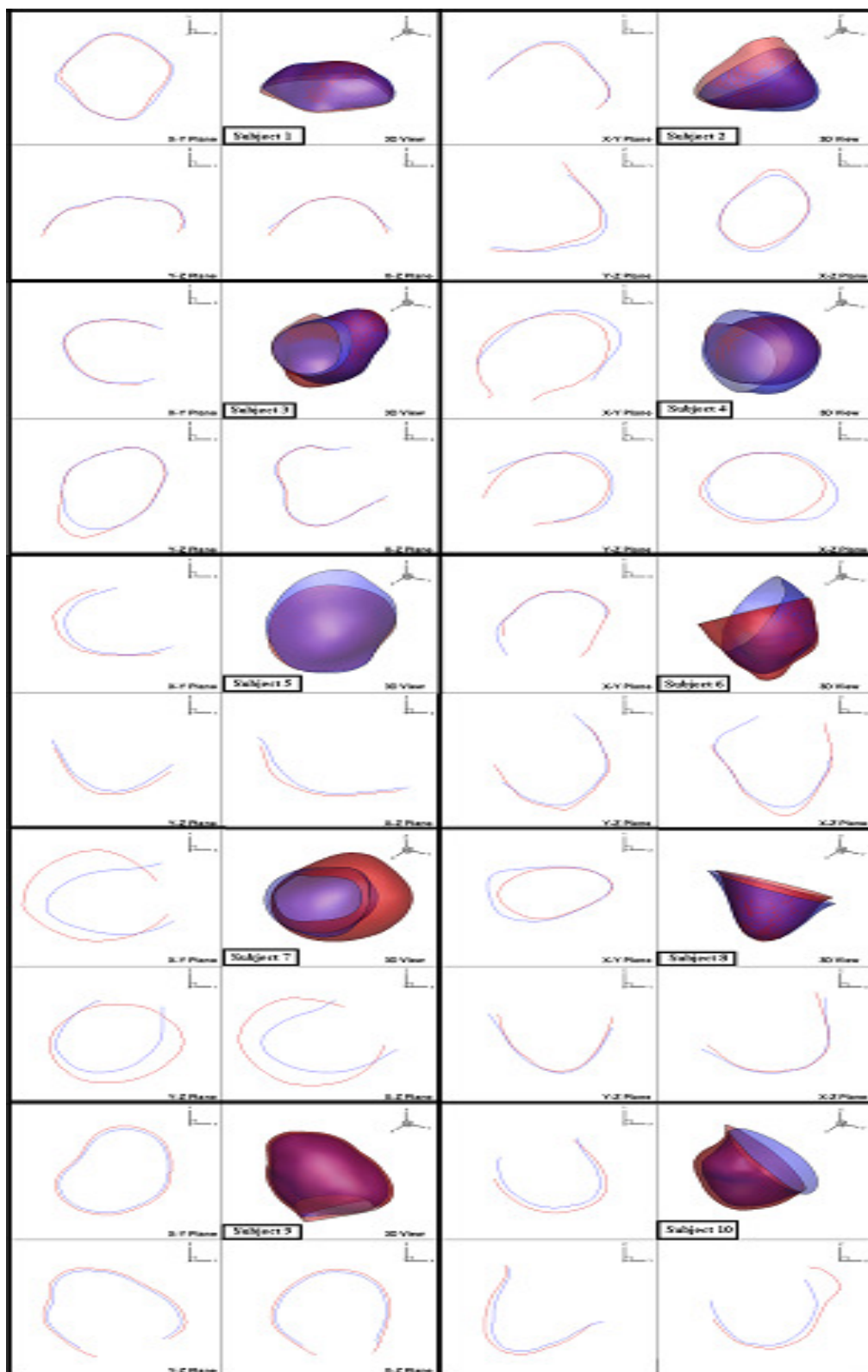


Figure 38: Three cross sections of all 10 aneurysm models. Highlighted in Red Models by User 1, in blue – Models by User 2

As seen in the study of sensitivity to modalities, discussed in Chapter 4, certain size and shape indices are inherently influenced by the location of the isolation plane chosen by each user. Also, observation of Figure 39 shows variation in neck plane selection between the two users. To eliminate subjectivity, if any, in the selection of the cutting plane, aneurysm isolation was performed by one of the users instead of two and index calculation was repeated for the newly isolated models.

8.3 Results and Discussion

The indices calculated for aneurysm models isolated using independent cutting planes and common cutting planes are shown in Table 9.

In order to better compare the morphometric indices generated for each user's isolated aneurysm model, a Bland Altman analysis was performed. Bland-Altman analysis assesses the agreement between users for all eleven indices calculated on aneurysm models isolated using independent and common cutting planes. For each index, the difference in measurement between the two users (y-axis) is plotted against their mean (x-axis). The line at the center of the plot represents the 'bias' which is the mean of the means. The dotted lines represent the limits of agreement ($\text{bias} \pm 1.96 * \text{std.dev of means}$). The Bland-Altman plot for each of the size indices calculated for aneurysm-models isolated using independent cutting planes and common cutting planes are shown in Figure 40. Similarly, the Bland-Altman plots for each of the shape indices are shown in Figure 41.

Indices	Independent Cutting Plane		Common Cutting Plane	
	User 1 Models	User 2 Models	User 1 Models	User 2 Models
Height (mm)	3.3 ± 2.1	3.6 ± 2.6	3.2 ± 2.0	3.3 ± 2.1
Max. Diameter (mm)	4.4 ± 1.7	4.4 ± 1.7	4.3 ± 1.7	4.4 ± 1.7
Neck Diameter (mm)	4.0 ± 1.1	3.8 ± 1.2	4.0 ± 1.2	3.8 ± 1.3
Aspect Ratio	0.8 ± 0.4	0.9 ± 0.5	0.8 ± 0.3	0.8 ± 0.4
Volume (mm ³)	54.0 ± 85.3	63.3 ± 103.5	52.9 ± 85.2	60.3 ± 99.2
Surface area (mm ²)	51.9 ± 55.8	58.6 ± 64.4	50.9 ± 55.7	55.8 ± 61.0
Bottleneck Factor	1.1 ± 0.2	1.2 ± 0.3	1.1 ± 0.2	1.1 ± 0.3
Bulge Location	0.1 ± 0.2	0.2 ± 0.2	0.1 ± 0.2	0.2 ± 0.2
Undulation Index	0.03 ± 0.01	0.02 ± 0.01	0.02 ± 0.01	0.02 ± 0.02
Non Sphericity Index	0.08 ± 0.04	0.1 ± 0.04	0.08 ± 0.03	0.09 ± 0.04

Table 9: Average and standard deviation of size and shape indices calculated across 10 aneurysm models.

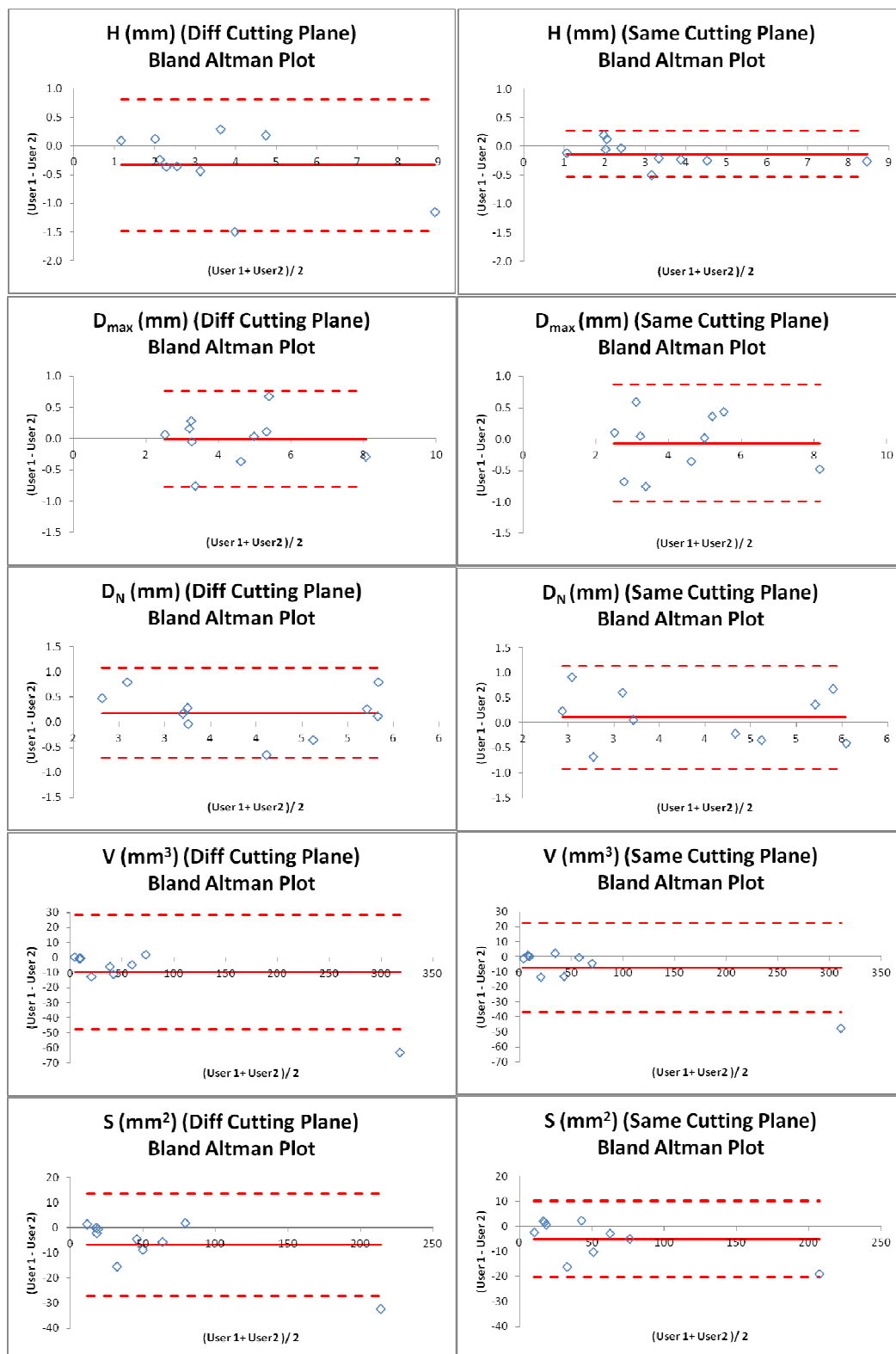


Figure 39: Bland-Altman plots for size indices calculated for each aneurysm model, isolated using different and same cutting planes.

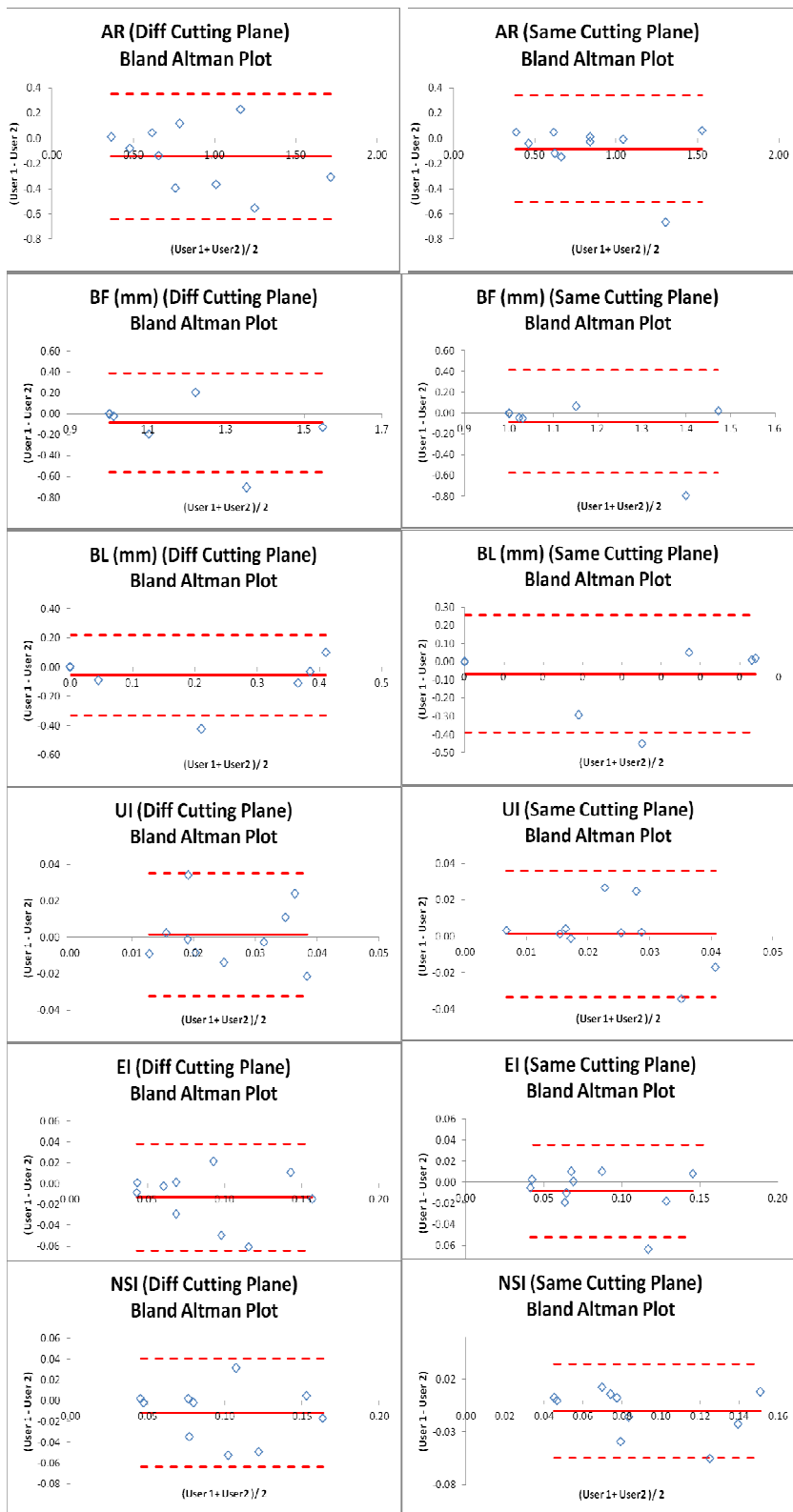


Figure 40: Bland-Altman plots for shape indices calculated for each aneurysm model, isolated using different and same cutting planes.

The Bland-Altman plot is a method to quantify the repeatability of a method. It can be done using the coefficient of repeatability which can be defined as:

$$\text{The coefficient of repeatability(CR)} = 1.96 * \sqrt{\frac{\sum (d_2 - d_1)^2}{n-1}}$$

where d_1 and d_2 are the two measurements made. The ideal CR, when a method is completely repeatable should be equal to zero. The CRs for each of the indices are listed in Table 10.

Domes Isolated With Different Planes		Domes Isolated With Same Planes	
Indices	CR	Indices	CR
Height (mm)	1.147070	Height (mm)	0.398455
Max. Diameter (mm)	0.765471	Max. Diameter (mm)	0.929561
Neck Diameter (mm)	0.765471	Neck Diameter (mm)	1.026989
Aspect Ratio	0.496545	Aspect Ratio	0.423620
Volume (mm ³)	37.837186	Volume (mm ³)	29.701554
Surface area (mm ²)	20.503732	Surface area (mm ²)	15.201111
Bottleneck Factor	0.472946	Bottleneck Factor	0.496858
Bulge Location	0.275060	Bulge Location	0.324069
Undulation Index	0.033651	Undulation Index	0.034733
Non Sphericity Index	0.051821	Non Sphericity Index	0.044219

Table 10: Coefficient of Repeatability (CR) calculated for models segmented by User1 and User 2.

From the table, it is seen that CR reduces for ten out of eleven of the indices while the same cutting plane is used. The measurement of aneurysm height (H) is found to improve significantly on using the same cutting plane. This is possibly because this index H is not only dependent upon the placement of the cutting place but is also dependent upon the angle of the cutting plane. The cutting plane angle defines the axis along which H is measured and thus, using the same cutting plane improves this index considerably. With the usage of same cutting, there is also a considerable improvement in V, SA and AR as can be seen by the reducing values of CR for these indices in Table 13. CR for some indices (Dmax, Dn, BF, BL, UI and NSI) increases with the use of the same cutting plane. While the increase is more drastic in some than in the others, this worsening of variability in measurement of these indices could point to the importance of segmentation at the neck region of the IA geometry. Increase in CR, in spite of using the same cutting plane on the 2 3D surface models segmented by 2 different users, shows that although the neck plane location and neck plane angle are similar, the differences in segmentation does causes some variability in index calculation.

8.4 Conclusion

In a large cohort study, segmentations performed by multiple users will cause a small amount of variability in the results. Variability in certain indices can be reduced by one user consistently choosing cutting planes to isolate the IA dome from its contiguous vasculature. But it is necessary that while interpreting the results CR calculated for each index be taken into account. Index measurements lower than the value of CR for that particular index should be disregarded or interpreted with utmost caution.

CHAPTER 9

LONGITUDINAL COHORT STUDY

9.1 Data Collection

A total of 198 study subjects were recruited at Penn State Hershey Medical Center, Massachusetts General Hospital, Thomas Jefferson University Hospital and University of Iowa Hospitals and Clinics. All had at least one unruptured IA and were placed on follow-up without immediate intervention. Scans were obtained in any one of the four modalities—Computed Tomography Angiography (CTA), Time-of-Flight Magnetic Resonance Angiography (TOF-MRA) and Contrast-Enhanced MRA (CE-MRA). Most scans were of the CTA modality as seen in Figure 41.

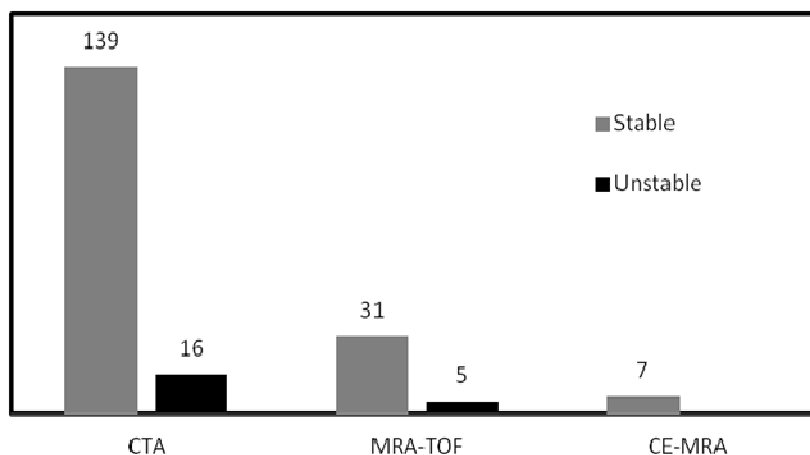


Figure 41: Bar chart showing number of patient scans in each of the three imaging modalities.

About 364 patients had been recruited and their initial scans were sent to our group from the clinics. Patient scans are transferred in a standard medical image format-DICOM. All collected images were inspected to ensure that they were suitable to be

included in the study. Images that were not of the required format (2D DICOM slices of 3D volumetric data), images of poor resolution and images with scanning artifacts could not be used for segmentation since they would not yield accurate 3D models. In total, 294 scans were reviewed and 198 patient-specific cerebral aneurysms were chosen for this study. Along with the dicom slices of the 3D volumetric scans, the clinically diagnosed location of the aneurysm was also provided. Further, additional relevant information (such as if the IA belonged to a multiple constellation, whether the aneurysm was fusiform or saccular and if there were aneurysms for that patient that were previously treated) was also provided by the clinics to our group. Our group was deliberately blinded from any information about the IA that might reveal growth or rupture information while these IAs were being followed. Initial scans were collected and the morphometric analysis was performed without receiving any information about their growth or rupture status.

IAs in the study were predominantly located in the anterior circulation as seen in Figure 42 where most of the IAs were ICA and MCA aneurysms.

The X and Y resolutions range from 0.20 to 0.86 mm with an average of 0.41 mm in each direction and the slice spacing (which is the resolution in the Z direction) ranged from 0.30 to 1.00 mm with an average of 0.64 mm.

Of the 198 aneurysms that were being followed 132 were single aneurysms and 66 IAs were part of a multiple constellation. These 66 aneurysms, that were part of multiple constellations, were from 57 unique patients.

All of the 198 IAs in this study were saccular in shape. Out of the scans that were reviewed, there were 2 aneurysms that contained thrombus and these 2 aneurysms were left out from the study as discussed earlier in Chapter 2.

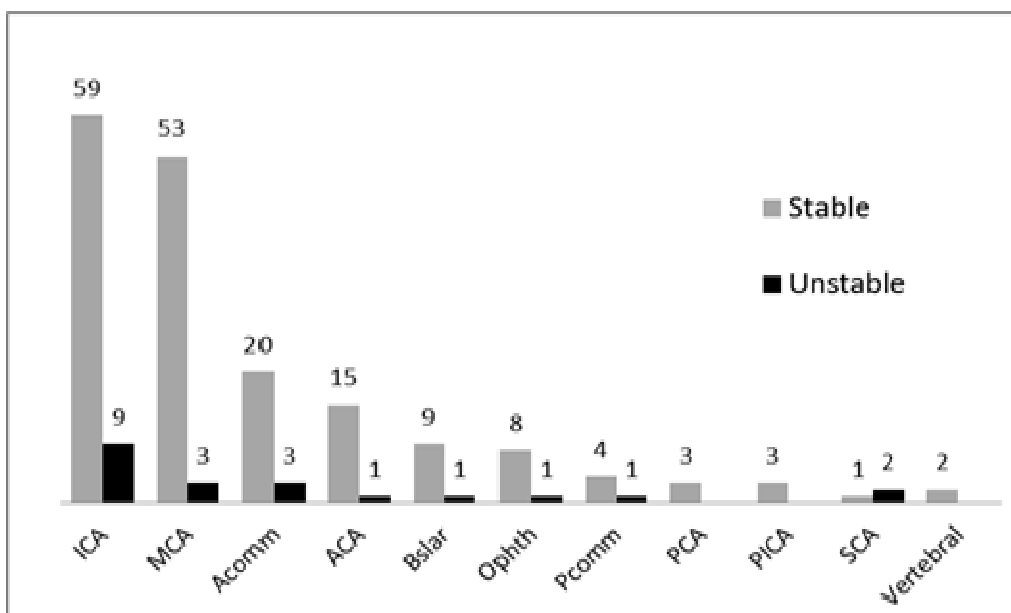


Figure 42: Bar chart showing the number of aneurysms at each location.

9.2 Segmentation and Isolation

Dicom images from the initial 3D scans of the 198 aneurysms were archived. The segmentation protocol discussed in Section 7.2.2 was used and each of these IAs were segmented by four user. All four users were trained by segmenting from scans of cerebral vasculature silicone phantom with an ACOM aneurysm. This silicone phantom is discussed in Section 5.2.2. Users started segmenting patient aneurysms after a certain level of comfort and expertise was attained with the segmentation methods and protocol. It was ensured that IA geometries along with all of their contiguous vasculature were segmented. The aneurysm dome was then isolated from its contiguous vasculature by one consistent user for all the 198 aneurysm models. 3D surface models of isolated IA domes were remeshed and these models in each of the 11 locations (listed in Figure 43) are each shown in Figure 44-51.



Figure 43:3D models of isolated ICA aneurysms.

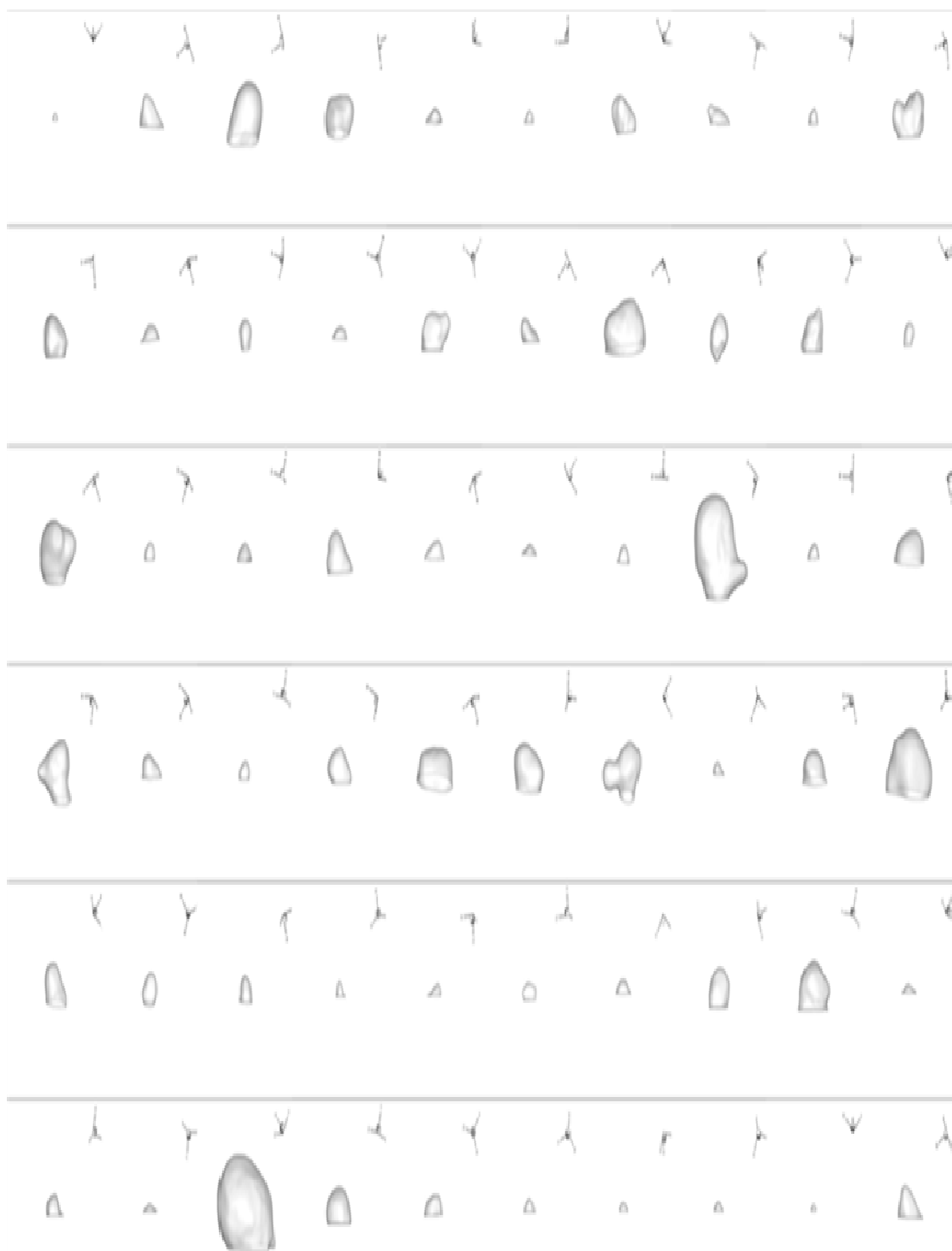


Figure 44: 3D models of isolated MCA aneurysms.

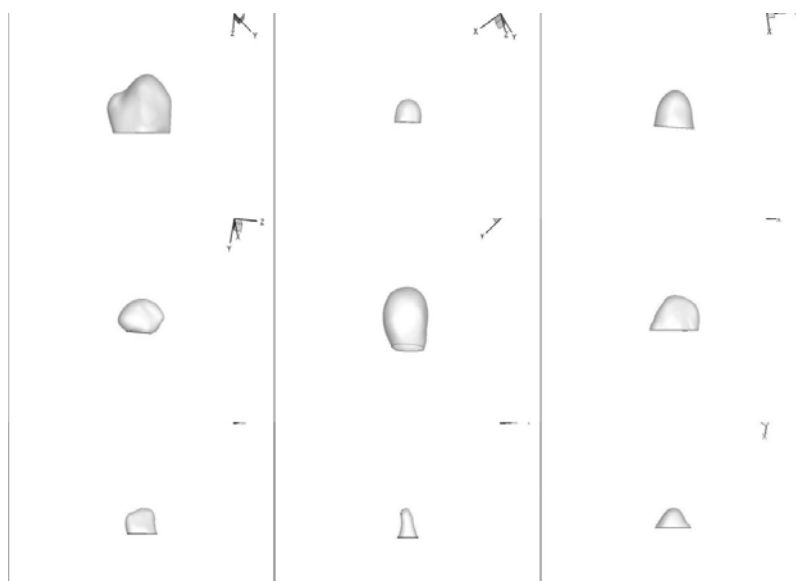


Figure 45: 3D models of isolated Ophthalmic aneurysms.

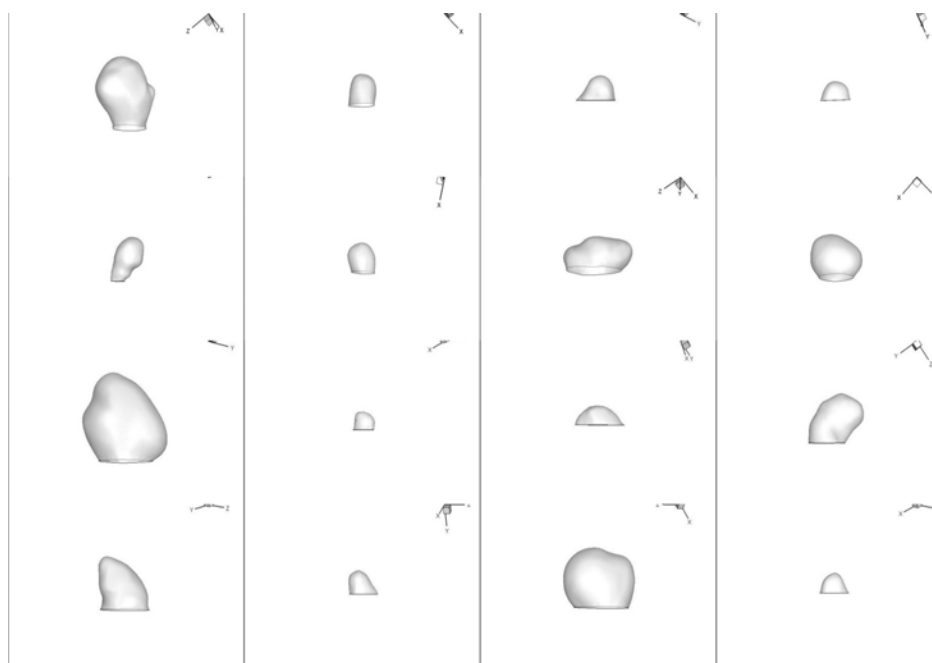


Figure 46: 3D models of isolated ACA aneurysms.

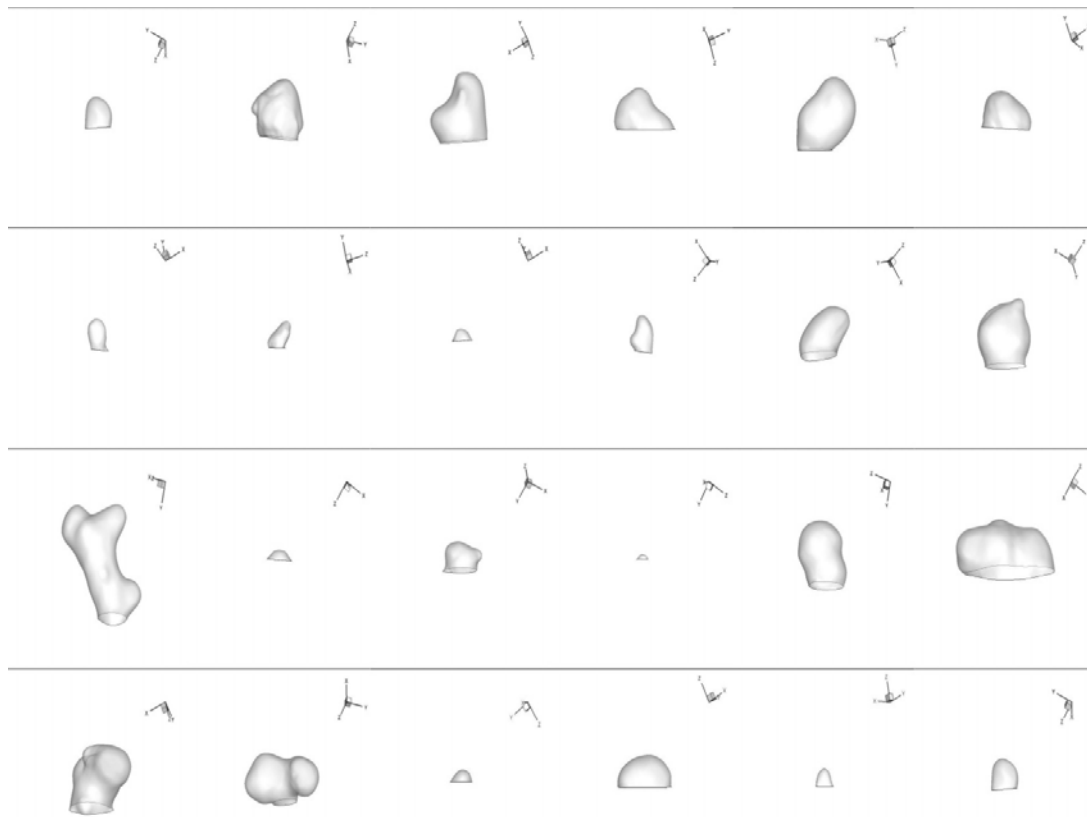


Figure 47:3D models of isolated AComm aneurysms.

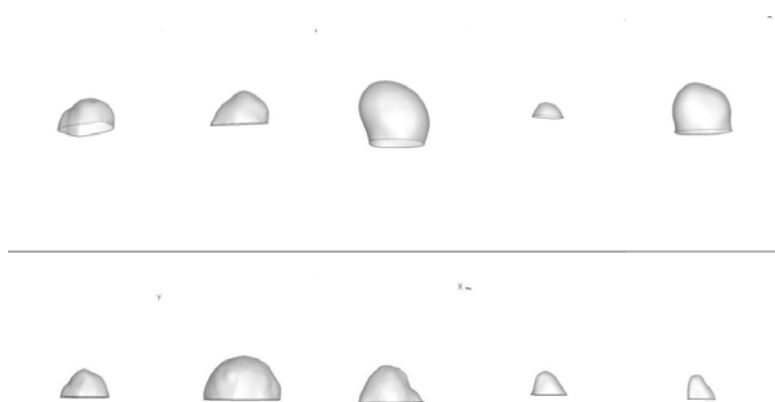


Figure 48:3D models of isolated Bslar aneurysms.

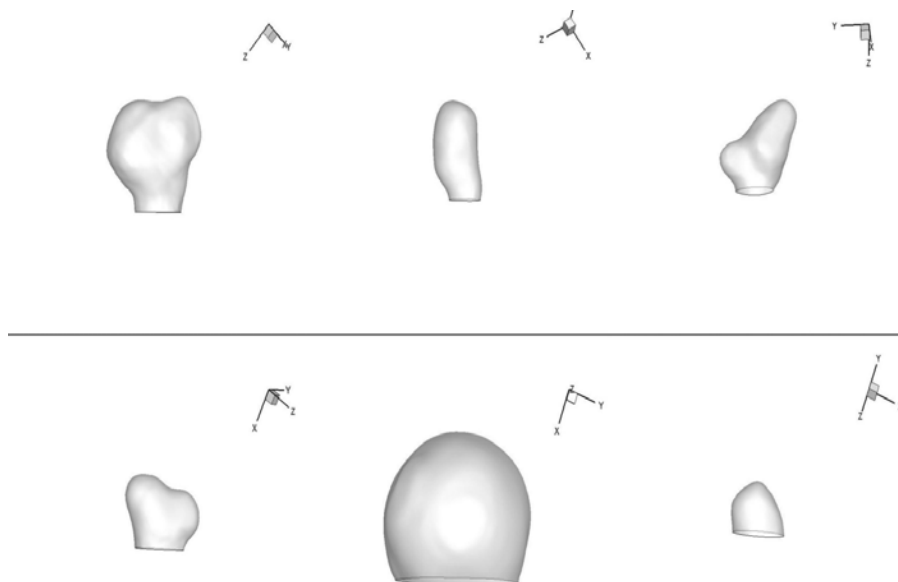


Figure 49:3D models of isolated PComm aneurysms.

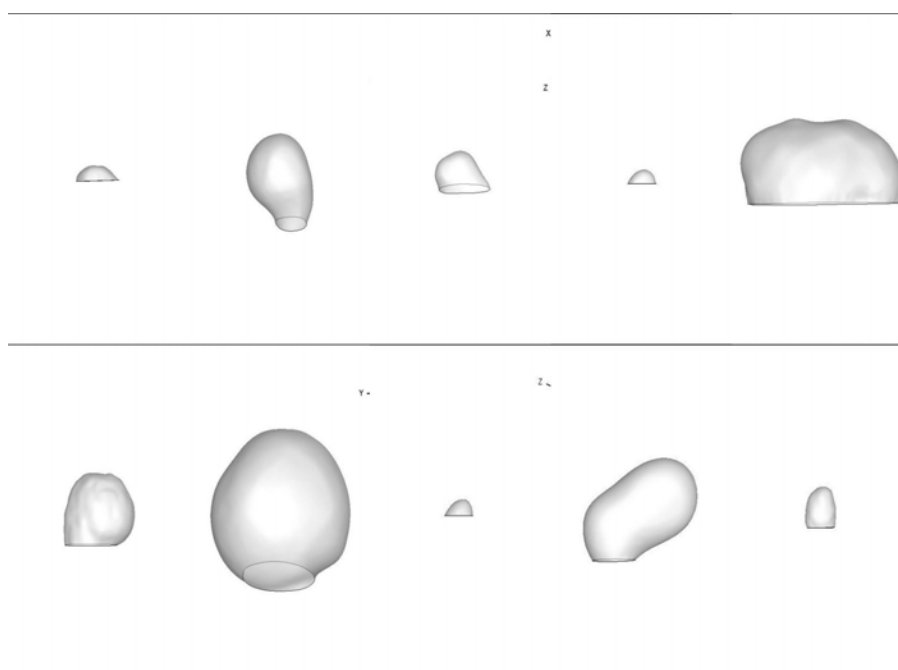


Figure 50:3D models of isolated aneurysms located at PCA, PICA, SCA and Vertebral arteries.

9.3 Morphometric Analysis of Initial Scans and Clinical Follow-up

After these 198 models were segmented, five size and six shape indices were calculated on the isolated aneurysm geometry: Size indices - Height (H), max. diameter (Dmax), neck diameter (Dn), volume (V), and surface area (SA); Shape Indices - Undulation index (UI), Aspect ratio (AR), Ellipticity index (EI), Non-sphericity index (NSI), Bulge Location (BL), and Bottleneck factor (BF); Wall Tension index - the 95th percentile max. principal stress (Peak Wall Stress - PWS).

Since researchers were blinded from the clinical status on growth or rupture during the morphometric analysis, follow-up statuses on each of these aneurysms were collected after the morphometric analysis was completed. During follow-up, aneurysms were labeled as “grown” or “stable” by radiologists in each clinical center upon examining angiograms or maximum intensity projections. As part of this clinical assessment, size measurements were made on the IA geometry during every follow-up visit and their growth status was determined by comparing measurements made on current scans to such measurements made on images from the previous visit. Study subjects were assigned to one of two groups based on clinical outcome: Unstable group (grown or ruptured) or Stable group (remained same or lesser size).

These 198 aneurysms were followed for an average of 607 days. Over the follow-up period, 26 were lost to follow up, 150 were found to be stable, 20 had grown, 1 deceased, 1 could not be located on the angiogram and none had ruptured. Also, of the total 198, 53 were electively treated during follow-up period.

Statistical analysis was then performed on the computed morphometric and wall tension indices. Non-parametric Mann-Whitney U-tests were performed for each morphometric index and peak wall stress to test for statistically significant difference between the stable ($n_1 = 150$) and the unstable group ($n_2 = 20$). None of the indices differentiated the two groups in a statistically significant manner.

Indices	Stable (N=150) (min–median–max)	Unstable (N=20) (min–median–max)	U test p-value
H (mm)	0.68–3.35–12.12	1.08–3.43–8.19	0.81
Dmax (mm)	1.51–4.24–16.44	2.08–3.54–8.72	0.11
Dn (mm)	1.51–3.86–15.58	1.33–3.30–8.26	0.08
V (mm ³)	0.75–29.42 –1371	2.26–24.12 –292.8	0.39
SA (mm ²)	3.22–42.88–495.1	6.92–35.86–177.5	0.45
AR	0.28–0.86–4.94	0.42–0.91–3.49	0.21
BF	1.00–1.02–2.16	1.00–1.04–2.67	0.68
BL	0.00–0.21–0.74	0.00–0.20–0.56	0.43
UI	0.001–0.021–0.230	0.002–0.019–0.106	0.89
EI	0.015–0.089–0.285	0.039–0.093–0.232	0.85
NSI	0.017–0.097–0.331	0.040–0.101–0.248	0.93
PWS (MPa)	0.073–0.356–1.012	0.140–0.322–0.670	0.38

Table 11: Range of measurement for each index measured on 199 aneurysm dome models.

In order to get a visual impression of the distribution of measured indices across the patient population, histograms of a few indices are listed in Figure 52, 53 and 54.

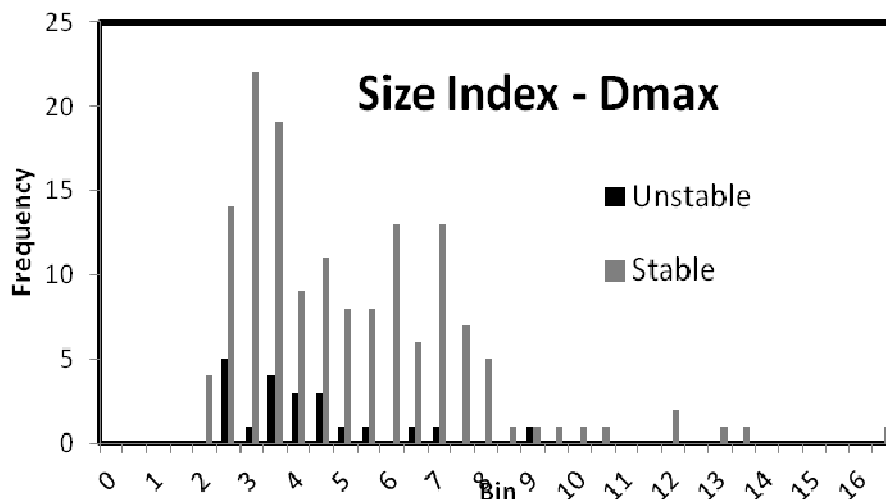


Figure 51: Histogram showing distribution of Dmax ranging from 1.4 to 16.4 mm.

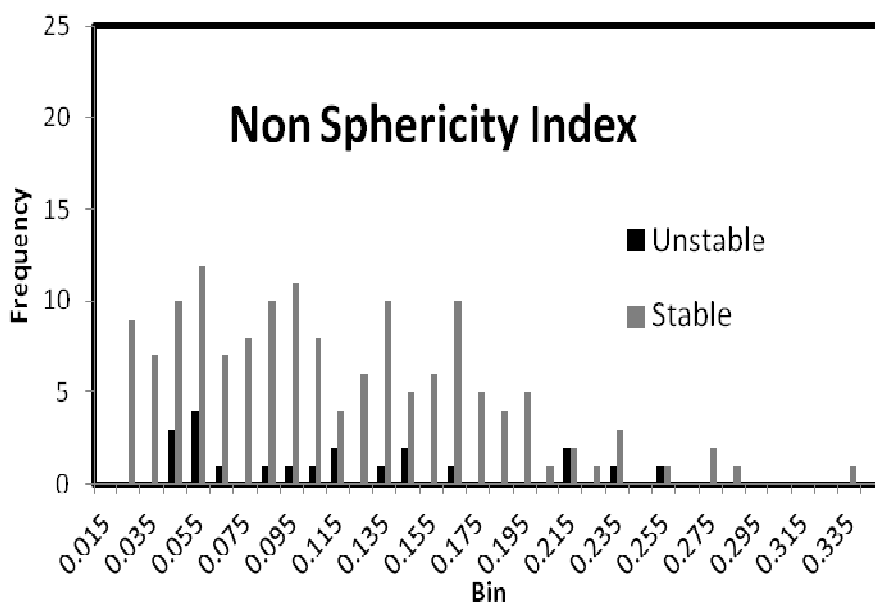


Figure 52: Histogram showing distribution of NSI ranging from 0.27 – 4.94.

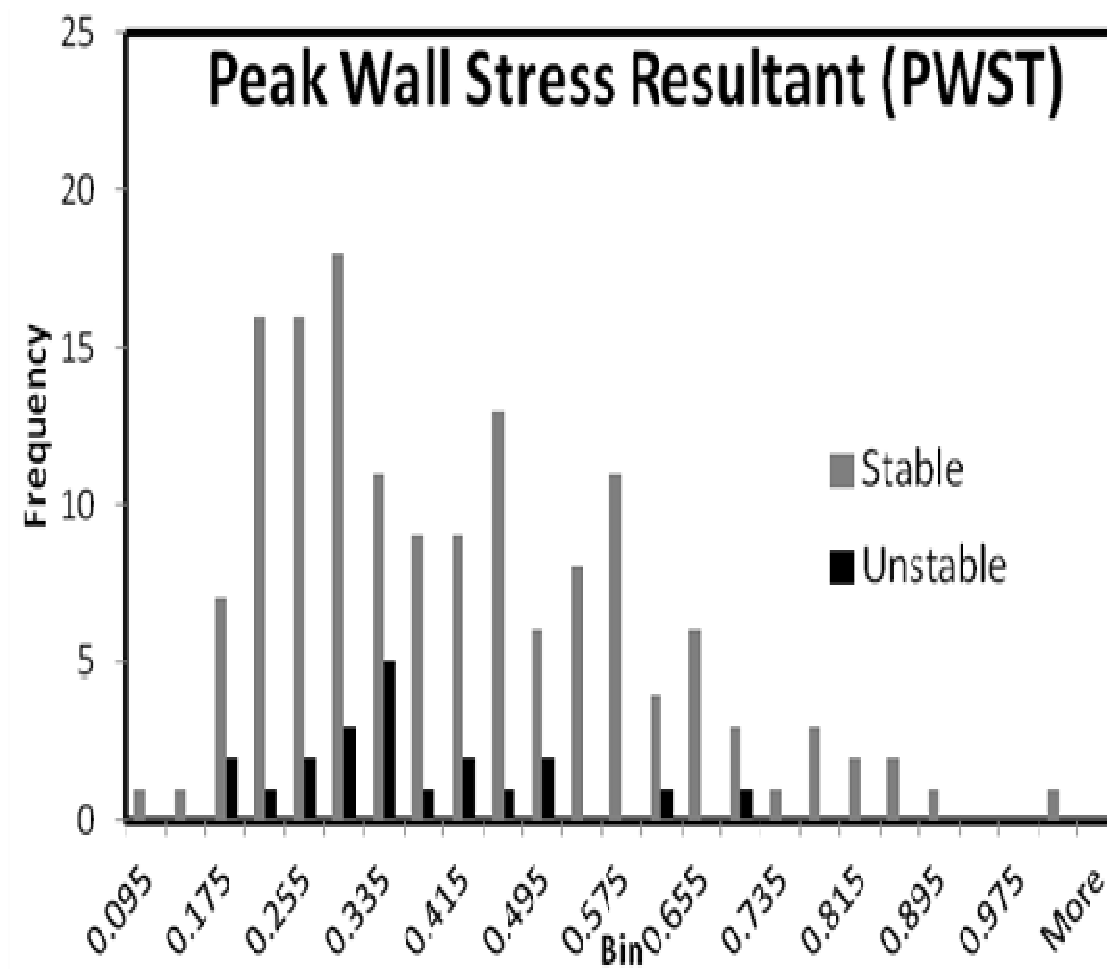


Figure 53: Histogram showing distribution of PWS ranging from 0.073 – 1.012 MPa.

Receiver Operating Characteristics (ROC) curve analysis was performed on each morphometric index to assess the predictability of risk rupture. ROC results were consistent with the Mann-Whitney U test findings i.e. none of the indices were able to distinguish unstable aneurysms from the stable ones. This can be observed in the ROC curves and the calculated Area under the curve (AUC) for each of these indices, shown in Figure 55 and Table 12 respectively.

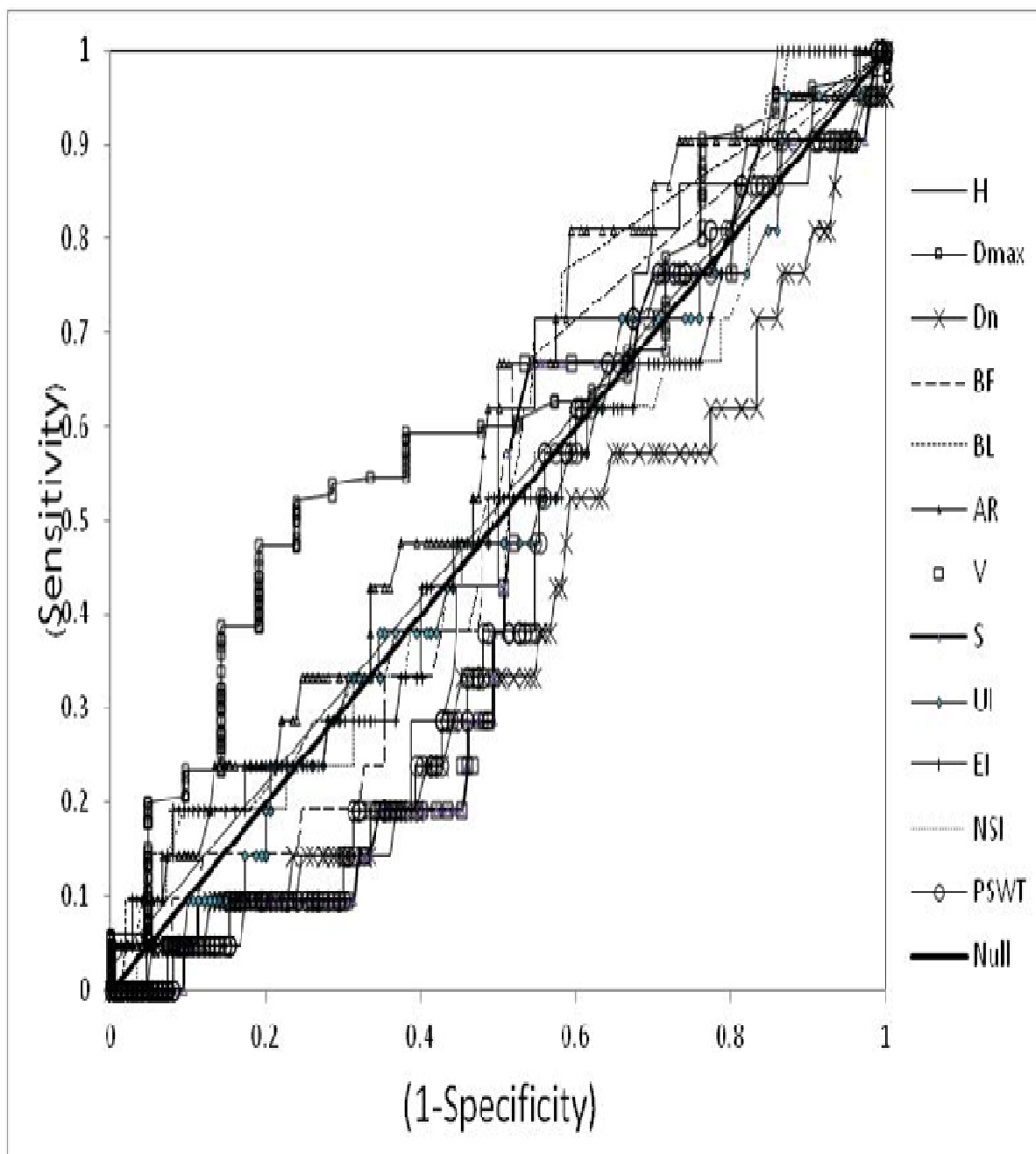


Figure 54: Receiver Operating Characteristics (ROC) curves for each index. “Null” represents zero predictive capability. Most indices are close to “Null” indicating the absence of their predictive capability.

Indices	H	Dmax	Dn	V	S	AR	BF	BL	UI	EI	NSI	PW S
AUC	0.47	0.39	0.38	0.44	0.45	0.58	0.51	0.55	0.49	0.51	0.50	0.44

Table 12: Area under the ROC curve (AUC) calculated for the each index. AUC of “Null” is 0.50.

9.4. Morphometric Analysis of Follow-up scans of Unstable Aneurysms

On detail reading of the radiology reports for the unstable group of aneurysms, increase in their size ranged from 0.5mm to 12mm in our study population. Some aneurysms, which were noted as larger in one dimension, were smaller in other dimensions.

In addition to clinical status of growth or rupture, clinical measurements of diameter were collected from the radiology reports in the clinical centers. It was available for 108 aneurysms and these 108 clinically-provided diameters were compared to maximum diameter (Dmax) calculated during the morphometric analysis. Comparison of clinical Dmax to measured Dmax of the initial aneurysm geometry shown in Figure 56 reveals a measurement error of ± 1 mm. 7 of the stable aneurysms were, in fact, “smaller” according to radiological measurements reported. Hence, reported measurements needed to be validated with a more consistent method of measurement and “growth” needed to be assessed further.

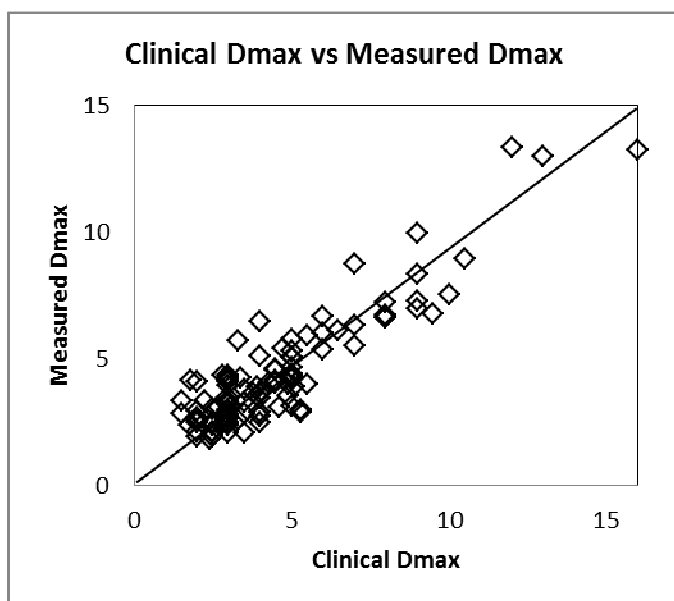


Figure 55: Comparison between maximum diameter measurements provided by clinics and maximum diameter data measured on isolated aneurysm models obtained after segmentation.

Latest follow-up scans of the 20 unstable aneurysms were collected from the clinical centers. Segmentations were performed on 17 of these aneurysms and their contiguous vasculature. Scan from 3 of these aneurysms could not be analysis due to the following reasons: 1) Scan quality insufficient for segmentation (2 ICAs) 2) Unavailability of 3D scan of IA before it was treated (AComm). The average (x, y, z) resolution of the 17 scans used for segmentation was 0.44 x 0.44 x 0.79 mm respectively. Users performing the segmentation process were blinded from growth or rupture status. During the analysis of the follow-up scans, aneurysm locations were identified and their segmentations were performed independently without referring to the analysis or geometries performed with the initial scans.

For qualitative assessment of change in IA morphology, geometries segmented from initial scans were registered with those segmented from latest follow-up scans. Using VMTK's centerlines algorithms [49], centerlines in both the initial and follow-up models of the aneurysms and their contiguous vasculature were computed. These models

were then registered using the VMTK's ICP registration algorithm [49]. Initial segmentations overlaid on follow-up segmentations are shown in the series of figures 57 – 60.

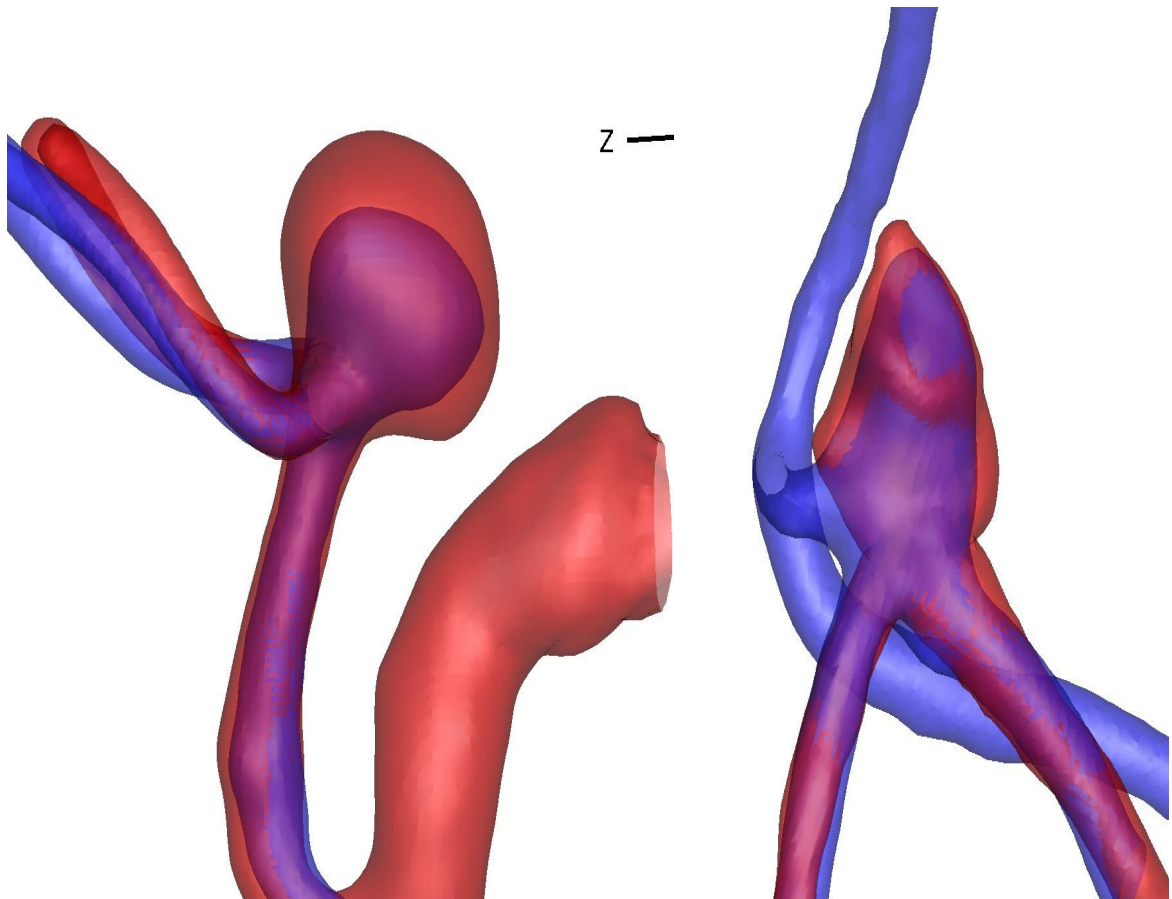


Figure 56: ACA aneurysms – initial (blue) and follow-up (red) segmentation. Follow-up segmentations show increase in aneurysms size.

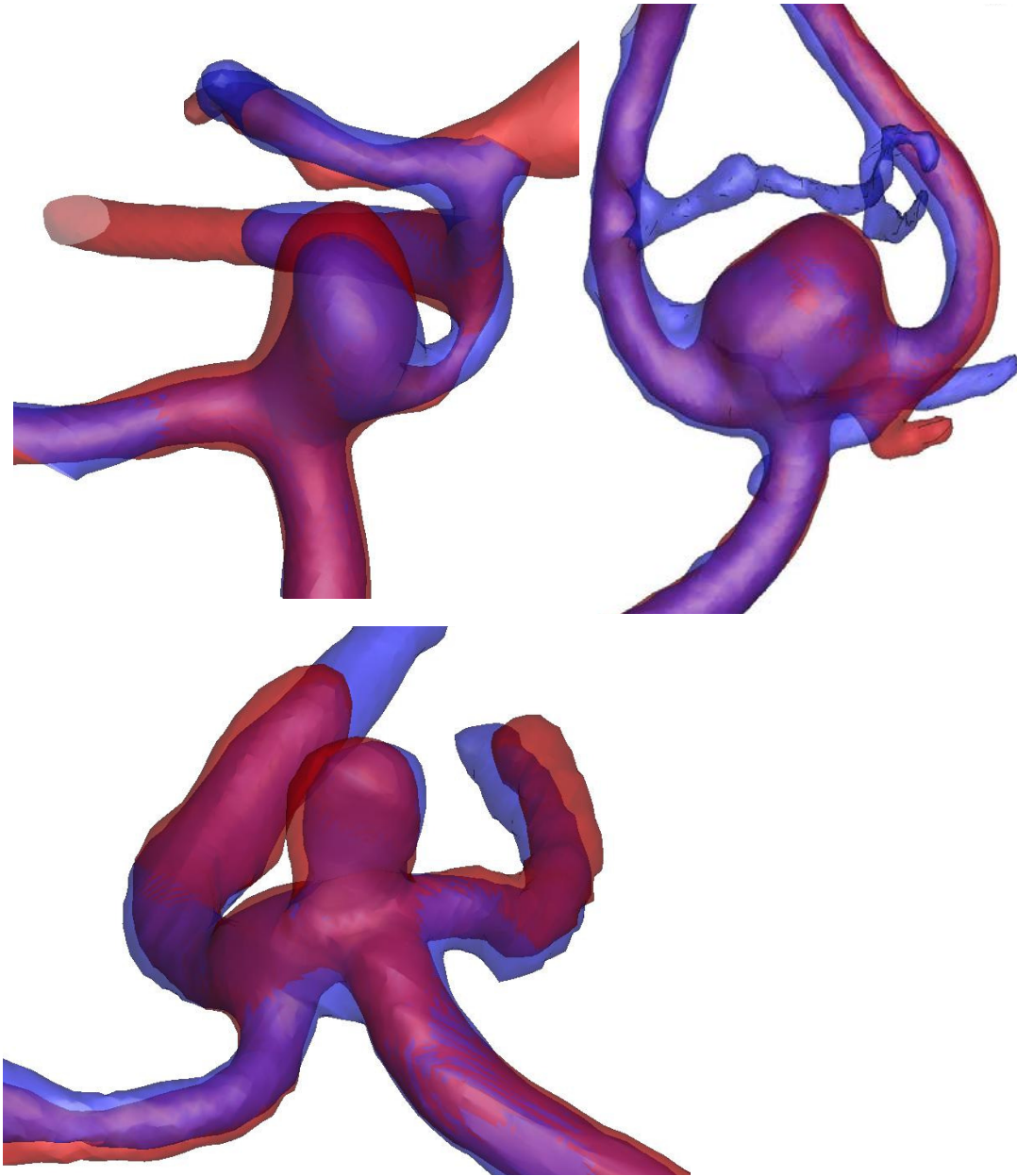


Figure 57: AComm aneurysms – initial (blue) and follow-up (red) segmentations. Follow-up segmentations show increased in aneurysm size.

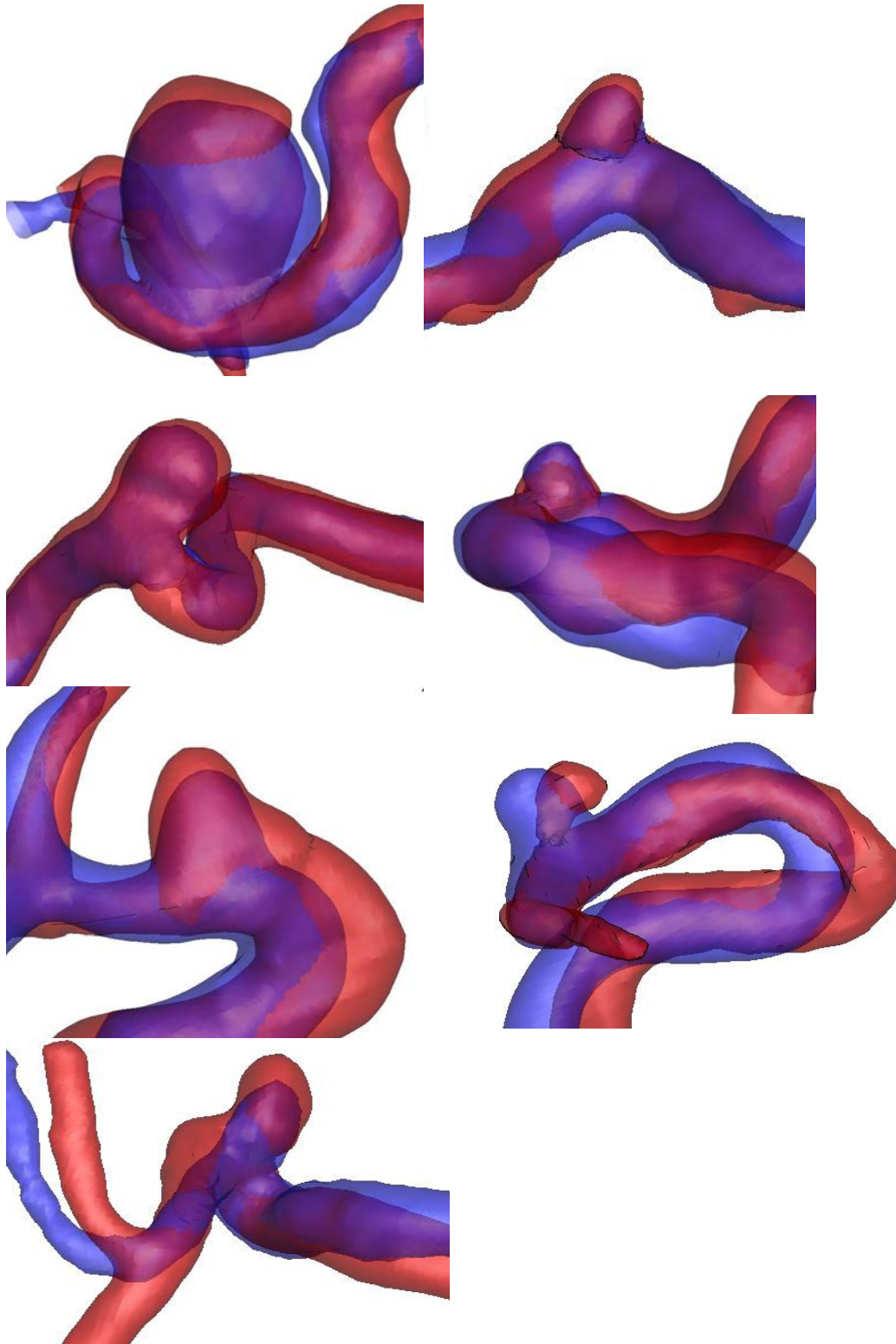


Figure 58: ICA aneurysms – initial (blue) and follow-up (red) segmentation. Follow-up segmentations show increase in aneurysms size.

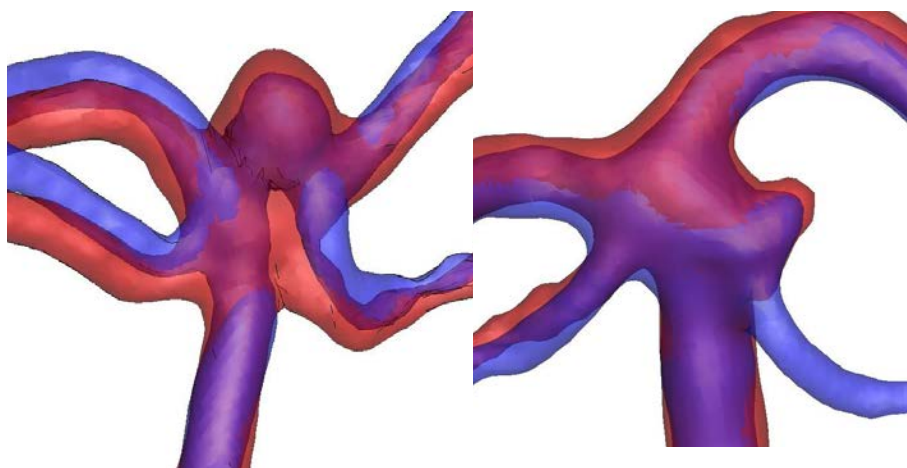


Figure 59: Basilar and SCA aneurysms – initial (blue) and follow-up (red) segmentation. Follow-up segmentations show increase in aneurysms size.

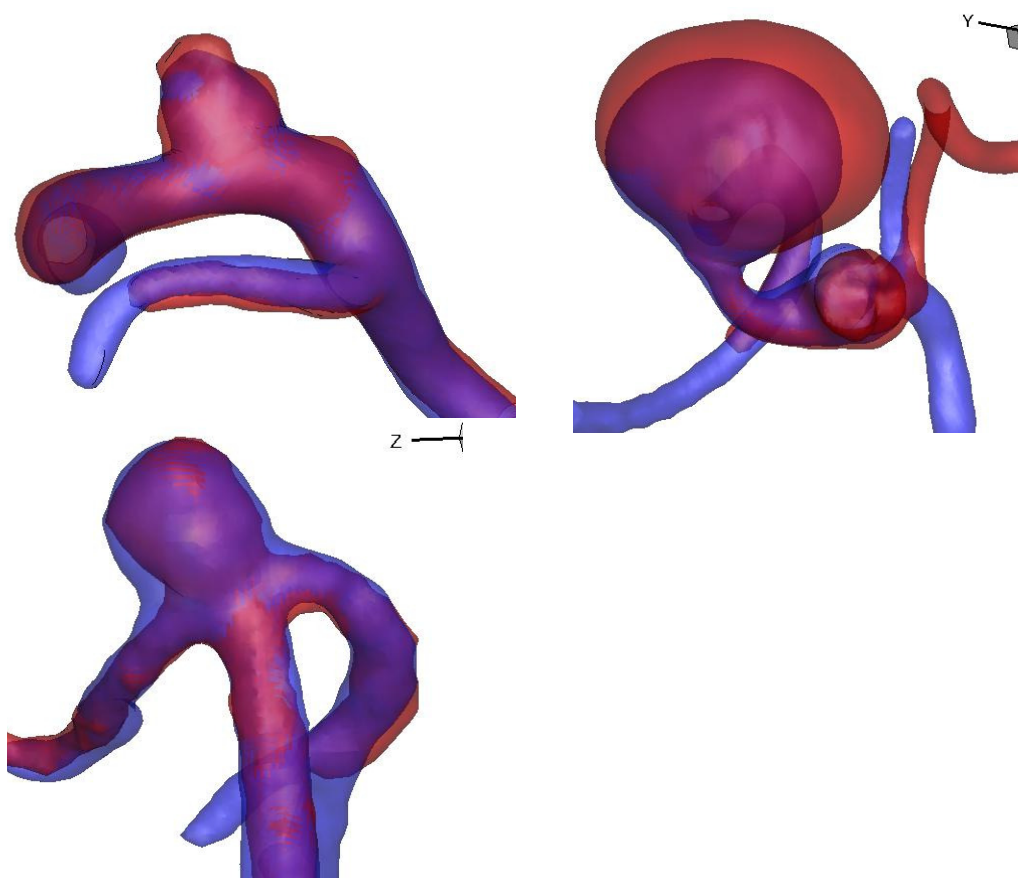


Figure 60: PComm and MCA aneurysms – initial (blue) and follow-up (red) segmentation. Follow-up segmentations show increase in aneurysms size.

For the quantitative assessment of “growth” or change in dimension from initial measurements to follow-up measurements, 5 size and 6 shape indices were calculated on the isolated aneurysm domes obtained from follow-up scan segmentations. Follow-up indices were then compared to the indices calculated for these aneurysms from the initial scans. This process was repeated in 17 aneurysms that were clinically determined to be unstable.

Indices	Change in Dimension		
	min	Median	max
H (mm)	-0.76	0.30	7.66
Dmax (mm)	-0.94	0.24	12.04
Dn (mm)	-1.91	0.25	8.29
AR	-0.50	0.02	1.09
BF	-0.02	3.5E-05	0.50
BL	-0.03	0.01	0.63
V	-22.44	6.45	1752.1
S	-12.25	7.02	576.68
UI	-0.09	0.02	0.15
EI	-0.10	0.02	0.13
NSI	-0.12	0.05	0.80
PWS	-0.46	0.04	0.58

Table 13: Increase in morphometric indices measured in 17 "unstable" aneurysms listed as min-median-max.

If “growth” is defined an increase in volume measured between initial and follow-up segmentations, 14 out of the 17 aneurysms had an increase in volume while 3 out of the 17 had a decrease in volume. In the 3 aneurysms that had decreased in volume (according to the comparison of morphometric analysis), 1 had increased in height by 0.34mm and the other 2 had increased in UI, EI and NSI. The overall assessment, from comparing the initial and follow-up morphometric analysis of “unstable” aneurysms, suggests that an aneurysm was deemed as clinically unstable if it appeared to have become bigger in volume, increased in size in one particular dimension or had developed irregular shape features. However, on comparing the amount of “growth” with the coefficient of repeatability (CR) obtained from the user sensitivity study, “growth” in most aneurysms was within the range of user variability. Measurement of indices and the observation of growth, especially in small aneurysms, fall within the margin of measurement error and cannot be used effectively to differentiate stable from unstable aneurysms. Therefore, in this study population, changes in IA morphology could not be confidently attributed to IA “growth”.

9.5 Discussion

Could aneurysm shape or some aggregate of size and shape be a risk factor for IA growth/rupture? We sought to test this hypothesis in a study design that is unique in many ways. It is the first large population study of longitudinal cohorts. The study population was prospectively recruited at multiple clinical sites. So far, most research groups, including ours, have studied ruptured aneurysms and compared them to unruptured in a retrospective fashion [24]. Although this is crucial to improve our understanding of the disease, identifying unstable aneurysms on their initial (unruptured) presentation aids in making treatment decisions. This study design helps better understand what aspects of unruptured IA geometry measured on initial presentation could potentially be used to make predictions instability of the lesion in future. Further,

patient population in this study was recruited from multiple clinical sites with a number of participating physicians. This helps eliminate selection biases that might occur from recruiting patients from the same clinical center. The use of patient data from multiple centers in multiple modalities increases the realism of the data collection process. This set of data contains all the realistic perturbations involved in the day-to-day assessment of unruptured intracranial aneurysms. Also, this study population was predominated by small aneurysms. While treatment decisions are straightforward in larger aneurysms, small aneurysms (<7mm) are usually placed on follow-up because of their lower risk of rupture. The physician's dilemma with whether to treat or to not treat IAs occurs predominantly in these smaller aneurysms. It is necessary that studies on unruptured IAs provide insights on the management of small IAs. 88% of IAs in our study population was less than 7 mm; these are precisely the kind where the operative decision needs to be made in the clinic. Small aneurysms are more difficult to analyze and are often not included in IA studies. This study provides more insight on tools that could be used for the improved management of small aneurysms. The hypothesis motivating this study is that aneurysm shape or some aggregate of size and shape may be a risk factor, especially in small aneurysms. Testing this hypothesis required that we quantify (i.e., characterize with numbers) the three-dimensional size and shape of the aneurysm. Novel methods drawn from fields such as computational geometry (e.g., ellipticity of the aneurysm) and biomechanics (e.g., pressure-induced tension in aneurysm tissue or blood flow characteristics) are leveraged to quantify the size and shape of IAs. This study has also used state-of-the-art 3D medical images, image processing techniques to capture shape features. Additionally, three independent studies were performed to assess different aspects of this multicenter, longitudinal cohort study. Each of these studies provides unique insights into the longitudinal cohort study and in turn, the understanding of intracranial aneurysm behavior. The role played by each of these independent studies in the assessment of the IA geometry in the longitudinal cohort study is discussed below.

9.5.1 Sensitivity to imaging modalities

This study was performed to assess the sensitivity of using scans from multiple modalities in this longitudinal cohort study. Regular clinical practice involves assessing intracranial aneurysms using scans of different modalities and the patient population of the longitudinal cohort study reflects this clinical reality. For purposes of the longitudinal cohort study, it was necessary to quantify the variability introduced in the segmented geometries and the calculated indices due to lumping data from multiple modalities in one study. In other words, if the same IA geometry was imaged using CTA, TOF-MRA, CE-MRA and 3DRA, will the segmented geometry look different (qualitative) and how much variability will the index measurements have (quantitative)? This question was answered using both a phantom geometry and using patient geometries. 3D segmentation, isolation and morphometric analysis on these IA geometries were performed using the same methods employed for the longitudinal cohort study. Comparisons of IA geometries obtained from scans of different modalities revealed that size and shape measures had minimal sensitivity to imaging modality in the IA geometries that were studied. In conclusion, the assessment of IA morphology was deemed to be not significantly affected by using data from scans of multiple modalities in the large cohort study. This allowed the longitudinal cohort study to contain data from different imaging modalities. However, in this study comparing modalities, patient IA geometries ranged in size from 4mm to 9mm while in the longitudinal cohort study they ranged from 1.5mm to 16mm. So, the effects of imaging modalities on smaller aneurysms were not analyzed. Clinical data collected for the longitudinal cohort study were predominantly CTAs (155) with a relatively low number of TOF-MRAs (36) and CE-MRAs (7). Although our group did not make a purposive decision on using CTA as a predominant imaging modality, this distribution in imaging modality provides more consistency in the analysis of smaller IA geometries as part of the longitudinal cohort study.

9.5.2 User Variability in the segmentation process

As part of the longitudinal cohort study, 198 aneurysms were analyzed and in order to handle the large volume of data, multiple users were to be involved in the 3D segmentation of IA geometries. Therefore, in addition to assessing sensitivity to imaging modalities, it was also necessary to assess the sensitivity of the 3D segmentation process when performed by multiple users. Ten aneurysms were selected from this large cohort and IA segmentation, dome isolation and morphometric analysis was performed on all of them by 2 different users. Although most surface features were captured by both the users in a similar fashion, there were differences in certain indices between the 2 users. Noteworthy differences were observed in the neck diameter measurements between the 2 users and so the morphometric analysis was repeated on IA domes isolated using the same cutting plane on models segmented by both users. This decreased variability in some indices while not on the others. This was because some indices were influenced by minor variations in the 3D segmentation in the neck area of the IA geometry. Hence a coefficient of repeatability was determined for each index to quantify variability in 3D surface models due to multiple users being involved in the segmentation process. This coefficient of repeatability was taken into account while assessing results of the longitudinal cohort study in addition to the dome isolation performed by a single user.

9.5.3 Role of Modeling Choices

Peak wall tension in IA geometry has been used as a combined measure of size and shape in this longitudinal cohort study of unruptured IAs. In the longitudinal cohort study, appropriate modeling parameters, that are to be applied across the patient population for the calculation of peak wall tension, were chosen after an assessment of the role of modeling choices was performed. For this assessment, a population of 26 IAs was used and peak wall tension was calculated in each of them using methods of different

levels of sophistication. While it is fair to assume that the closer the analysis is to physiological conditions the more accurate the results, do these assumptions change the stratification of IAs when they are applied uniformly across the patient population? This longitudinal cohort study did not include any patient specificity in the stress analysis other than the patient-specific IA geometries. Pressure, boundary conditions, wall thickness and material model of these IA geometries were to be kept consistent across the population since they were not available at a patient specific level. Additional patient-specific morphological information like presence of thrombus, contact constraints with skull, etc were not modeled since the purpose of this index in the study was to serve as an index of morphology. Results of this study showed that peak wall tension can be calculated using simpler methods without the simplicity on methodology causing much variation in inferences. In other words, the stratification of aneurysms based on simpler modeling parameters were almost the same as the stratification based on more sophisticated methods. Based on those results, the peak wall tension in this longitudinal cohort study was calculated by performing forward finite element analysis on the isolated IA dome using a hyperelastic polynomial material with a fixed neck and a pressure of 100 mmHg applied to its inner wall. This serves as an effective index of morphology with the size (not shape) of the IA geometry having a predominant effect on the index.

9.5.4 Limitations

Overall, results from this first longitudinal cohort study of unruptured IAs are not consistent with the hypothesis. There are however limitations in this study that should be considered in this context. First, the indices studied do not capture some key geometric features (e.g., size ratio [8], angulation of the IA with parent vessel) and hemodynamic characteristics. The study population size may not be powered enough considering the number of indices and the variances in the indices noted. There may be a selection bias in the study population. That is, the physician may judiciously be choosing out and treating

risky unruptured IAs leaving only those unruptured IAs which are predisposed to remain stable. Fifty three out of 198 aneurysms were electively treated during follow-up reducing average followup period of the study. Most IAs in the study were small resulting in poorer signal to noise ratio. Average x, y and z resolution of 3D diagnostic images used in this study was 0.4 x 0.4 x 0.6 mm. This resolution does not lend itself to analyzing geometrical features in small aneurysms and sometimes, in assessing minor changes in IA morphology. Also, noise in measurements at the clinic to ascertain growth status and in segmentation at the analysis lab may introduce some fuzziness in the numbers. The isolation of the sac from the vessels involves subjectivity that may affect estimates as well.

9.5.5 Future Studies

For future analysis, this cohort of aneurysms should be analyzed with additional morphometric indices that address the limitations of the indices used currently. An automatic method of aneurysm isolation should be used so that it does not introduce user variability into the analysis. Hemodynamic metrics and their potential correlations with the morphometric indices should be calculated. This would reveal effects of blood flow in IAs and its relationship with various flow patterns to shape features. Also, in addition to the current cohort of unruptured intracranial aneurysms placed on follow-up, two other patient cohorts should be considered – unruptured intracranial aneurysms chosen for immediate treatment and intracranial aneurysms that were ruptured at first presentation. Prospective studies that include these cohorts could eliminate the selection bias in IAs that are placed on follow-up.

9.6 Conclusion

In conclusion, the results of this large population cohort study are not consistent with the hypothesis that many previously reported metrics of aneurysm morphology can serve as prognostic indicators of longitudinal outcome. The results of this study show that

size or shape measures obtained from initial presentation of unruptured IAs, in this patient population, is not predictive of instability. Additional studies comparing patient cohorts containing unruptured aneurysms that were placed on follow-up vs. unruptured aneurysms that were treated immediately would provide more insights on the representativeness of this study's patient population. Therefore, if this study population is representative of the general population of unruptured intracranial aneurysms, IA morphology measured in terms of the size and shape indices will not be able to differentiate stable from unstable aneurysms.

REFERENCES

1. Weir, B., *Unruptured intracranial aneurysms: a review*. J Neurosurg, 2002. **96**(1): p. 3-42.
2. Rinkel, G.J., et al., *Prevalence and risk of rupture of intracranial aneurysms: a systematic review*. Stroke, 1998. **29**(1): p. 251-6.
3. Wiebers, D., *Unruptured intracranial aneurysms: natural history, clinical outcome, and risks of surgical and endovascular treatment*. lancet, 2003. **362**.
4. Juvela, S., M. Porras, and K. Poussa, *Natural history of unruptured intracranial aneurysms: probability of and risk factors for aneurysm rupture*. J Neurosurg, 2008. **108**(5): p. 1052-60.
5. Molyneux, A.J., et al., *International subarachnoid aneurysm trial (ISAT) of neurosurgical clipping versus endovascular coiling in 2143 patients with ruptured intracranial aneurysms: a randomised comparison of effects on survival, dependency, seizures, rebleeding, subgroups, and aneurysm occlusion*. lancet, 2005. **366**(9488): p. 809-17.
6. Molyneux, A., et al., *International Subarachnoid Aneurysm Trial (ISAT) of neurosurgical clipping versus endovascular coiling in 2143 patients with ruptured intracranial aneurysms: a randomised trial*. lancet, 2002. **360**(9342): p. 1267-74.
7. *Unruptured intracranial aneurysms--risk of rupture and risks of surgical intervention. International Study of Unruptured Intracranial Aneurysms Investigators*. N Engl J Med, 1998. **339**(24): p. 1725-33.
8. Villablanca, J.P., et al., *Detection and Characterization of Very Small Cerebral Aneurysms by Using 2D and 3D Helical CT Angiography*. AJNR Am J Neuroradiol, 2002. **23**(7): p. 1187-1198.
9. Winn, H.R., et al., *The long-term outcome in patients with multiple aneurysms. Incidence of late hemorrhage and implications for treatment of incidental aneurysms*. J Neurosurg, 1983. **59**(4): p. 642-51.
10. Ujiie, H., et al., *Clinical analysis of incidentally discovered unruptured aneurysms*. Stroke, 1993. **24**(12): p. 1850-6.
11. Rosenørn, J. and V. Eskesen, *Does a safe size-limit exist for unruptured intracranial aneurysms?* Acta Neurochirurgica, 1993. **121**(3): p. 113-118.
12. Juvela, S., M. Porras, and O. Heiskanen, *Natural history of unruptured intracranial aneurysms: a long-term follow-up study*. J Neurosurg, 1993. **79**(2): p. 174-82.
13. Asari, S. and T. Ohmoto, *Natural history and risk factors of unruptured cerebral aneurysms*. Clin Neurol Neurosurg, 1993. **95**(3): p. 205-14.
14. Crompton, M.R., *Mechanism of growth and rupture in cerebral berry aneurysms*. Br Med J, 1966. **1**(5496): p. 1138-42.

15. Hademenos, G.J., et al., *Anatomical and morphological factors correlating with rupture of intracranial aneurysms in patients referred for endovascular treatment*. *Neuroradiology*, 1998. **40**(11): p. 755-60.
16. Sarwar, M., et al., *Growing intracranial aneurysms*. *Radiology*, 1976. **120**(3): p. 603-7.
17. Ujiie, H., et al., *Is the aspect ratio a reliable index for predicting the rupture of a saccular aneurysm?* *Neurosurgery*, 2001. **48**(3): p. 495-502; discussion 502-3.
18. Ujiie, H., et al., *Effects of size and shape (aspect ratio) on the hemodynamics of saccular aneurysms: a possible index for surgical treatment of intracranial aneurysms*. *Neurosurgery*, 1999. **45**(1): p. 119-29; discussion 129-30.
19. Ma, D., et al., *Size ratio for clinical assessment of intracranial aneurysm rupture risk*. *Neurol Res*, 2010. **32**(5): p. 482-6.
20. Beck, J., et al., *Difference in configuration of ruptured and unruptured intracranial aneurysms determined by biplanar digital subtraction angiography*. *Acta Neurochir (Wien)*, 2003. **145**(10): p. 861-5; discussion 865.
21. Dhar, S., et al., *Morphology parameters for intracranial aneurysm rupture risk assessment*. *Neurosurgery*, 2008. **63**(2): p. 185-96; discussion 196-7.
22. Tremmel, M., et al., *Influence of intracranial aneurysm-to-parent vessel size ratio on hemodynamics and implication for rupture: results from a virtual experimental study*. *Neurosurgery*, 2009. **64**(4): p. 622-30; discussion 630-1.
23. Rahman, M., et al., *Size ratio correlates with intracranial aneurysm rupture status: a prospective study*. *Stroke*, 2010. **41**(5): p. 916-20.
24. Raghavan, M.L., B. Ma, and R.E. Harbaugh, *Quantified aneurysm shape and rupture risk*. *J Neurosurg*, 2005. **102**(2): p. 355-62.
25. Simkins, T.E. and W.E. Stehbens, *Vibrations recorded from the adventitial surface of experimental aneurysms and arteriovenous fistulas*. *Vasc Surg*, 1974. **8**(3): p. 153-65.
26. Hademenos, G.J., et al., *A nonlinear mathematical model for the development and rupture of intracranial saccular aneurysms*. *Neurol Res*, 1994. **16**(5): p. 376-84.
27. Kyriacou, S.K. and J.D. Humphrey, *Influence of size, shape and properties on the mechanics of axisymmetric saccular aneurysms*. *J Biomech*, 1996. **29**(8): p. 1015-22.
28. Shah, A.D., et al., *Further Roles of Geometry and Properties in the Mechanics of Saccular Aneurysms*. *Computer Methods in Biomechanics and Biomedical Engineering*, 1997. **1**(2): p. 109 - 121.
29. Millan, R.D., et al., *Morphological characterization of intracranial aneurysms using 3-D moment invariants*. *IEEE Trans Med Imaging*, 2007. **26**(9): p. 1270-82.
30. Seshaiyer, P., et al., *Multiaxial Mechanical Behavior of Human Saccular Aneurysms*. *Computer Methods in Biomechanics and Biomedical Engineering*, 2001. **4**(3): p. 281 - 289.

31. Isaksen, J.G., et al., *Determination of wall tension in cerebral artery aneurysms by numerical simulation*. Stroke, 2008. **39**(12): p. 3172-8.
32. Reeps, C., et al., *The impact of model assumptions on results of computational mechanics in abdominal aortic aneurysm*. J Vasc Surg, 2010. **51**(3): p. 679-88.
33. Humphrey, J.D., *Review: Computer Methods in Membrane Biomechanics*. Comput Methods Biomech Biomed Engin, 1998. **1**(3): p. 171-210.
34. Toth, M., et al., *Sterically inhomogenous viscoelastic behavior of human saccular cerebral aneurysms*. J Vasc Res, 1998. **35**(5): p. 345-55.
35. Steiger, H.J., et al., *Strength, elasticity and viscoelastic properties of cerebral aneurysms*. Heart Vessels, 1989. **5**(1): p. 41-6.
36. Scott, S., G.G. Ferguson, and M.R. Roach, *Comparison of the elastic properties of human intracranial arteries and aneurysms*. Can J Physiol Pharmacol, 1972. **50**(4): p. 328-32.
37. Ma, B., et al., *Nonlinear anisotropic stress analysis of anatomically realistic cerebral aneurysms*. J Biomech Eng, 2007. **129**(1): p. 88-96.
38. Zhou, X., et al., *Patient-Specific Wall Stress Analysis in Cerebral Aneurysms Using Inverse Shell Model*. Annals of Biomedical Engineering, 2010. **38**(2): p. 478-489.
39. Cebal, J.R., et al., *Quantitative characterization of the hemodynamic environment in ruptured and unruptured brain aneurysms*. AJNR Am J Neuroradiol, 2011. **32**(1): p. 145-51.
40. Cebal, J.R., et al., *Characterization of cerebral aneurysms for assessing risk of rupture by using patient-specific computational hemodynamics models*. AJNR Am J Neuroradiol, 2005. **26**(10): p. 2550-9.
41. Steiger, H.J., *Pathophysiology of development and rupture of cerebral aneurysms*. Acta Neurochir Suppl (Wien), 1990. **48**: p. 1-57.
42. Liou, T.M. and S.N. Liou, *A review on in vitro studies of hemodynamic characteristics in terminal and lateral aneurysm models*. Proc Natl Sci Counc Repub China B, 1999. **23**(4): p. 133-48.
43. Steiger, H.J., et al., *Hemodynamic stress in terminal saccular aneurysms: a laser-Doppler study*. Heart Vessels, 1988. **4**(3): p. 162-9.
44. Tateshima, S., et al., *In vitro measurement of fluid-induced wall shear stress in unruptured cerebral aneurysms harboring blebs*. Stroke, 2003. **34**(1): p. 187-92.
45. Xiang, J., et al., *Hemodynamic-morphologic discriminants for intracranial aneurysm rupture*. Stroke, 2011. **42**(1): p. 144-52.
46. Antiga, L., B. Ene-Iordache, and A. Remuzzi, *Computational geometry for patient-specific reconstruction and meshing of blood vessels from MR and CT angiography*. IEEE Trans Med Imaging, 2003. **22**(5): p. 674-84.

47. Piccinelli, M., et al., *A framework for geometric analysis of vascular structures: application to cerebral aneurysms*. IEEE Trans Med Imaging, 2009. **28**(8): p. 1141-55.
48. Antiga, L., et al., *Geometric reconstruction for computational mesh generation of arterial bifurcations from CT angiography*. Comput Med Imaging Graph, 2002. **26**(4): p. 227-35.
49. Antiga, L., *Patient-Specific Modeling of Geometry and Blood Flow in Large Arteries*, in *DIPARTIMENTO DI BIOINGEGNERIA*. 2002, POLITECNICO DI MILANO: Milano.
50. Osborn, A.G.J., John M, *Diagnostic Cerebral Angiography*. 1999: Lippincott Williams & Wilkins.
51. Kraysenbühl, H.Y., Mahmut Gazi; Huber, Peter; Bosse, George *Cerebral Angiography*. 1982: Thieme.
52. Ture, U., et al., *Giant pericallosal artery aneurysm: case report and review of the literature*. Neurosurg Rev, 2001. **24**(2-3): p. 151-5.
53. Ma, B., R.E. Harbaugh, and M.L. Raghavan, *Three-dimensional geometrical characterization of cerebral aneurysms*. Ann Biomed Eng, 2004. **32**(2): p. 264-73.
54. Ma, B., *Modeling the geometry, hemodynamics and tissue mechanics of cerebral aneurysms*, in *Biomedical Engineering 2004*, University of Iowa: Iowa City.
55. Green, D. and D. Parker, *CTA and MRA: Visualization without catheterization*. Seminars in Ultrasound, CT, and MRI, 2003. **24**(4): p. 185-191.
56. Anzalone, N., et al., *Follow-up of coiled cerebral aneurysms at 3T: Comparison of 3D time-of-flight MR angiography and contrast-enhanced MR angiography*. American Journal of Neuroradiology, 2008. **29**(8): p. 1530-1536.
57. Bash, S., et al., *Intracranial vascular stenosis and occlusive disease: evaluation with CT angiography, MR angiography, and digital subtraction angiography*. AJNR Am J Neuroradiol, 2005. **26**(5): p. 1012-21.
58. Chappell, E.T., F.C. Moure, and M.C. Good, *Comparison of computed tomographic angiography with digital subtraction angiography in the diagnosis of cerebral aneurysms: a meta-analysis*. Neurosurgery, 2003. **52**(3): p. 624-31; discussion 630-1.
59. Doerfler, A., et al., *Multimodal imaging in the elastase-induced aneurysm model in rabbits: A comparative study using serial DSA, MRA and CTA*. Rofo-Fortschritte Auf Dem Gebiet Der Rontgenstrahlen Und Der Bildgebenden Verfahren, 2004. **176**(4): p. 590-596.
60. Ferre, J.C., et al., *Time-of-flight MR angiography at 3T versus digital subtraction angiography in the imaging follow-up of 51 intracranial aneurysms treated with coils*. Eur J Radiol, 2009. **72**(3): p. 365-9.

61. Kouskouras, C., et al., *Intracranial aneurysms: evaluation using CTA and MRA. Correlation with DSA and intraoperative findings*. *Neuroradiology*, 2004. **46**(10): p. 842-850.
62. Majoie, C.B., et al., *MR angiography at 3T versus digital subtraction angiography in the follow-up of intracranial aneurysms treated with detachable coils*. *AJNR Am J Neuroradiol*, 2005. **26**(6): p. 1349-56.
63. Tanoue, S., et al., *Three-dimensional reconstructed images after rotational angiography in the evaluation of intracranial aneurysms: surgical correlation*. *Neurosurgery*, 2000. **47**(4): p. 866-71.
64. Wardlaw, J.M. and P.M. White, *The detection and management of unruptured intracranial aneurysms*. *Brain*, 2000. **123 (Pt 2)**: p. 205-21.
65. Fahrig, R., et al., *A three-dimensional cerebrovascular flow phantom*. *Med Phys*, 1999. **26**(8): p. 1589-99.
66. Piotin, M., et al., *CT angiography, MR angiography and rotational digital subtraction angiography for volumetric assessment of intracranial aneurysms. An experimental study*. *Neuroradiology*, 2003. **45**(6): p. 404-9.
67. Ford, M.D., et al., *Characterization of volumetric flow rate waveforms in the normal internal carotid and vertebral arteries*. *Physiol Meas*, 2005. **26**(4): p. 477-88.
68. Ford, M.D., et al., *An objective approach to digital removal of saccular aneurysms: technique and applications*. *Br J Radiol*, 2009. **82 Spec No 1**: p. S55-61.
69. G. Taubin, T.Z., and G. Golub., *Optimal Surface Smoothing as Filter Design*. *Fourth European Conference on Computer Vision*. Fourth European Conference on Computer Vision (ECCV'96). **and IBM Research Technical Report RC-20404, March 1996.**
70. Raghavan, M.L., et al., *Three-dimensional finite element analysis of residual stress in arteries*. *Ann Biomed Eng*, 2004. **32**(2): p. 257-63.
71. Lu, J., X. Zhou, and M.L. Raghavan, *Inverse method of stress analysis for cerebral aneurysms*. *Biomech Model Mechanobiol*, 2008. **7**(6): p. 477-86.
72. Speelman, L., et al., *Patient-specific AAA wall stress analysis: 99-percentile versus peak stress*. *Eur J Vasc Endovasc Surg*, 2008. **36**(6): p. 668-76.
73. Sekhar, L.N. and R.C. Heros, *Origin, growth, and rupture of saccular aneurysms: a review*. *Neurosurgery*, 1981. **8**(2): p. 248-60.
74. Toth, M., et al., *Are there systemic changes in the arterial biomechanics of intracranial aneurysm patients?* *Pflugers Arch*, 2000. **439**(5): p. 573-8.
75. Laaksamo, E., et al., *Involvement of mitogen-activated protein kinase signaling in growth and rupture of human intracranial aneurysms*. *Stroke*, 2008. **39**(3): p. 886-92.
76. Yoshimura, K., et al., *Regression of abdominal aortic aneurysm by inhibition of c-Jun N-terminal kinase*. *Nat Med*, 2005. **11**(12): p. 1330-8.

77. Ahmad, S., et al., *Direct evidence for endothelial vascular endothelial growth factor receptor-1 function in nitric oxide-mediated angiogenesis*. *Circ Res*, 2006. **99**(7): p. 715-22.
78. Morello, F., A. Perino, and E. Hirsch, *Phosphoinositide 3-kinase signalling in the vascular system*. *Cardiovasc Res*, 2009. **82**(2): p. 261-71.
79. Frosen, J., et al., *Remodeling of saccular cerebral artery aneurysm wall is associated with rupture: histological analysis of 24 unruptured and 42 ruptured cases*. *Stroke*, 2004. **35**(10): p. 2287-93.
80. Kilic, T., et al., *Expression of structural proteins and angiogenic factors in normal arterial and unruptured and ruptured aneurysm walls*. *Neurosurgery*, 2005. **57**(5): p. 997-1007; discussion 997-1007.
81. Frosen, J., et al., *Growth factor receptor expression and remodeling of saccular cerebral artery aneurysm walls: implications for biological therapy preventing rupture*. *Neurosurgery*, 2006. **58**(3): p. 534-41; discussion 534-41.

APPENDIX

Segmentation Protocol

```

#!/bin/bash

#####

#####

# Script:      CARP.sh                #
# Task:        Moves user through a VMTK segmentation session with      #
#              explicit branch processes                                #
# Requirements:                                     #
# #Eye of Gnome image viewer                                #
# # image file ".C_o_W.png"                                #
# VMTK                                                    #
# message_display.sh                                     #
# get_dicom_path.sh                                     #
# get_location,sh                                       #
# get_patient_path.sh                                   #
# get_dicom_path.sh                                     #

#####

#####

#              global variables                                #

#####

#####

SCRIPTNAME=$(basename ${0} .sh)

# Zenity variables

TITLE=""

```

```
WIDTH=325
# Number of parameters needed (Edit line 55 logic)
NUMOFPARAMS=0
# Code testing parameters
DEBUGFILENAMES=1 # Zero=ON
DEBUGCOUNT=0
# exit status definitions
EXIT_SUCCESS=0
EXIT_FAILURE=1
EXIT_ERROR=2
EXIT_BUG=10
# variables for option switches with default values
VERBOSE="n"
OPTFOLDER=""
# variables for aneurysm segmentation
NOW=""
FILENAME=""
LOGIC=""
INITIAL=""
#PICPATH="/var/tmp/dmwelch/uiowa/bash"
#PICFILE=".CoW.png"
PATIENTPATH=""
PATIENT_NUM=""
DICOMPAT=""
TYPE=""
LEVEL=""
MESSAGE=""
```

```

AIRLEVEL=""
BONELEVEL=""
LEVELTYPE=""
ANEURYSM_NUM=1
ANEURYSM=1 #Equals false unless needed

#####

#####

#           functions           #

#####

#####

function usage {
    echo "Usage: ${SCRIPTNAME} [-h] [-v] [-i] [-o folder]" >&2
    [[ ${#} -eq 1 ]] && exit ${1} || exit ${EXIT_FAILURE}
}

function debug {
    if [[ $DEBUGFILENAMES -eq 0 ]] ; then
        echo "${DEBUGCOUNT} -> $1"
        DEBUGCOUNT=$(( ${DEBUGCOUNT} + 1 ))
    fi
}

function interest_volume {
    zenity --question --width=$WIDTH --title=${TITLE} --text="Create a new
VOI?" --ok-label="_Yes" --cancel-label="_No"
    case $? in
        0) # If creating a new VOI, get the location to name correctly

```

```

    . get_location.sh ;;

1) # If using an old VOI, select it from a list
    FILENAME=`zenity --width=$WIDTH --title=${TITLE} --
filename=${PATIENTPATH}/ --file-selection --title="Select VOI to use"
    FILENAME=`basename ${FILENAME%%'.vti'}` #Strip off folder
information
    . message_display.sh "Showing VOI selected. Type \"q\" in render
window to proceed"
    vmtkimagereader -ifile ${PATIENTPATH}/${FILENAME}.vti --pipe
vmtkimageviewer # Show user the voi they choose
    debug $FILENAME ;;
-1)
    exit ${EXIT_FAILURE} ;;
esac
}

function create_sigmoid {
    zenity --width=$WIDTH --title="${TITLE}" --question --text="Does this VOI
need $1 corrections?" --ok-label="_Yes" --cancel-label="_No"
    case $? in
        0)
            create_feature ;;
-1 | 1)
            ;;
        *)
            echo $? ; exit ${EXIT_BUG}
    esac
}

```

```

}

function air_feature {
    LEVEL=`zenity --entry --title="${TITLE}" --width=$WIDTH --text="Enter
the value for air" --cancel-label="_Done"`
    while [[ $? -eq 0 ]] ; do
        AIRLEVEL=$LEVEL; . message_display.sh "Displaying potential air
feature"

        vmtkimagereader -ifile ${PATIENTPATH}/${FILENAME}.vti --pipe
vmtkmarchingcubes -l ${AIRLEVEL} --pipe vmtkrenderer --pipe vmtkimageviewer --
pipe vmtksurfaceviewer

        LEVEL=`zenity --entry --title="${TITLE}" --width=$WIDTH --text="Enter
the value for air" --cancel-label="_Done"`
    done

    LEVEL=$AIRLEVEL #Needed b/c last zenity call in while loop erases value
for LEVEL!
}

function bone_feature {
    LEVEL=`zenity --entry --title="${TITLE}" --width=$WIDTH --text="Enter
the value for bone" --cancel-label="_Done"`
    while [[ $? -eq 0 ]] ; do
        BONELEVEL=$LEVEL; . message_display.sh "Displaying potential bone
feature"

        vmtkimagereader -ifile ${PATIENTPATH}/${FILENAME}.vti --pipe
vmtkmarchingcubes -ifile ${PATIENTPATH}/${FILENAME}.vti -l ${BONELEVEL} -
-pipe vmtkrenderer --pipe vmtkimageviewer --pipe vmtksurfaceviewer

```



```

LEVEL=`zenity --entry --title="${TITLE}" --width=$WIDTH --text="Enter
the value for bone" --cancel-label="_Done"

```

```
done
```

```

LEVEL=$BONELEVEL #Needed b/c last zenity call in while loop erases
value for LEVEL!

```

```
}
```

```
function create_feature {
```

```

    zenity --question --width=$WIDTH --title=${TITLE} --text="Is there already
a(n) ${TYPE} file?" --ok-label="_Yes" --cancel-label="_No"

```

```
case $? in
```

```
0) # Already a file
```

```

    LEVEL=`zenity --file-selection --title="${TITLE}: Select ${TYPE} file"
--filename="${PATIENTPATH}/"

```

```
case $? in
```

```
0)
```

```
;;
```

```
1)
```

```
echo "No file selected."
```

```
. quit.sh ;;
```

```
-1)
```

```
echo 'Zenity has caused an error!' # Something happened with zenity
```

```
exit ${EXIT_ERROR} ;;
```

```
*)
```

```
echo $? ; exit ${EXIT_BUG}
```

```
esac
```

```
# Removes front and back from filename, leaving only LEVEL value
```

```

LEVEL=${LEVEL%%.vti}
LEVEL=${LEVEL##*${FILENAME}}_${TYPE}_
# Now we need to pass the level value to the correct container variable
if [[ ${TYPE} == 'air' ]]; then
    AIRLEVEL=${LEVEL}
elif [[ ${TYPE} == 'bone' ]]; then
    BONELEVEL=${LEVEL}
else
    echo "Error assigning level values"; exit ${EXIT_BUG}
fi
;;
1) # No file
    ${TYPE}_feature
    if [[ ! -f
${PATIENTPATH}/${FILENAME}_${TYPE}_${LEVEL}_lvlset.vti ]] ; then
        . message_display.sh "Create the feature correction now. Select
        \"isosurface\"\\n'
                                for the segmentation method and enter the value you
        have\\n'
                                previously decided upon. Evolve at 300 0 0 1."
        vmtklevelsetsegmentation -ifile
${PATIENTPATH}/${FILENAME}.vti -ofeatureimagefile
${PATIENTPATH}/${FILENAME}_${TYPE}_${LEVEL}.vti -ofile
${PATIENTPATH}/${FILENAME}_${TYPE}_${LEVEL}_lvlset.vti
        vmtkimagefeaturecorrection -ifile
${PATIENTPATH}/${FILENAME}_${TYPE}_${LEVEL}.vti -levelsetfile

```

```

${PATIENTPATH}/${FILENAME}_${TYPE}_${LEVEL}_lvlset.vti -scalefrominput 0
-ofile ${PATIENTPATH}/${FILENAME}_${TYPE}_sigmoid.vti

        fi ;;

    esac

}

function image_feature {
    vmtkimagecompose -ifile
    ${PATIENTPATH}/${FILENAME}_bone_${BONELEVEL}_lvlset.vti -i2file
    ${PATIENTPATH}/${FILENAME}_air_${AIRLEVEL}_lvlset.vti -negatei2 1 -ofile
    ${PATIENTPATH}/${FILENAME}_both_lvlset.vti
    vmtkimagefeaturecorrection -ifile
    ${PATIENTPATH}/${FILENAME}_bone_${BONELEVEL}.vti -levelsetsfile
    ${PATIENTPATH}/${FILENAME}_both_lvlset.vti -scalefrominput 0 -ofile
    ${PATIENTPATH}/${FILENAME}_both_sigmoid.vti
}

function segment {
    if [[ -f ${PATIENTPATH}/${NEWFILENAME}_initial.vti ]] ; then # IS
initial file
        if [[ ! -f ${PATIENTPATH}/${FILENAME}_bone_sigmoid.vti && ! -f
    ${PATIENTPATH}/${FILENAME}_air_sigmoid.vti ]] ; then # NO sigmoid file
            vmtklevelsetsegmentation -ifile ${PATIENTPATH}/${FILENAME}.vti -
initiallevelsetsfile ${PATIENTPATH}/${NEWFILENAME}_initial.vti -ofile
    ${PATIENTPATH}/${NEWFILENAME}_segm.vti
        else # IS initial & has sigmoid(s)

```

```

if [[ -f ${PATIENTPATH}/${FILENAME}_bone_sigmoid.vti && -f
${PATIENTPATH}/${FILENAME}_air_sigmoid.vti ]] ; then
    if [[ ! $AIRLEVEL == "" && ! $BONELEVEL == "" ]]; then
        image_feature
        . message_display.sh "Both air and bone corrections detected" ;
LEVELTYPE="both"
    fi
else
    if [[ -f ${PATIENTPATH}/${FILENAME}_bone_sigmoid.vti ]] ; then
        . message_display.sh "Only bone correction detected" ;
LEVELTYPE="bone"
    else
        . message_display.sh "Only air correction detected" ;
LEVELTYPE="air"
    fi
    fi
    vmtklevelsetsegmentation -ifile ${PATIENTPATH}/${FILENAME}.vti -
featureimagefile ${PATIENTPATH}/${FILENAME}_${LEVELTYPE}_sigmoid.vti -
initiallevelsetsfile ${PATIENTPATH}/${NEWFILENAME}_initial.vti -ofile
${PATIENTPATH}/${NEWFILENAME}_segm.vti
    fi
else # NO initial file
    if [[ ! -f ${PATIENTPATH}/${FILENAME}_bone_sigmoid.vti && ! -f
${PATIENTPATH}/${FILENAME}_air_sigmoid.vti ]] ; then # NO sigmoid file
        vmtkimageinitialization -ifile ${PATIENTPATH}/${FILENAME}.vti -
olevelsetsfile ${PATIENTPATH}/${NEWFILENAME}_initial.vti

```

```

vmtklevelsetsegmentation -ifile ${PATIENTPATH}/${FILENAME}.vti -
initiallevelsetsfile ${PATIENTPATH}/${NEWFILENAME}_initial.vti -ofile
${PATIENTPATH}/${NEWFILENAME}_segm.vti
else # NO initial & has sigmoid(s)
    if [[ -f ${PATIENTPATH}/${FILENAME}_bone_sigmoid.vti && -f
${PATIENTPATH}/${FILENAME}_air_sigmoid.vti ]] ; then
        image_feature
        . message_display.sh "Both air and bone corrections detected" ;
LEVELTYPE="both"
    else
        if [[ -f ${PATIENTPATH}/${FILENAME}_bone_sigmoid.vti ]] ; then
            . message_display.sh "Only bone correction detected" ;
LEVELTYPE="bone"
        else
            . message_display.sh "Only air correction detected" ;
LEVELTYPE="air"
        fi
    fi
    vmtkimageinitialization -ifile ${PATIENTPATH}/${FILENAME}.vti -
olevelsetsfile ${PATIENTPATH}/${NEWFILENAME}_initial.vti
    vmtklevelsetsegmentation -ifile ${PATIENTPATH}/${FILENAME}.vti -
initiallevelsetsfile ${PATIENTPATH}/${NEWFILENAME}_initial.vti -featureimagefile
${PATIENTPATH}/${FILENAME}_${LEVELTYPE}_sigmoid.vti -ofile
${PATIENTPATH}/${NEWFILENAME}_segm.vti
    fi
fi
REPLY=""

```

```

.message_display.sh "Please record the evolution smoothing parameters
                    you used and the vessels they were applied to:
                    Type \"q\" or \"Q\" to quit"
while [[ ! $REPLY == "q" && ! $REPLY == "Q" ]]; do
    read ;
    if [[ ! $REPLY == "q" && ! $REPLY == "Q" ]]; then
        echo "Level set evolution parameters for ${NEWFILENAME}:
${REPLY} on " `date` 1>>${PATIENTPATH}/params${ANEURYSM_NUM}
        fi
    done
}

function combine {
    VESSEL=`zenity --file-selection --filename=${PATIENTPATH}/ --
title="${TITLE}: Select vessel file"; VESSEL=${VESSEL%%'.vti'}
    ANEURYSM=`zenity --file-selection --filename=${PATIENTPATH}/ --
title="${TITLE}: Select aneurysm file"; ANEURYSM=${ANEURYSM%%'.vti'}
    vmtkimagecompose -ifile ${VESSEL}.vti -i2file ${ANEURYSM}.vti -
operation min -ofile ${PATIENTPATH}/${FILENAME}_combined_seg.vti --pipe
vmtkmarchingcubes -i @vmtkimagecompose.o --pipe vmtksurfaceviewer
    vmtkimageslice -spacing 0.25 0.25 0.25 -ifile ${VESSEL}.vti -ofile
${VESSEL}_sub.vti
    vmtkimageslice -spacing 0.25 0.25 0.25 -ifile ${ANEURYSM}.vti -ofile
${ANEURYSM}_sub.vti
    YESNO=1
    while [[ ! $YESNO == 0 ]] ; do

```

```

SHIFT=`zenity --entry --title="${TITLE}" --width=$WIDTH --text="Enter
the value to shrink (0-1)"`

case $? in
    0)
        vmtkimageshiftscale -ifile ${VESSEL}_sub.vti -shift $SHIFT -ofile
        ${VESSEL}_sub_shrunked.vti
        vmtkimageshiftscale -ifile ${ANEURYSM}_sub.vti -shift $SHIFT -
        ofile ${ANEURYSM}_sub_shrunked.vti
        vmtkimagecompose -ifile ${VESSEL}_sub_shrunked.vti -i2file
        ${ANEURYSM}_sub_shrunked.vti -operation min -ofile
        ${PATIENTPATH}/${FILENAME}_combined_seg.vti --pipe vmtkmarchingcubes -i
        @vmtkimagecompose.o --pipe vmtksurfaceviewer
        zenity --question --title="$TITLE" --text="Is this satisfactory?" --ok-
        label="_Yes" --cancel-label="_No"
        YESNO=$?;;
    -1|1)
        . quit.sh ;;
    *)
        ;;
esac

done

echo "Shift scale value is ${SHIFT} for ${FILENAME}_seg.vtp on "`date`
1>>${PATIENTPATH}/params${ANEURYSM_NUM}
}

#####

#####

#                main program                #

```

```

#####
#####
# the options -h for help should always be present. Options -v and
# -o are examples. -o needs a parameter, indicated by the colon ":"
# following in the getopt call
while getopt ':o:vh' OPTION ; do
    case ${OPTION} in
        v) VERBOSE=y ;;
        o) OPTFOLDER="${OPTARG}" ;;
        i) INITIAL=y ;; #This is the first segmentation and the dicom folder needs
read
        h) usage ${EXIT_SUCCESS} ;;
        \?) echo "unknown option \"-${OPTARG}\"." >&2 ; usage
${EXIT_ERROR} ;;
        :) echo "option \"-${OPTARG}\" requires an argument." >&2 ; usage
${EXIT_ERROR} ;;
        *) echo "Impossible error. parameter: ${OPTION}" >&2 ; usage
${EXIT_BUG} ;;
    esac
done
# skip parsed options
shift $(( OPTIND - 1 ))
# if you want to check for a minimum or maximum number of arguments, do it
here
if [[ $# -lt $NUMOFPARAMS ]] ; then
    echo 'Wrong number of parameters' >&2
    usage ${EXIT_ERROR} ; exit

```



```

fi
# loop through all arguments
for ARG ; do
    if [[ ${VERBOSE} = y ]] ; then
        echo -n 'argument: '
    fi
    echo ${ARG}
done

# Needed on BIOMOST000, BIOMOST007, BIOMOST008
export PYTHONPATH=/usr/css/opt/vmtk-0.8/lib:/usr/css/opt/vmtk-
0.8/lib/vmtk:/usr/css/opt/vtk-5.4.2/lib64/python2.6/site-packages
export LD_LIBRARY_PATH=/usr/css/opt/vtk-5.4.2/lib/vtk-
5.4:/usr/css/opt/InsightToolkit-3.16.0/lib/InsightToolkit:/usr/css/opt/vmtk-
0.8/lib:/usr/css/opt/vmtk-0.8/lib/vmtk

NOW=`date`
xhost +local:$USER

#####

#####

# The filename is used as a description of the content of the file so #
# we carefully construct the filename based on the patient number, the #
# aneurysm location, the stage of segmentation, and possibly the user #
# and date. #
# The function 'get_patient_path.sh' prompts the user to enter the #
# patient number and returns the global variables PATIENT_NUM & #
# PATIENTPATH. #
# 'aneurysm_num.sh' has user select the location and side of the #
# aneurysm and appends that to the filename. The aneurysms are numbered#

```

```

# by alphabetical order. Users should segment in that order to maintain#
# file coherence. #
# 'get_dicom_path.sh' loads the dicom data IF IT HAS NOT ALREADY BEEN
#
# READ- the function searches for a file named "..._all.vti" and if not #
# present, it produces it. #
#####
#####
. get_patient_path.sh; FILENAME=$PATIENT_NUM; debug $FILENAME
. echo $FILENAME
aneurysm_num.sh
. get_dicom_path.sh
#####
#####
# For multiple aneurysms, loop the script to do them all in one session #
# This is the master control of the program: it controls the flow of the #
# script and makes branching between tasks easier to follow and edit. #
#####
#####
COUNT=1
while [[ $COUNT -le $ANEURYSM_NUM ]] ; do
# Loop following code or ask to select which to do
FILENAME="${PATIENT_NUM}_${COUNT}"; debug $FILENAME
interest_volume # Create a volume of interest for this anatomy
zenity --width=$WIDTH --title="{TITLE}" --question --text="Would you
like to segment this VOI?" --ok-label="_Yes" --cancel-label="_No"
case $? in

```

```

0) # If yes, are there air or bone corrections needed?
    TYPE="air"; create_sigmoid $TYPE;
    TYPE="bone"; create_sigmoid $TYPE;
    for NEWFILENAME in "${FILENAME}_vessel"
"${FILENAME}_aneurysm"; do #Sets NEWFILENAME variable during loop
        debug $NEWFILENAME
        if [[ -f ${PATIENTPATH}/${NEWFILENAME}_segm.vti ]]; then #
This has a previous completed segmentation
            zenity --width=$WIDTH --title="${TITLE}" --question --
text="Would you like to use the existing segmented model\n for $NEWFILENAME?" --
ok-label="_Yes" --cancel-label="_No"
            case $? in
                0)
                    . message_display.sh "Examine this previous model for
ommissions. Type \"q\" in render window to proceed"
                    vmtkimagereader -ifile
${PATIENTPATH}/${NEWFILENAME}_segm.vti --pipe vmtkmarchingcubes -l 0.0 --
pipe vmtkrenderer --pipe vmtkimagereader -ifile
${PATIENTPATH}/${FILENAME}.vti --pipe vmtkimageviewer --pipe
vmtksurfaceviewer # Show model to user and proceed
                    ;;
                1)
                    segment # If there is a previous model but we want to make a
new one...
                    ;;
            esac
        else

```

```

        segment # If there is no previous model, make one...
    fi
done
combine
;;
-1 | 1)
    ;; # No, do nothing
esac

zenity --width=$WIDTH --title="{TITLE}" --question --text="Would you
like to mesh a segmentation?" --ok-label="_Yes" --cancel-label="_No"
case $? in
    0)
        . reconstruct.sh ;;
    *) # We either don't want to mesh OR we only have a VOI and no surface
        ;;
esac

if [[ ${FILENAME} == *CoW* ]] ; then
    echo "Renaming CoW files"
    for ii in `find . -name "CoW" -type f` ; do
        mv $ii "${ii%}_${COUNT}_"*}_${ii##*_}${COUNT}_""
    done
    COUNT=${COUNT}; # Don't advance the count for CoW
else
    COUNT=${COUNT}+1;
fi

FILENAME=${PATIENT_NUM}; debug $FILENAME # Reset the filename
done

```

```

exit ${EXIT_SUCCESS}

#!/bin/bash

ANEURYSM_NUM=`zenity --list --width=400 --
title="${TITLE}:\n'How many aneurysms?" --list --radiolist
--column="Aneurysms" --column="Number" TRUE 1 FALSE 2 FALSE
3 FALSE 4 FALSE 5 FALSE 6 FALSE 7 FALSE 8 FALSE 9 --print-
column 2`
# Recursion loop needed for multiple aneurysm cases
case $? in
0) ;;
1) ANEURYSM_NUM=1 ;; # All patients have
at least ONE aneurysm
-1) echo 'Zenity has caused an error!' #
Something happened with zenity
exit ${EXIT_ERROR} ;;
esac

#!/bin/bash

if [[ ! -f ${PATIENTPATH}/${PATIENT_NUM}_all.vti ]] ;
then # If dicom folder hasn't been created as .vti
#`mipav -inputDIR $PATIENTPATH`

DICOMPATH=`zenity --filename="${PATIENTPATH}" --
file-selection --directory --title="${TITLE}: Select image
directory"`
case $? in
0)
echo $DICOMPATH
ANSWER= `zenity --question --text="Are the
images saved as DICOM?"`
case $? in
0)
READERNUM=1
echo $READERNUM
echo $DICOMPATH ;;
1)
IMGPATH=`zenity --
filename="${DICOMPATH}" --file-selection --title="${TITLE}:
Select image file"`
case $? in
0)

```

```

        echo $IMGPATH ;;
    1)
        echo "No file selected.
Exiting..." ; . quit.sh ;;
    -1)
        echo 'Zenity has caused an
error!' # Something happened with zenity
        exit ${EXIT_ERROR} ;;
    *)
        echo $? ; exit ${EXIT_BUG} ;;
esac
    READERNUM=2
    echo $READERNUM;;
    -1)
        echo 'Zenity has caused an error!' #
Something happened with zenity
        exit ${EXIT_ERROR} ;;
    *)
        echo $? ; exit ${EXIT_BUG} ;;
esac;;
1)
    echo "No file selected. Exiting..." ; .
quit.sh ;;
    -1)
        echo 'Zenity has caused an error!' #
Something happened with zenity
        exit ${EXIT_ERROR} ;;
    *)
        echo $? ; exit ${EXIT_BUG} ;;
esac

        #if [[ ! -f ${PATIENTPATH}/DICOMDIR ]] ; then
        #    `gdcmgendir -r -i ${DICOMPATH} -o
${PATIENTPATH}DICOMDIR 2>/dev/null`
        #    case $? in
        #        0)
        #            ;;
        #        *)
        #            for j in `ls
${DICOMPATH}/*`; do
        #                `gdcmmconv -V --raw --
force -i $j -o ${PATIENTPATH}/DICOM/$j 2>/dev/null`
        #                if [[ $? -ne 0 ]] ;
then
        #                    break

```

```

#                                     fi
#                                     done
#                                     `gdcmgendir -r -i
${PATIENTPATH}/DICOM -o ${PATIENTPATH}DICOMDIR 2>/dev/null`
#                                     case $? in
#                                     0)
#
DICOMPATH="${PATIENTPATH}/DICOM" ;;
#                                     *)
#                                     echo "Could not
create DICOMDIR" #Failed twice to create DICOMDIR file
#                                     rm -rf
${PATIENTPATH}/DICOM ;; # Remove DICOM folder created above
#                                     esac ;;
#                                     esac
#fi
if [ ${READERNUM} = "1" ] ; then
    vmtkimagereader -f dicom -d $DICOMPATH --pipe
vmtkimagewriter -ofile ${PATIENTPATH}/${FILENAME}_all.vti
else
    echo $READERNUM
    vmtkimagereader -ifile $IMGPATH --pipe
vmtkimagewriter -ofile ${PATIENTPATH}/${FILENAME}_all.vti
fi
fi

#!/bin/bash

function get_side {
    `zenity --question --width=150 --title="VOI
Orientation" --text="Which side of the patient is it on?" -
-ok-label="_Right" --cancel-label="_Left"` # Potential bug:
Clicking "Close" will signal a choice of "Right"
    case $? in
        0) FILENAME=${FILENAME}_right ;;
        1) FILENAME=${FILENAME}_left ;;
        -1) echo "Exiting..." ; . quit.sh;;
    esac
}

function userGUI {
    CHOICE1=`zenity --list --width=500 --
height=400 --title="${TITLE}: Aneurysm Location" --list --
radiolist --column="Aneurysms" --column="Location" --
column="Code" --hide-column=3 FALSE "Anterior Cerebral
Artery" 1 FALSE "Anterior Communicating Artery" 2 FALSE
"Basilar" 3 FALSE "Circle of Willis" 4 FALSE "Interior

```

```
Carotid Artery" 5 FALSE "Middle Cerebral Artery" 6 FALSE
"Ophthalmic Artery" 7 FALSE "Posterior Cerebral Artery" 8
FALSE "Posterior Communicating Artery" 9 FALSE "Other" 10 -
-print-column 3 `
```

```

        case $? in
            0) ;;
            -1 | 1) echo "Exiting..." ; . quit.sh;;
        esac

        case $CHOICE1 in
            1) FILENAME=${FILENAME}_ACA ;
get_side;;
            2) FILENAME=${FILENAME}_AComm ;; # No
'side'
            3) FILENAME=${FILENAME}_Bslar ;; # No
'side'
            4) FILENAME=${FILENAME}_CoW ;; # No
'side' and remove the numeral
            5) FILENAME=${FILENAME}_ICA ;
get_side;;
            6) FILENAME=${FILENAME}_MCA ;
get_side;;
            7) FILENAME=${FILENAME}_Ophth ;
get_side;;
            8) FILENAME=${FILENAME}_PCA ;
get_side;;
            9) FILENAME=${FILENAME}_PComm ;
get_side;;
            10) LOCATION=`zenity --entry --
title="${TITLE}" --text="Enter VOI location:" --entry-text
"location"`
                case $? in
                    0)
FILENAME=${FILENAME}_${LOCATION} ;;
                    -1 | 1) echo "No location entered" ; .
get_location.sh ;;
                esac
                ;;
        esac

    }
    #####
#####
#
#
```



```

#
main program
#
#
#####
#####
#if [ -e "${PICPATH}/${PICFILE}" ] ; then
#    ( `eog -f "${PICPATH}/${PICFILE}"` | userGUI
) # Displays help image simultaneously with zenity GUI
#    wait # Do not proceed until picture is closed
#else
    userGUI
#fi
zenity --width=$WIDTH --title="${TITLE}" --info --
text='Selecting VOI. Press "i" to initiate VOI selector.'
vmtkimagevoiselector -ifile
${PATIENTPATH}/${PATIENT_NUM}_all.vti -ofile
${PATIENTPATH}/${FILENAME}.vti --pipe vmtkimagemipviewer -
display 0 -ofile ${PATIENTPATH}/${FILENAME}_mip.vti # Set
display to 1 to show MIPS during runtime

if [[ $DEBUGFILENAMES -eq 0 ]] ; then
    echo "${DEBUGCOUNT} -> ${FILENAME}" ;
DEBUGCOUNT=$(( ${DEBUGCOUNT} + 1 ))
fi

#!/bin/bash
#function get_patient_path
PATIENT_NUM=0
#####
#####
if [[ $TITLE = "" ]] ; then
    TITLE="Patient Data"
fi

PATIENTPATH=`zenity --file-selection --directory --
title="${TITLE}: Select destination folder" --
filename="/media/"`
case $? in
0)    echo "${PATIENTPATH} selected";;
1)    echo "No path selected."
    . quit.sh ;;
-1)   echo 'Zenity has caused an error!' #
Something happened with zenity
    exit ${EXIT_ERROR} ;;

```

```

*)          echo $? ; exit ${EXIT_BUG};;
esac

while [[ $PATIENT_NUM -lt 1001 || $PATIENT_NUM -ge
5000 || $PATIENT_NUM%1000 -eq 0 ]] ; do # -.10 will break
out of the while loop! Need to investigate!
    if [[ $PATIENT_NUM == Train* || $PATIENT_NUM ==
test ]]; then # If this is a training set, name the files
Train...
        break
    fi
    PATIENT_NUM=`zenity --entry --title="${TITLE}"
--width=200 --text="Enter the patient ID _number:"`
    case $? in
        0)          ;;
        1)          echo "No patient number given."
                    . quit.sh ;;
        -1)         echo 'Zenity has caused an
error!' # Something happened with zenity
                    exit ${EXIT_ERROR} ;;
        *)          echo $? ; exit ${EXIT_BUG}
    esac
done

#!/bin/bash

#function message_display{
#####
#####
#       Output a string with a border
#
#       Arguments:
#
#       1.       string
#
#####
#####
length=''
str=''
# exit status definitions
EXIT_SUCCESS=0
EXIT_FAILURE=1
EXIT_ERROR=2
EXIT_BUG=10

function string
{

```

```
#####
#           Emulate the old BASIC function
"string$" #
#           Arguments:
#
#           1.      character
#
#           2.      length
#
#####
local string_length # local variable
# Fatal error if required arguments are
missing
if [[ "$1" = "" || "$2" = "" ]]; then
    echo "message_display,string: INTERNAL
ERROR - arguments not passed correctly"
    exit $EXIT_BUG # if arguments NOT
passed to function, fatal error
fi

# Make sure that argument 2 is actually a
number
string_length=$(echo "$2" | awk '/^[0-9]*$/ {
print $0 }')
if [ -z "$string_length" ]; then
    echo "message_display,string: INTERNAL
ERROR - argument must be a number"
    exit $EXIT_BUG
fi

# Make the string
awk -v char=$1 -v len=$string_length '
BEGIN {
    str = ""
    for (i=0; i < len; i++) {
        str = str char
    }
    print str
}'

} # end of string

# Fatal error if required arguments are missing
if [ "$1" = "" ]; then
    echo "message_display: missing argument 1"
```

```

        exit $EXIT_FAILURE
    fi

    length=$(echo $1 | awk '{ print length($0) }')
    str=$(string "-" $length)
    if [[ $? -ne 0 ]]; then # If the function string exits
in an abnormal way, kill program with error code
        echo $str
        exit $EXIT_ERROR
    fi
    echo ""
    echo $str
    echo $1
    echo $str
    echo ""

#!/bin/bash
#####
#####
# Script: reconstruct.sh
#
# Task:          This script searches for files
ending in _segm.vti and #
#               passes the batch of them through a meshing
and centerline #
#               analysis. Other methods will be implemented
in future #
#               This can be run as a stand-alone
program. #
# Author:       Dave Welch
#
# Contact:      david.m.welch@gmail.com
#
# Date:         10 Feb, 2010
#
# Licence:      Copyright (C) 2010 David M. Welch
#
#
# This program is free software: you can redistribute
it and/or modify #
# it under the terms of the GNU General Public
License as published by #
# the Free Software Foundation, either version 3 of
the License, or #
# (at your option) any later version.
#

```

```

#
#
#   This program is distributed in the hope that it
will be useful, #
#   but WITHOUT ANY WARRANTY; without even the
implied warranty of #
#   MERCHANTABILITY or FITNESS FOR A PARTICULAR
PURPOSE. See the #
#   GNU General Public License for more details.
#
#
#   You should have received a copy of the GNU
General Public License #
#   along with this program. If not, see
<http://www.gnu.org/licenses/>. # #
#
#####
#####
#####
#####
#
#
#           global variables
#
#
#
#####
#####
SCRIPTNAME=$(basename ${0} .sh)

# Number of parameters needed (Edit line 55 logic)
NUMOFPARAMS=0

EXIT_SUCCESS=0
EXIT_FAILURE=1
EXIT_ERROR=2
EXIT_BUG=10

# variables for option switches with default values
VERBOSE="n"
OPTFILE=""
LICENSE="COPYING"

#####
#####

```

```

#
#
#           functions
#
#
#####
#####
function usage {
    echo "Usage: ${SCRIPTNAME} [-h] [-v] [-c] [-o
arg] file ..." >&2
    [[ ${#} -eq 1 ]] && exit ${1} || exit
${EXIT_FAILURE}
}

function copyright {
    DIR=`find / -type d -name "name" 2>/dev/null`
    exec < "${DIR}/${LICENSE}"
    while read LINE ; do
        echo ${LINE}
    done
}

#####
#####
#
#
#           main program
#
#
#####
#####

# the options -h for help should always be present.
Options -v and
# -o are examples. -o needs a parameter, indicated by
the colon ":"
# following in the getopt call
while getopt ':o:vhc' OPTION ; do
    case ${OPTION} in
        c)          copyright
                    ;;
        v)          VERBOSE=y
                    ;;
        o)          OPTFILE="${OPTARG}"
                    ;;
    esac
done

```

```

        h)  usage ${EXIT_SUCCESS}
            ;;
        \?) echo "unknown option \"-${OPTARG}\"."
>&2
            usage ${EXIT_ERROR}
            ;;
        :)  echo "option \"-${OPTARG}\" requires an
argument." >&2
            usage ${EXIT_ERROR}
            ;;
        *)  echo "Impossible error. parameter:
${OPTION}" >&2
            usage ${EXIT_BUG}
            ;;
    esac
done

# skip parsed options
shift $(( OPTIND - 1 ))

# if you want to check for a minimum or maximum number
of arguments,
# do it here
if [[ $# -ne $NUMOFPARAMS ]] ; then
    echo "Wrong number of parameters" >&2
    usage ${EXIT_ERROR}
fi

# loop through all arguments
for ARG ; do
    if [[ ${VERBOSE} = y ]] ; then
        echo -n "argument: "
    fi
    echo ${ARG}
done
if [[ -z ${PATIENTPATH} ]] ; then
    . get_patient_path.sh
    # Needed on BIOMOST000
    export PYTHONPATH=/usr/css/opt/vmtk-
0.8/lib:/usr/css/opt/vmtk-0.8/lib/vmtk:/usr/css/opt/vtk-
5.4.2/lib64/python2.6/site-packages
    export LD_LIBRARY_PATH=/usr/css/opt/vtk-
5.4.2/lib/vtk-5.4:/usr/css/opt/InsightToolkit-
3.16.0/lib/InsightToolkit:/usr/css/opt/vmtk-
0.8/lib:/usr/css/opt/vmtk-0.8/lib/vmtk
fi

```

```

INPUT=`zenity --file-selection --
filename=$PATIENTPATH/ --title="Select segm file to mesh" `
# Manasi wants Tecplot ASAP here!
###vmtkmarchingcubes -ifile ${INPUT} --pipe
vmtksurfacesubdivision -method loop -ofile
${INPUT%%segm.vti}mesh.vtp --pipe vmtksurfacetomesh --pipe
vmtkmeshscaling -scale 0.1 --pipe vmtkmeshwriter -f tecplot
-ofile ${INPUT%%segm.vti}mesh.dat # Write tecplot file in
cgs units, not in mm, that is C^2continuous

vmtkmarchingcubes -ifile ${INPUT} --pipe
vmtksurfacetriangle --pipe vmtksurfacewriter -f tecplot -
ofile ${INPUT%%.vti}.dat # Tecplot files need .dat
extention, but no interior manipulations

# # #Automatically cut ends by identifying endpoints
to centerlines
# # # vmtksurfacereader -ifile
${INPUT%%segm.vti}mesh.vtp --pipe vmtkcenterlines -ofile
${INPUT%%segm.vti}ctrlines.vtp --pipe vmtkendpointextractor
--pipe vmtkbranchclipper --pipe vmtksurfaceconnectivity -
cleanoutput 1 --pipe vmtkrenderer --pipe vmtksurfaceviewer
-opacity 0.25 --pipe vmtksurfaceviewer -i
@vmtkcenterlines.voronoidiagram -array
MaximumInscribedSphereRadius --pipe vmtksurfaceviewer -i
@vmtkcenterlines.o --pipe vmtksurfacewriter -ofile
${INPUT%%segm.vti}clip.vtp # Did we get them all?
# # # `zenity --question --width=150 --
title="Automated Clipping" --text="Did this clip the
surface accurately?" --ok-label="_Yes" --cancel-
label="_No" `
# # # case $? in
# # #     0)                ;;
# # #     -1 | 1)           ;;
# # #                     vmtksurfacereader -ifile
${INPUT%%segm.vti}clip.vtp --pipe vmtkbranchclipper -ofile
${INPUT%%segm.vti}clip.vtp --pipe vmtksurfacereader --pipe
vmtkcenterlines -seedselector openprofiles -ofile
${INPUT%%segm.vti}ctrlines.vtp --pipe vmtkrenderer --pipe
vmtksurfaceviewer -opacity 0.25 --pipe vmtksurfaceviewer -i
@vmtkcenterlines.voronoidiagram -array
MaximumInscribedSphereRadius --pipe vmtksurfaceviewer -i
@vmtkcenterlines.o ;;
# # # esac
# # #
# # # # Add flow extensions

```



```
# # # vmtksurfacereader -ifile  
${INPUT%%segm.vti}clip.vtp --pipe vmtkcenterlines -  
seedselector openprofiles --pipe vmtkflowextensions -  
adaptivelength 1 -extensionratio 20 -normalestimationratio  
1 -interactive 0 --pipe vmtksurfacewriter -ofile  
${INPUT%%segm.vti}flow.vtp --pipe vmtksurfacetomesh --pipe  
vmtkmeshscaling -scale 0.1 --pipe vmtkmeshwriter -f tecplot  
-ofile ${INPUT%%segm.vti}flow_mesh.dat
```

```
tecplot ${INPUT%%.vti}.dat  
exit ${EXIT_SUCCESS}
```

```
#!/bash/bin  
echo 'Application terminated by user.'  
exit ${EXIT_SUCCESS}
```